



**Politecnico di Milano**

---

SCHOOL OF INDUSTRIAL AND INFORMATION ENGINEERING  
Master of Science in Energy Engineering

MASTER THESIS

**SOLAR-ASSISTED HEAT PUMP WITH PVT:  
MODELLING AND PRELIMINARY EXPERIMENTAL  
INVESTIGATION**

Student

**Giovanni Mattei**

**ID 836338**

Supervisor

**Prof. Giampaolo Manzolini**

Co-supervisor

**Ing. Riccardo Simonetti**

---

**Academic Year 2015–2016**

Giovanni Mattei: *Solar-assisted heat pump modelling and preliminary experimental investigation* | Master Thesis in Ingegneria Energetica - Energy Engineering, Politecnico di Milano.

© Copyright December 2016.

---

Politecnico di Milano:

[www.polimi.it](http://www.polimi.it)

Scuola di Ingegneria Industriale e dell'Informazione:

[www.ingindinf.polimi.it](http://www.ingindinf.polimi.it)

---

# Ringraziamenti

Desidero esprimere qui la mia gratitudine verso tutte le persone che mi hanno accompagnato in questi mesi e questi anni di università.

Desidero ringraziare il Prof. Manzolini e l'Ing. Simonetti per i consigli e il supporto nel lavoro di questi mesi.

Un grazie anche alla mia famiglia, per l'affetto con cui mi ha accompagnato. Grazie anche agli zii Ines e Giancarlo, per la loro presenza amorevole. Grazie agli amici di sempre (Francesco, Francesco, Lorenzo, Giorgia, Andrea, Simone e Enrico) che nonostante la lontananza mi sono rimasti accanto in questi anni, e a tutti gli amici conosciuti in università. In particolare Alberto, fondamentale compagno di studi.

Ma il ringraziamento più importante va senza dubbio a Maria Clotilde, fonte costante di sostegno e incoraggiamento. Grazie per l'amore con cui mi ha accompagnato ogni giorno, anche nei momenti più difficili.



*A Maria Clotilde*



# Indice

<b>1</b>	<b>Introduction</b>	<b>1</b>
1.1	Global challenges . . . . .	1
1.2	European and Italian context . . . . .	3
1.3	Subject of the work . . . . .	4
<b>2</b>	<b>Solar energy exploitation</b>	<b>5</b>
2.1	Solar Energy . . . . .	5
2.1.1	The Sun . . . . .	5
2.1.2	Effect of the atmosphere . . . . .	5
2.1.3	Sun position . . . . .	7
2.1.4	Incidence angle . . . . .	9
2.2	PV . . . . .	10
2.2.1	Photovoltaic effect . . . . .	10
2.2.2	p-n junction . . . . .	10
2.2.3	Performances . . . . .	11
2.2.4	PV technologies . . . . .	13
2.3	Solar thermal . . . . .	14
2.3.1	General aspects . . . . .	14
2.3.2	Efficiency . . . . .	15
2.4	PVT . . . . .	18
2.4.1	General aspects . . . . .	18
2.4.2	Heat recovery . . . . .	19
2.5	Heat pumps and solar systems . . . . .	20
2.5.1	Heat pump . . . . .	20
2.5.2	Solar assisted heat pumps . . . . .	22
2.5.3	IEA SHC programme . . . . .	23
2.5.4	Direct-expansion SAHP . . . . .	23
2.5.5	Indirect expansion SAHP . . . . .	24

---

<b>3</b>	<b>Methodology</b>	<b>27</b>
3.1	Solar modules . . . . .	27
3.1.1	Thermal performance . . . . .	27
3.1.2	Electrical performance . . . . .	29
3.2	Heat pump . . . . .	30
3.2.1	Model selection . . . . .	30
3.2.2	Evaporator . . . . .	30
3.2.3	Compressor . . . . .	31
3.2.4	Condenser . . . . .	33
3.2.5	Design conditions . . . . .	35
3.2.6	Off-design . . . . .	35
3.3	Numerical solution . . . . .	38
3.4	Model recap . . . . .	39
3.5	Annual simulation . . . . .	40
3.5.1	Considered cases . . . . .	40
3.5.2	Performance maps . . . . .	41
3.5.3	Storage . . . . .	42
3.5.4	Thermal load . . . . .	42
3.5.5	Weather Data . . . . .	43
3.5.6	Control logic . . . . .	43
3.6	Economic Analysis . . . . .	44
3.6.1	Investment cost . . . . .	44
3.6.2	Net Cash Flow . . . . .	45
3.6.3	Investment evaluation . . . . .	47
<b>4</b>	<b>Experimental campaign</b>	<b>49</b>
4.1	System configuration . . . . .	49
4.1.1	Heat Pump . . . . .	49
4.1.2	Solar modules . . . . .	49
4.1.3	Measuring apparatus . . . . .	51
4.2	Experimental results . . . . .	52
4.2.1	SAHP . . . . .	52
4.2.2	PVT cooling effect . . . . .	58
4.3	Conclusions . . . . .	60
<b>5</b>	<b>Results</b>	<b>63</b>
5.1	Performance Maps . . . . .	63
5.2	Daily results - Winter . . . . .	64



---

5.3	Daily results - Mid-season . . . . .	67
5.4	Annual and monthly results . . . . .	69
5.4.1	Load supply . . . . .	69
5.4.2	Primary Energy . . . . .	74
5.5	Economic results . . . . .	78
5.6	System with PV and thermal modules. . . . .	81
<b>6</b>	<b>Conclusions</b>	<b>87</b>
<b>A</b>	<b>Technical specifications</b>	<b>91</b>
A.1	Compressors . . . . .	91
A.2	Solar modules . . . . .	92
	<b>Acronyms</b>	<b>101</b>



# Abstract

Solar-assisted heat pump(SAHP) is a promising system for domestic hot water production and buildings heating. In this work the results of a preliminary experimental campaign on a small-size heat pump prototype with PVT are presented and a numerical model of the system is developed. Tests showed the relations between performances and ambient operating parameters, and the beneficial effects of PVT use in this application; also limits and problems found out during tests are presented and discussed. In the work SAHP with PVT systems of various sizes are numerically modelled and investigated. The model shows that the systems can cover up to 50% of a reference domestic load, reducing by 60% the primary energy demand with costs analogous to conventional solutions. Results also demonstrate the advantages of SAHP systems with respect to air-source ones, because evaporation can occur at temperatures higher than ambient one. The use of PVT is justified by a comparison with an analogous system equipped with conventional thermal collectors and PV: fixed the overall collectors' area, the solution with PVT is more efficient and leads to a better economic sustainability.

**Keywords:** Solar-assisted heat pump, heat pump, PVT, model, domestic heating



# Sommario

Le pompe di calore elio-assistite sono una promettente soluzione per la produzione di acqua calda sanitaria e riscaldamento domestico. In questa tesi vengono presentati i risultati di una campagna sperimentale preliminare su un prototipo di piccola taglia con PVT e viene sviluppato un modello numerico del sistema. Le prove sperimentali evidenziano il legame tra prestazioni e parametri ambiente e gli effetti positivi dell'utilizzo dei PVT; vengono riscontrati problemi di funzionamento che portano le prestazioni al di sotto delle aspettative. Il modello numerico viene sviluppato per soluzioni di diversa taglia. Le soluzioni proposte permettono di coprire fino al 50% del carico termico dell'utenza di riferimento riducendo del 60% il fabbisogno di energia primaria, con costi analoghi a una soluzione convenzionale. L'utilizzo dell'energia solare all'evaporatore porta vantaggi rispetto alle macchine ad aria, poiché l'evaporazione può avvenire a temperature superiori a quella ambiente. La bontà dell'utilizzo dei moduli PVT viene dimostrata attraverso una comparazione con un sistema SAHP con collettori termici e PV convenzionali: a parità di superficie, l'utilizzo dei PVT rende il sistema sia più efficiente sia energeticamente sia economicamente.

**Keywords:** pompa di calore elio-assistita, pompa di calore, PVT, modello, riscaldamento.



# Chapter 1

## Introduction

### 1.1 Global challenges

From the beginning of the industrial revolution, the world faced great technological developments and started to use new energy resources based on fossil fuels, such as coal, oil and natural gas. The use of such resources provides also today reliable and efficient energy supply to the world: heating, power generation, transportation, etc. In figure 1.1 we can see that, according to the International Energy Agency [1], energy demand increased in the last decades. However, energy reserves of oil and natural gas does not seem to decrease [2], thanks to the discovery of new reserves with recent extraction technologies. The massive use of fossil fuel energy sources is creating serious environmental issues: according to the Intergovernmental Panel on Climate Change,  $CO_2$  concentration in atmosphere is constantly increasing, with possible dramatic consequences in terms of atmospheric temperature rise due to greenhouse effect. [3]

Renewable energy sources and efficient energy conversion systems become funda-

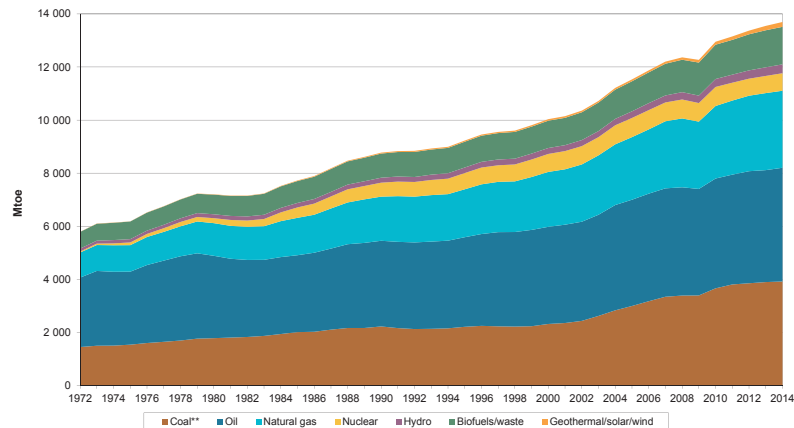


Figure 1.1: World Total Primary Energy Supply - IEA

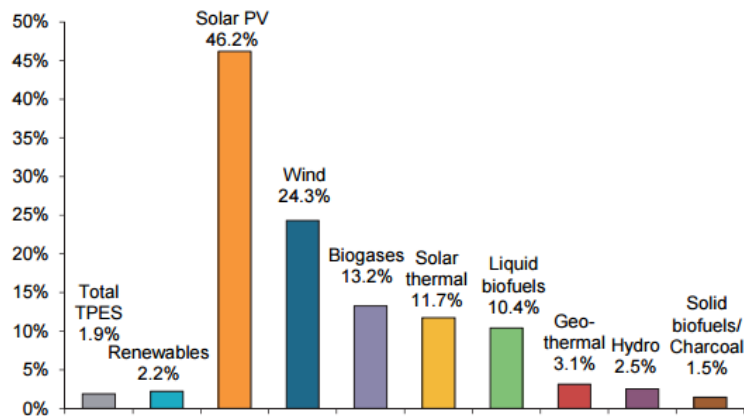


Figure 1.2: Annual growth rates of world renewables supply from 1990 to 2014. [4]

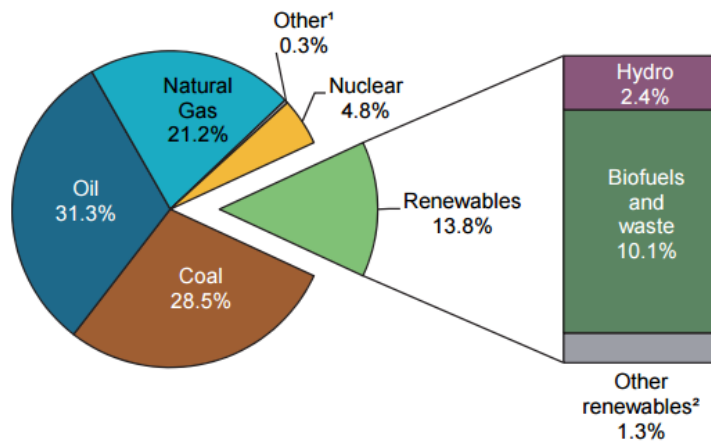


Figure 1.3: 2014 fuel shares in world total primary energy supply. [4]

mentals in order to supply energy in a sustainable way, with the lowest environmental impact possible.

Governments and policy makers pushed towards the use of such resources with incentives and simplified regulations. In figure 1.2 we can see that the result is a huge growth of renewable energy production, in particular for PV and Wind.

However, we can see in figure 1.3 that this growth is less relevant in absolute terms, since the share of renewable energy on the Total Primary Energy Supply is 13.8% (1894 Mtoe). Furthermore, this 13.8% is mainly due to solid biofuels and charcoal (Figure 1.4), widely used in developing countries for residential heating and cooking. Solar (and tide) energy has a share of 2.5% on the total of renewables, but with a huge growth rate. Italy is certainly part of this trend: PV installed capacity reached 12773 MW in 2011 from 431 of 2008, and in 2015 was 18892 MW. [5]

In the next decades, the extent of the growth rate of renewable energy share and the introduction of innovative technologies for their exploitation and integration will



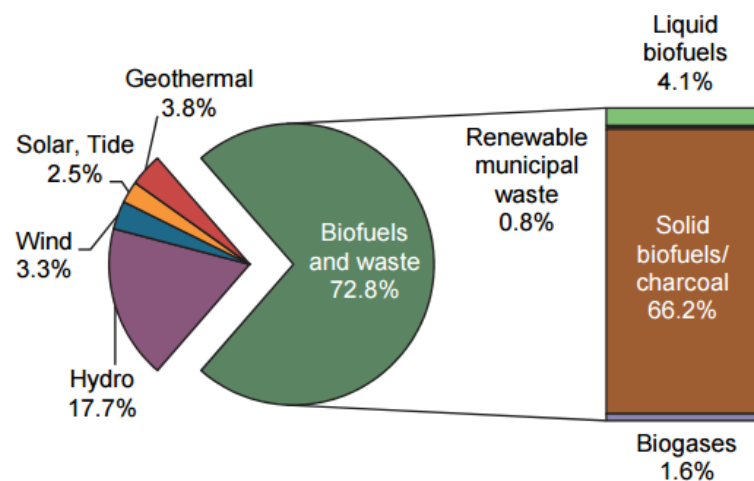


Figure 1.4: 2014 product shares in world renewable energy supply. [4]

be fundamental for the reduction of carbon dioxide emissions and for the achievement of the global goals stated by governments at international level.

## 1.2 European and Italian context

European Union in 2007 set three main binding targets in order to contrast climate change and energy dependence from other countries. The goals set in the directives are:

- 20% green house gases emissions reduction by 2020 with respect to 1990 levels.
- 20% reduction of primary energy use by 2020 with respect to the forecast consumption. In order to achieve this goal, the parameter to improve is *efficiency*.
- 20% share of renewable energy in EU 2020 total final consumption.

Such targets are shared among EU members with specific and binding targets according to Directive 2009/28/EC. [6] In 2005, Italy's renewable energy share was 5.2%, and in 2020 should reach 17%.

According to GSE[7], Italy reached its target in 2014 (17.1%): Figure 1.5 shows that actual values are much higher than the roadmap stated by the government. This result is referable both to the efforts made in the previous years in terms of subsidies and to the decrease of the total energy consumption due to the economic crisis.

In Figure 1.6 we can see the contribution of each technology to renewable energy exploitation. The main contribution is given by biofuels for thermal applications

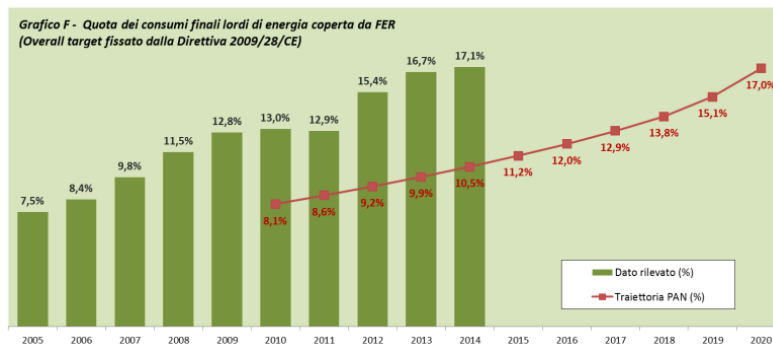


Figure 1.5: Renewable energy contribution to gross final energy consumption in Italy. [7]

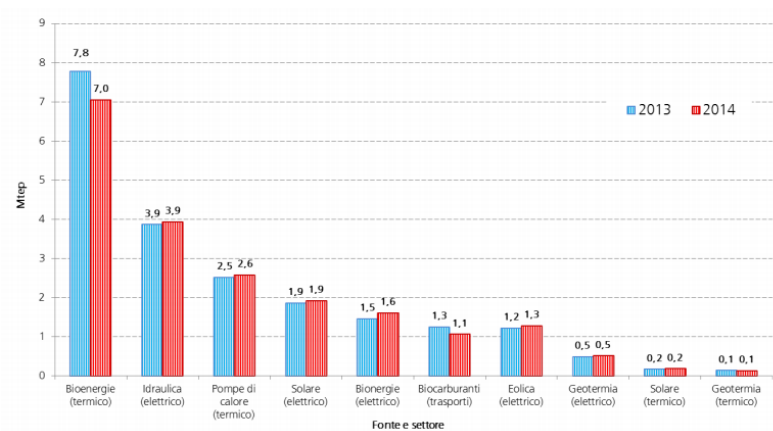


Figure 1.6: Renewable energy exploitation in Italy by source. [7]

and hydro power. But an important role is played also by heat pumps and PV, that grew significantly in the last five years.

### 1.3 Subject of the work: Solar Driven Heat Pump

In the context described in this chapter an interesting technology is represented by solar-assisted heat pumps. This solution is a combination of solar modules and a heat pump, that in this way can absorb heat from the sun.

Solar collectors can be either conventional thermal collectors or PVT ones.

In this work is described the development of a numerical model in MATLAB<sup>®</sup> code of a plant installed at SolarTech Lab, Energy department of Politecnico di Milano, and its preliminary experimental study.

# Chapter 2

## Solar energy exploitation: state of the art

The aim of the chapter is to give an overview of the main technologies treated in this work. The first section (2.1) gives a description of the Sun and the solar radiation. Then, the main technologies for its exploitation are discussed: photo-voltaic (2.2), solar thermal (2.3), photo-voltaic-thermal (2.4). In the last section (2.5) the solar-assisted heat pump technology is discussed, a combination of solar-thermal (or PVT) collectors and heat pumps.

### 2.1 Solar Energy

#### 2.1.1 The Sun

The Sun is composed mainly by hydrogen and helium, that are, respectively, 75% and 25% of its mass. Hydrogen undergoes to nuclear fusion reactions, producing  $3.845 \cdot 10^{20}$  MW of thermal power.

#### 2.1.2 Effect of the atmosphere

Earth's atmosphere is reached approximately by  $1.74 \cdot 10^{14}$  W of solar radiation, with an average irradiance equal to  $1367 \text{ W/m}^2$  [8]. This radiation, passing through the atmosphere, is subject to variations due to atmospheric scattering and absorption. [9]

- Scattering is produced by interaction between radiation and air molecules, water and dust, depending on wavelength  $\lambda$  and particles size.

At small wavelengths, scattering occurs according to Rayleigh theory; dust and water affect scattering at higher wavelengths, according to Moon.

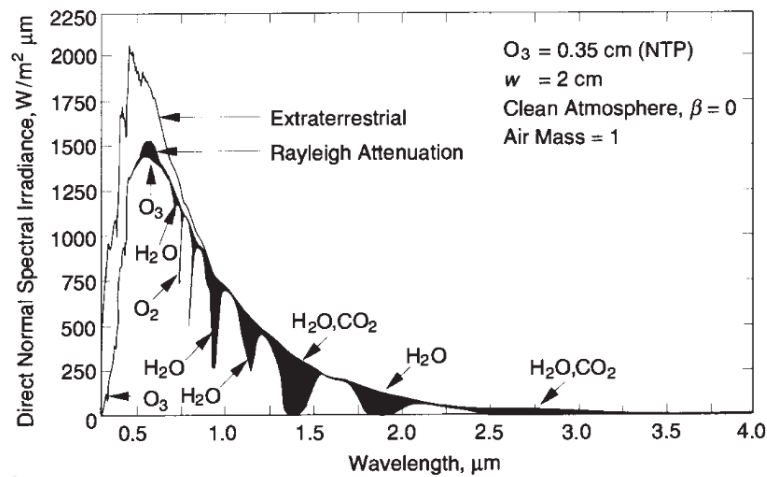


Figure 2.1: Effect of Rayleigh scattering and atmospheric absorption on spectral distribution of beam irradiance. [9]

- Absorption is due to ozone, water vapour and carbon dioxide. In Figure 2.1 we can see that each substance affects the spectrum at a specific wavelength.

The effect of scattering and absorption is shown in figure 2.1: the upper curve is the spectrum of the radiation outside the atmosphere, and the lower one is the spectrum at the sea level. The extraterrestrial spectrum can be assumed to be the spectrum of a black-body at 5777 K, according to Planck's law, with a peak in the visible region. Because of such effects, the radiation reaching Earth's surface is much lower than the extraterrestrial one, and the effect of the single species can be observed in the figure.

However, solar radiation on Earth's surface can be classified in two components:

- *beam* or *direct* irradiance, that comes directly from the sun;
- *diffuse* or *scattered* irradiance, coming from all the directions of the sky.

The proportion between the two components depends on many factors, such as the presence of clouds (i.e. water droplets) and air pollution (i.e. dust, particulate matter).

Depending on the relative position between Sun and a point on Earth's surface, the radiation covers different lengths in the atmosphere (fig. 2.2) with different attenuation and scattering effects. This fact is taken into account with the Air Mass parameter, representing the ratio between the distance covered and the thickness of the atmosphere:

$$AM = \frac{1}{\sin \gamma} \quad (2.1)$$

where  $\gamma$  is the solar altitude (i.e. the angle between the horizon and the sun).

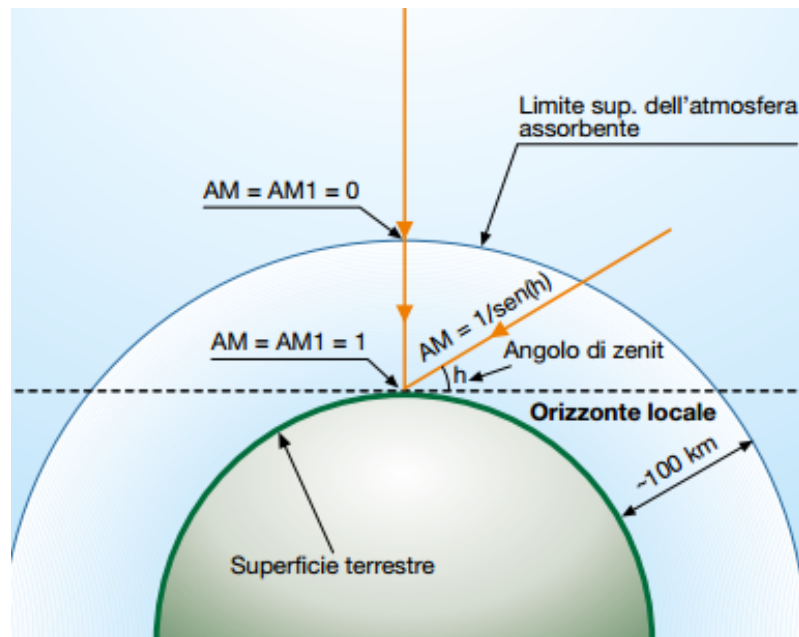


Figure 2.2: Air mass at different solar altitudes. [10]

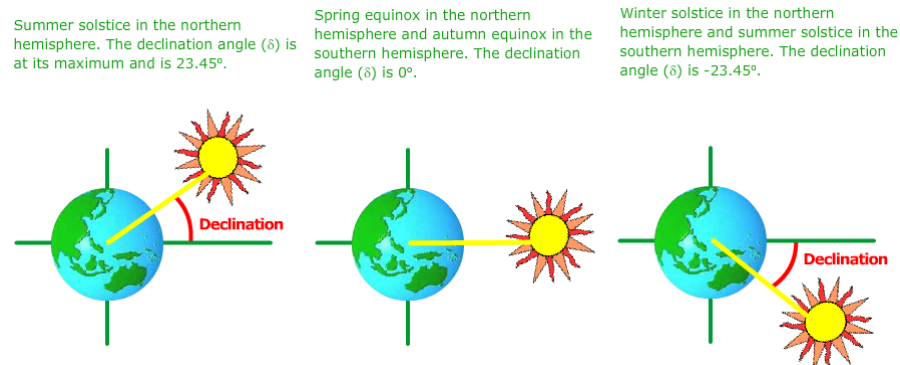


Figure 2.3: Declination change during the year. [11]

### 2.1.3 Sun position

The knowledge of sun's position is fundamental in order to calculate the radiation received by a surface on the earth's surface.

#### Declination

The first change of relative position that is taken into account is the variation of the declination. In figure 2.3 is shown that declination is the angle between Earth's rotation and the sun. The change of this angle is evident during the year: during summer days the path of the sun is higher in the sky than in winter ones.

Declination can be computed according to the following equation:

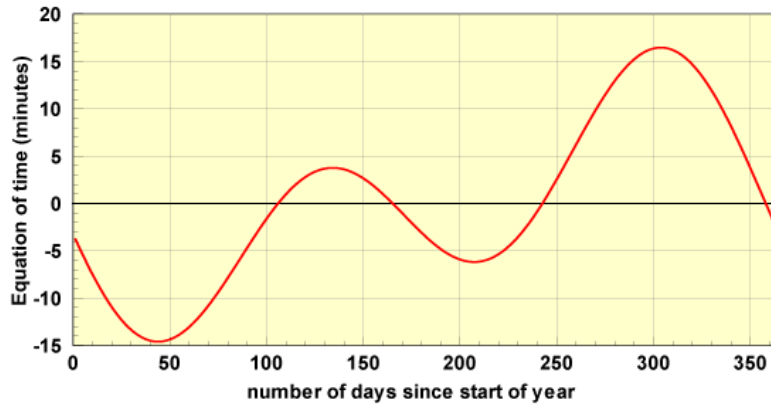


Figure 2.4: Equation of time. [11]

$$\delta = 23.45 \cdot \sin\left(\frac{360(d_n + 284)}{365}\right) \quad (2.2)$$

where  $d_n$  is the day of the year and  $\delta$  is expressed in degrees.

### Equation of time

The equation of time takes into account the change of the orbital velocity of the Earth. Such changes affect the time required by the Earth to accomplish a rotation on its axis with respect to the sun. The value of the equation of time (measured in minutes) is calculated as follows.[12]

$$B = 360 \frac{n - 1}{365} \quad (2.3)$$

$$E_n = 229.18 \cdot (0.000075 + 0.001868 \cos(B) - 0.03277 \sin(B) + \dots - 0.014615 \cos(2B) - 0.04080 \sin(2B)) \quad (2.4)$$

where  $n$  is the day of the year.

The equation is plotted in figure 2.4.

### Hour angle

The hour angle of a point on the earth's surface is defined as "*the angle through which the earth would turn to bring the meridian of the point directly under the sun*".[13]

It can be evaluated with the following equation.

$$\omega = (t_s - 12) \cdot 15 \quad (2.5)$$

where  $t_s$  is the solar time, measured in hours

$$t_s = t - \frac{\phi_{long} - \phi_{std}}{15} + \frac{E_n}{60} \quad (2.6)$$

and  $\phi_{long}$  and  $\phi_{std}$  are, respectively, local longitude and standard longitude, measured in degrees.

### Zenith and Azimuth angles

With the previous correlations it is possible to determine the relative position of the sun with respect to the earth in a defined time and place.

The position is determined with two angular coordinates:

- Zenith angle  $\theta_z$  : angle between sun rays and the vertical (i.e. the normal to the earth's surface);
- Azimuth angle  $\gamma_s$ : angle on the horizontal plane between the projection of the sun and the south.

Solar altitude is sometimes used instead of zenith, since it is defined as the complementary (i.e. the angle between sun rays and horizontal plane).

Zenith and Azimuth, in light of the previous considerations, can be computed as follows.

$$\cos(\theta_z) = \sin \delta \sin \phi + \cos \delta \cos \phi \cos \omega = \sin \gamma_s \quad (2.7)$$

$$\cos(\gamma_s) = \frac{\sin \gamma_s \sin \phi - \sin \delta}{\cos \gamma_s \cos \psi} \text{sign}(\psi) \quad (2.8)$$

#### 2.1.4 Incidence angle

Now it is possible to calculate the incidence angle  $\theta_s$ , defined as the angle between the normal to a generic surface with a tilt angle  $\beta$  and sun rays.

$$\begin{aligned} \cos \theta_s = & \sin \delta \sin \phi \cos \beta - \sin \delta \cos \phi \sin \beta \cos \gamma + \dots \\ & + \cos \delta \sin \phi \sin \beta \cos \gamma \cos \omega + \cos \delta \sin \gamma \sin \omega \sin \beta \end{aligned} \quad (2.9)$$

Therefore, direct and diffuse components of the irradiance can be computed as follows

$$G_{dir} = I_{DNI} \cos \theta_s \quad (2.10)$$

$$G_{diff} = I_{GHI} - I_{dir} \quad (2.11)$$

where  $G_{DNI}$  is the *Direct Normal irradiance*, that is the irradiance referred to a surface normal to the rays, and  $G_{GHI}$  is the *Global Horizontal Irradiance*, that is the overall irradiance received by a horizontal surface.

## 2.2 PV

### 2.2.1 Photovoltaic effect

An important technology for solar energy exploitation is the photovoltaic one, that converts the solar radiation into electric power.

Photovoltaic effect is a specific case of photoelectric effect, and can occur on particular materials, called semi-conductors, when they are hit by a photon. When this happens, if the energy of the photon is sufficiently high, an electron is released and can be collected with a particular diode circuit called p-n junction.

Photovoltaic effect can be well explained with the band gap theory. The band gap is an energy range where electrons are not stable. Therefore, they can exist either in the valence band (lower energy level) or in the conduction band (higher energy level). Depending on the energy gap, materials are classified as follows:

- $E_g < 5 \text{ eV}$ : insulators. The electron can not move from one band to the other.
- $0 < E_g < 5 \text{ eV}$ : semiconductors. If the electron has enough energy, it can move from valence to conduction band.
- $E_g < 0 \text{ eV}$ : conductors. Electrons are free to move and current can flow, because the two bands are overlapped.

The energy of the photon is calculated with the following equation

$$E_{ph} = h\nu \quad (2.12)$$

where  $h$  is Planck's constant and  $\nu$  is the wavelength.

Therefore only if the photon has a wavelength higher than a specific value depending on the material it will free an electron.

### 2.2.2 p-n junction

When an electron passes from valence to conduction band, a *hole* is created in the valence band. A hole can be assumed to be a positive charge due to the lack of the electron. The electron-hole couple tends to recombine spontaneously, releasing energy as heat or light. The PV cell inhibits recombination and takes advantage of



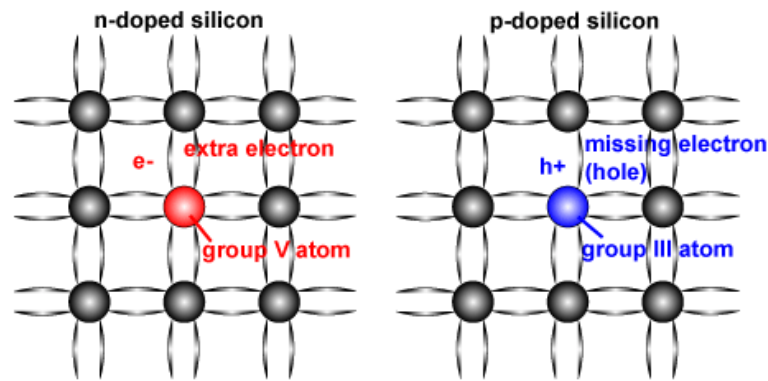


Figure 2.5: n-type and p-type silicon crystal lattice.[11]

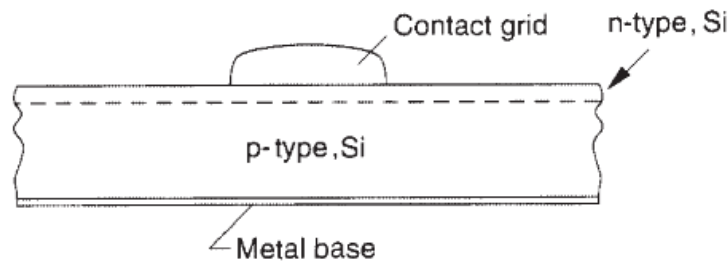


Figure 2.6: Cross section of a silicon solar cell.[9]

this phenomenon.

An obstacle to recombination is built in silicon cells with the p-n junction. Silicon semiconductor behaviour can be improved adding different atoms to the crystal lattice: this process is called *doping*. In figure 2.5 we can see that the addition of a group V atom produces the presence of an extra electron, while with the addition of a group III atom the effect is the presence of an extra hole. Once p-type and n-type silicon are put in contact, as shown in figure 2.6, the electrons can flow through the junction only in a single direction, and the junction works as a diode; therefore, if the two sides are externally connected with an electric circuit, the electrons will flow through it generating a current.

### 2.2.3 Performances

The efficiency of a solar cell is affected by several factors:

- Energy gap(1): all the photons with energy lower than the energy gap does not produce any useful effect.
- Energy gap(2): all the photons with energy higher than the energy gap dissipate as heat the extra energy that is not used in terms of photovoltaic effect.

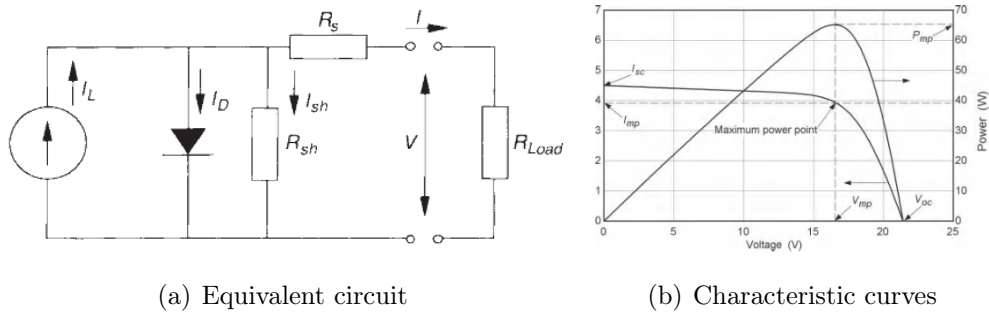


Figure 2.7: Model and I-V curve of a PV cell. [9]

- Optical losses(1): the glass cover is not perfectly transparent, and the cell itself has an absorptance lower than one, so part of the incident radiation is reflected or absorbed.
- Optical losses(2): the metal circuit on the top of the cell shadows the lower part.
- Recombination losses: holes and electrons can recombine before they are collected by the circuit.
- Joule losses: ohmic voltage drop due to electric resistivity of the materials.

Part of such losses can be modelled with the equivalent circuit of the PV cell, represented in figure 2.7 a); in the circuit we can note the presence of  $R_{sh}$  and  $R_s$  that represent, respectively, the effect of recombination and joule losses. The effect of such losses can be observed in figure 2.7 b), representing the I-V curve of a cell. Ideally, the curve should reach both the axes orthogonally: ohmic losses affect the slope of the curve in the high-voltage region, while recombination losses decrease the voltage in high-current region.

The shape of the curve (i.e. the losses) determines the *fill factor* of the cell, defined as follows:

$$FF = \frac{P_{mpp}}{V_{oc}I_{sc}} \quad (2.13)$$

where  $P_{mpp}$  is the power at the maximum power point,  $V_{oc}$  is the open circuit voltage and  $I_{sc}$  is the short circuit current.

The efficiency can be defined as the maximum power that the cell can produce with respect to the incident power.

$$\eta = \frac{P_{mpp}}{P_{in}} \quad (2.14)$$

Moreover, starting from the model of the electric circuit previously described, the operating curve I-V can be determined as well by means of the following equations.

[14]

$$I_{sc} = I_{sc,ref} \frac{G}{G_{ref}} (1 + \alpha(T_c - T_{c,ref})) \quad (2.15)$$

$$V_{oc} = V_{oc,ref} (1 + \beta(T_c - T_{c,ref})) + A \ln \frac{G}{G_{ref}} \quad (2.16)$$

where  $\alpha$  and  $\beta$  are parameters provided by the manufacturers.

Electric power can be computed as well with a similar correlation:

$$P_{el} = P_{el,ref} \frac{G}{G_{ref}} (1 + \gamma(T_c - T_{c,ref})) \quad (2.17)$$

The main issue is to determine sufficiently accurately the operating temperature of the cells. A commonly used procedure, adopted also in this work, is described in the following lines. [12]

In order to estimate cell temperature  $T_c$  it's possible to use the *Nominal Operating Cell Temperature* (NOCT). NOCT is provided by manufacturers, and it's determined testing the modules under the following conditions:

- Ambient temperature  $T_{amb,NOCT} = 20$  °C;
- Irradiance  $G_{NOCT} = 800$  W/m<sup>2</sup>;
- Wind speed 1 m/s;
- No heat convection on the back (the module is positioned on a surface).

Once NOCT is known, the following correlation is proposed in order to estimate  $T_c$ :

$$T_c = T_{amb} + \frac{NOCT - T_{amb,NOCT}}{G_{NOCT}} \cdot G \quad (2.18)$$

## 2.2.4 PV technologies

PV technologies can be classified as follows:

### Conventional cells

Mono-silicon and multi-silicon cells, that together cover the larger part of the market. Mono-silicon reach 25% efficiency in lab and is more expensive; poly-silicon reach 20% efficiency in lab and is less expensive.

### Thin-film

This technology differs from mono and poly-silicon ones for the thickness of the layer and the manufacturing process: the thickness is around 1  $\mu m$  (100 $\mu m$  for conventional

silicon cells) and is produced via vapour deposition, resulting in a reduction of the cost. However, thin-film technology generally suffers lower efficiencies, leading to higher structure costs for a fixed nominal power with respect to silicon modules. An advantage of thin-film cells is that can be manufactured on flexible supports.

Different thin-film technologies are present on the market:

- Amorphous silicon: lab efficiency can reach 12.5%, but decreases with time because the energy gap passes from 1.2eV to 1.8eV.
- Cadmium telluride (Cd-Te): lab efficiency can reach 18.7% and the manufacturing process is quite low-cost. The main issue is the toxicity of cadmium if released to the ambient.
- CIGS(Copper Indium Gallium Selenide): lab scale efficiency can reach 18%;
- GaAs: high-efficiency technology used also in space applications.

### Multi-junction

Multi-junction and multi-layer technologies consist in a combination of cells with different energy gap. If the light is split into components with different wavelength, and each component is sent to a cell with a suitable energy gap, conversion efficiency will increase.

In figure 2.8 we can see that this result can be obtained spatially splitting the radiation or stacking the cells.

### Dye-sensitized

This technology is still a research topic, but seems to be promising in terms of costs reduction with respect to conventional technologies.

## 2.3 Solar thermal

### 2.3.1 General aspects

Solar thermal plants are designed to transfer the incoming thermal power from the sun to a fluid. This heat can be used for domestic or industrial applications. The key component of such plants are the collectors, and many models and configurations are available on the market.

In figure 2.9 are represented the main models and the relative characteristics: unglazed absorbers are suitable for low-temperature applications; glazed flat-plate collectors for

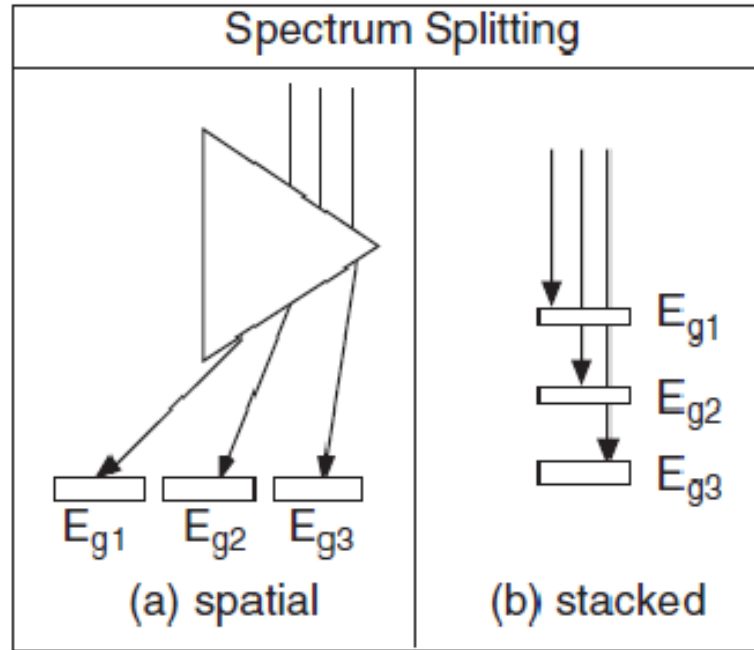


Figure 2.8: Multi-layer and multi-junction principle. [12]

medium-temperature applications and more complex collectors for high temperature ones. The application range, in fact, is strictly related to the thermal performance, that increases with the insulation, and so the cost, of the collector.

In this work the analysis is focused on flat-plate collectors, that is the technology adopted in the experimental part.

### 2.3.2 Efficiency

Flat-plate collectors are generally used for low or medium temperature applications, and they are characterized by a simple mechanical structure and the absence of optical concentration.

In Figure 2.10 we can see the cross section of a typical flat-plate collector. The incoming radiation passes through the protective layers and is captured by the absorber, that transfers the heat to the tube welded on its back.

The efficiency of the modules can be split in two terms:

$$\eta_{tot} = \eta_{opt}\eta_{th} \quad (2.19)$$

Each of the two components takes into account different losses.

Optical efficiency is defined as the part of heat that reaches the absorber with

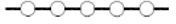
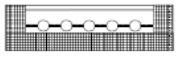
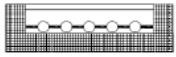
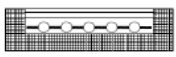


	principle	$\eta_0$ [ ]	U [W/m <sup>2</sup> K]	collector working temp.	appropriate application areas
simple absorber		0.90	20	15 – 30 °C	swimming pool
simple flat-plate collector with glass cover (FP)		0.80	4	30 – 80 °C	hot water
FP with selective surface (SS)		0.80	3	40 – 90 °C	hot water space heating
FP with double anti- reflective coated glazing and gas filling		0.80	2.5	50 – 100 °C	hot water space heating cooling
evacuated tube collector with SS (ETC)		0.65	2	90 – 130 °C	space heating cooling process heat
ETC with compound parabolic concentrator (CPC)		0.60	1	110 – 200 °C	space heating cooling process heat

Figure 2.9: Types of collectors and applications. [12]

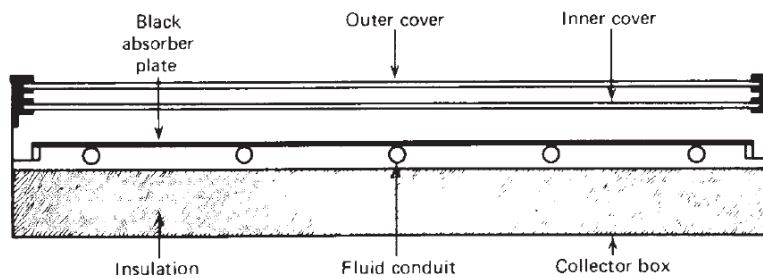


Figure 2.10: Cross section of a flat plate collector. [9]

respect to the overall incident radiation. Incident radiation can be computed as

$$\dot{Q}_{inc} = G \cdot A \quad (2.20)$$

and the radiation that reaches the absorber as

$$\dot{Q}_{abs} = \dot{Q}_{inc} \cdot (\rho\tau)_{cover} \cdot \alpha_{abs} \quad (2.21)$$

Where  $G$  is the irradiance,  $A$  is the area of the module,  $\rho$  the reflectance,  $\tau$  the transmittance and  $\alpha$  the absorptance.

$\rho$ ,  $\tau$  and  $\alpha$ , however, depend on the incidence angle  $\theta_s$ .

This behaviour is taken into account with the Incidence Angle Modifier (IAM), a function of  $\theta_s$ . Therefore, optical efficiency is calculated with the following equation.

$$\eta_{opt} = \eta_{opt,ref} \cdot IAM \quad (2.22)$$

where  $\eta_{opt,ref}$  is the optical efficiency at  $\theta_s = 0$ .

Thermal efficiency is defined as the ratio between the power absorbed by the receiver and the power available to the fluid. The first term is described in equation (2.21). The second can be computed as

$$\dot{Q}_{htf} = \dot{Q}_{abs} - \dot{Q}_{loss} \quad (2.23)$$

This heat transfer problem, modelled according to Oppenheim's method, is represented in figure 2.11, where  $S$  is the absorbed radiation per unit area. In a simplified approach, heat losses can be computed as the sum of a convective and a radiative component:

$$Q_{loss} = hA(T_{abs} - T_{amb}) + \sigma\varepsilon A(T_{abs}^4 - T_{amb}^4) \quad (2.24)$$

Therefore, the overall efficiency of the solar thermal module becomes

$$\eta = \frac{Q_{htf}}{Q_{inc}} = \frac{Q_{abs} - Q_{loss}}{Q_{inc}} = \eta_{opt} - \frac{Q_{loss}}{Q_{inc}} \quad (2.25)$$

If the module works at quite low temperatures, as usually happens for flat-plate ones, equation 2.24 can be linearized, so that the losses are function of the temperature difference and an overall heat exchange coefficient.

$$\eta = \eta_{opt} - \frac{UA(T_{abs} - T_{amb})}{GA} \quad (2.26)$$

Such coefficients are provided by manufacturers in the datasheets, with the addition

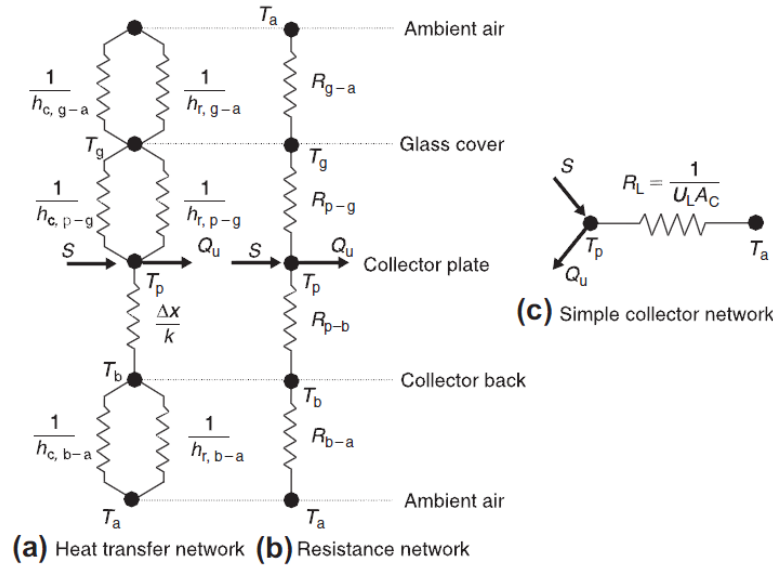


Figure 2.11: Thermal network for a single collector; case (c) represents a simplified approach. [13]

of a quadratic term if linearization is not accurate enough.

$$\eta = \eta_{opt} - k_1 \frac{\Delta T_{abs-amb}}{G} - k_2 \frac{\Delta T_{abs-amb}^2}{G} \quad (2.27)$$

This lumped parameters approach is adopted in this study, since it allows to predict sufficiently accurately the behaviour of the solar collectors without particular analytical and computational issues.

According to equation (2.27), thermal efficiency increases when  $G$  increases: thermal losses depend only on the operating temperature of the module, while the energy transferred to the fluid depends on  $G$ .

Moreover, we can see in figure 2.12 that each collector finds an optimal operating range application and, as said before, simple modules are suitable for low-temperature applications while complex ones for high-temperatures.

## 2.4 PVT

### 2.4.1 General aspects

Photovoltaic-thermal modules are a combination of PV and thermal technology. Conventional PV modules can convert only a small part of the incoming energy into electric power, so the remaining part is dissipated as heat. PVT collectors recover part of that heat, improving first-law efficiency of the module. Therefore, this technology has two useful outputs: electric and thermal power.



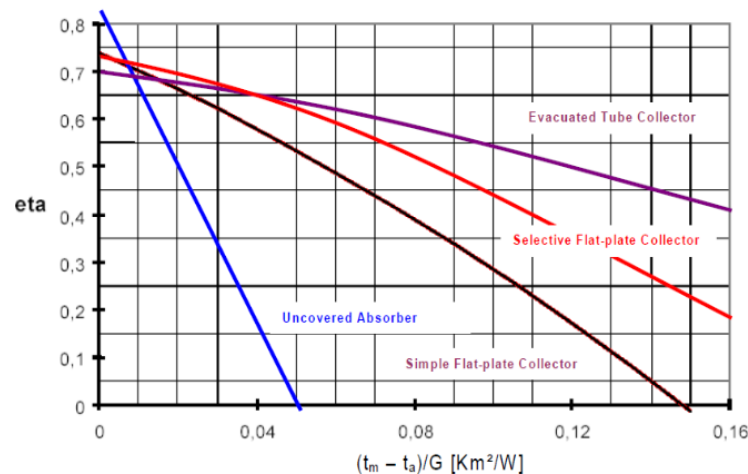


Figure 2.12: Plot of equation 2.27 for diverse collectors.

One of the main advantages of this technology is that the cooling effect of the fluid flowing in the collector can increase the electric efficiency of the cells (cfr. (2.17)). During summer this advantage could turn into a drawback, because the heat demand is generally low and the radiation high, resulting in high cell temperatures.

An important result of this technology is that, at the same conditions, the overall energy produced by two PVT modules is higher than the energy produced by a PV module and a thermal one.[15] In other words, PVT technology reach higher first-law efficiency.

An interesting application of PVT technology are solar assisted heat pumps: thanks to the low temperature of the fluid thermal losses are reduced, and the cooling effect of the refrigerant can improve significantly electrical efficiency. In fact, evaporation temperature generally ranges from  $+15^\circ\text{C}$  to  $-20^\circ\text{C}$ .

### 2.4.2 Heat recovery

PVT collectors can be distinguished in two main technologies, represented in figure 2.13:

- Sheet and tube;
- Roll-bond.

The first is by now a conventional technology, and consists in a metal sheet on the back of the solar module that collects thermal power transferring it to an adherent tube. On the market are available modules equipped with silicon cells and sheet and tube heat exchanger.

With roll bond technology there is no tube on the back of the module, and the

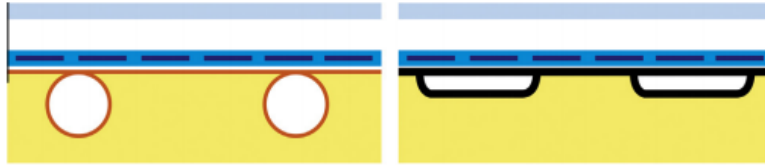


Figure 2.13: Sheet and tube (left) and roll bond (right) configurations of PVT modules. [16]

fluid passes through two metal sheets, pressed each other in order to leave a specific channel pattern. In this way the contact area can be higher, and the channel pattern can follow more complex designs. Also for this reason roll-bond collectors can reach thermal efficiencies higher than sheet and tube ones. [17]

## 2.5 Heat pumps and solar systems

Solar-driven heat pump and solar-assisted heat pump systems are a combination of heat pump and solar technologies. In such system the evaporator receives heat coming from a solar collector. The result is that the thermal power can be provided at a temperature higher than the ambient one, improving the COP.

### 2.5.1 Heat pump

The heat pump is a device that transfers heat from a lower temperature to a higher one through the interposition of a thermodynamic cycle between heat source and heat sink.

#### Thermodynamic cycle

In the plant scheme of figure 2.14 is shown that the working fluid undergoes 4 transformations:

- 1  $\rightarrow$  2 Compression
- 2  $\rightarrow$  3 Desuperheating and condensation
- 3  $\rightarrow$  4 Isoenthalpic throttling
- 4  $\rightarrow$  1 Evaporation

During compression process pressure and temperature of the fluid, in vapour phase, increase, and the fluid exits the compressor as superheated vapour. The heat is

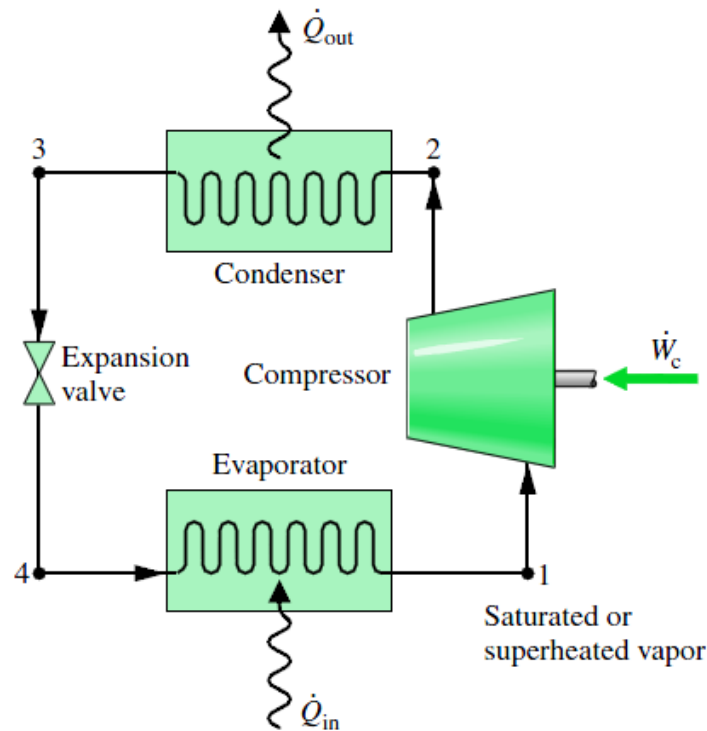


Figure 2.14: Heat pump scheme.[18]

released during condensation to the hot sink. After that, the fluid undergoes a throttling process, with a sudden decrease of pressure and temperature. Now the fluid can absorb heat from the heat source at low temperature during evaporation process and enter the compressor again.

In real machines, however, after evaporation process, a small superheating is required in order to avoid suction of liquid by the compressor, that should elaborate only vapour. Moreover, compression process is not isentropic and a small desuperheating occur after condensation.

### Performances

A heat pump, differently from household boilers or electric resistances, draws large part of the energy from the environment as heat at low temperature and a smaller one as electricity for the compressor.

Therefore, the efficiency is measured with the COP parameter, defined in eq 2.28 as the ratio between the useful effect (i.e.  $Q_h$ , the heat released by the condenser) and the energy expense (i.e.  $W_c$ , the power absorbed by the compressor).

$$COP = \frac{Q_c}{W_c} = \frac{W_c + Q_e}{W_c} = 1 + \frac{Q_e}{Q_c} \quad (2.28)$$

This parameter is higher than one, because the machine draws heat from the environment. COP value depends strongly on environment temperature and hot sink temperature: the higher is the temperature difference, the higher is the compression ratio and the power absorbed by the compressor. This fact makes the heat pump more suitable for low and medium temperature applications, such as domestic hot water production or low temperature space heating.

Heat pumps can draw heat from diverse sources: heat pump can be, for example, ground-source (or geothermal) or air-source heat pumps. Another possible option, still under development, is to use solar energy for the evaporation process. This technology, called solar-driven or solar-assisted heat pump, is investigated in this work and described in the following subsections.

### 2.5.2 Solar assisted heat pumps

In a solar assisted heat pump system, the evaporator receives heat coming from a solar collector. The result is that the thermal power can be provided at a temperature higher than the ambient one, improving the COP.

This system is called "solar-driven heat pump" (SDHP) or "solar-assisted heat pump" (SAHP).

The first effort to utilize solar thermal energy coupled with heat pumps is referable to Sporn and Ambrose in 1955 [19]. During the last decades many systems have been proposed and investigated, but we could classify them in two main groups:

- Direct expansion (DX-SAHP)
- Indirect expansion (IDX-SAHP)

In **direct expansion** solar-assisted heat pumps the evaporator is made by a solar collector. Therefore the working fluid of the heat pump cycle flows directly in the solar panel.

In **indirect expansion** solar assisted heat pumps the solar collector is not the evaporator, and the two components communicate with an heat exchanger. [20]

The main drawback of this technology is that, if not connected with auxiliary heat exchangers, such as an air evaporator, it can work only if there is solar radiation available. Dual-source heat pumps, thanks to the auxiliary evaporator, can draw heat from the ambient when solar radiation is not favourable;

Performances of SAHP systems depend also on the elasticity of the system, that is the possibility to adapt to different power inputs and heat demands. Chaturvedi et al. [21] stressed the importance of variable speed compressors in order to reach this goal.

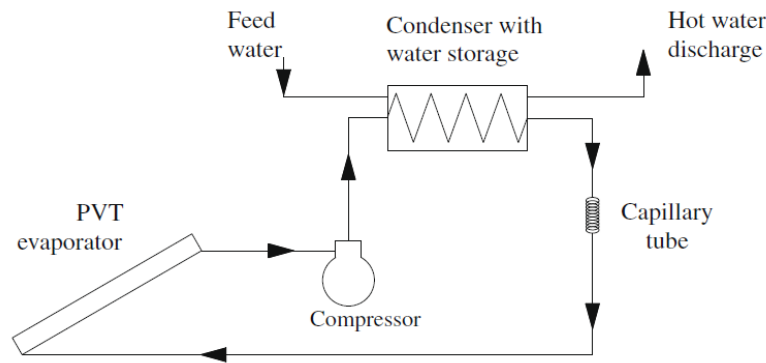


Figure 2.15: Schematic diagram of a DX-SAHP system.[25]

Kamel et al. [22] and Buker et al. [23] in their works presented an overview of the studies on this topic.

### 2.5.3 IEA Solar Heating and Cooling programme, Task44.

The Solar Heating and Cooling Programme was established in 1977 by the International Energy Agency. Its mission is to "advance international collaborative efforts for solar energy to reach the goal set in the vision of contributing 50% of the low temperature heating and cooling demand by 2030." Many researchers from all the world contributed to this programme with their work.

The technology studied in this thesis, solar-assisted heat pumps, have been investigated by the participants of Annex 38 and Task 44 of the IEA Heat Pump Programme and the Solar Heating and Cooling Implementing Agreements. The results of this programme are presented in the book by Hadorn, *Solar and Heat Pump Systems for Residential Buildings* [24].

### 2.5.4 Direct-expansion solar-assisted heat pump

In this configuration the solar collector acts as evaporator. As we can see in the schematic of the system in Figure 2.15, the working fluid flows directly in the solar module. The solar module can be a simple thermal collector or an integrated photovoltaic-thermal(PVT) module. With a PVT module both electric and thermal power are produced.

In heating applications water temperature should reach values at least equal to 40°C. This working condition decreases the thermal efficiency of the modules and the cooling effect of the PV cells (if present), with penalties in terms of electric efficiency. The use of PV evaporators can decrease operating cell temperatures and increase thermal efficiency. Moreover, refrigerant temperature is steady because the working

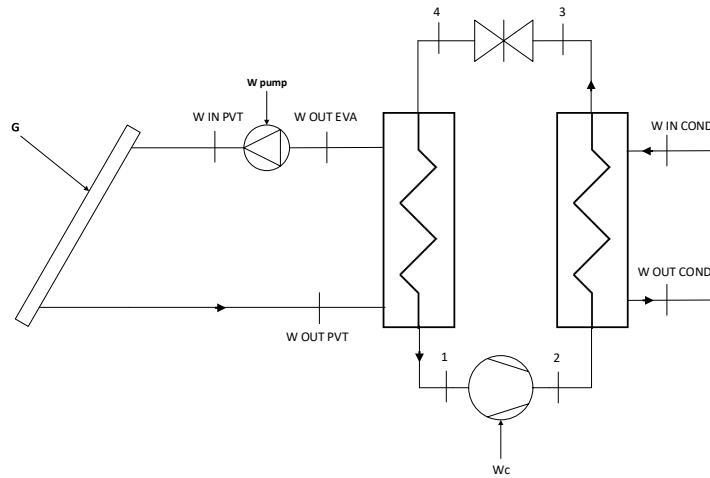


Figure 2.16: Schematic of indirect expansion solar-assisted heat pump.

fluid is changing phase, keeping constant the thermal efficiency.

### 2.5.5 Indirect expansion solar assisted heat pump

Indirect expansion solar assisted heat pumps differ from direct expansion ones for a fundamental arrangement: the solar collector is not the evaporator of the heat pump. Although they work together, they can be considered as two individual systems that interact by means of an heat exchanger, generally a flat-plate one.

A schematic of this configuration is proposed in figure 2.16.

With respect to DX-SAHP systems, indirect ones suffer a slightly higher temperature of the fluid flowing inside solar collectors (usually a water-glycol mixture), resulting in a lower thermal efficiency and lower power produced if the collector is a PVT panel; moreover, water-glycol mixture is not evaporating, and temperature is different in different points of the collector.

In IDX-SAHP, however, a thermal storage can be placed also on the solar collector side, in order to dump sudden solar radiation changes; moreover, since solar modules and heat pump are decoupled, it could be simpler to fix possible malfunctions.

Solar collectors and heat pumps can be coupled in different ways.

Kaygusuz et al. [26] investigated a IDX-SAHP system operated in diverse configurations, schematically represented in Figure 2.17. In Figure 2.18 we can see that dual and parallel modes reached the highest "free" energy contributions. Notice that the solar contribution in solar and parallel mode is the same, but parallel configuration can draw heat from ambient air when solar collectors do not provide enough heat (or heat at too low temperature). However, parallel configuration suffers a low average

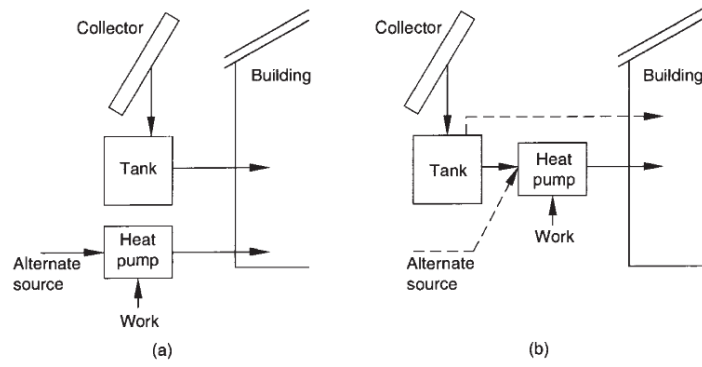


Figure 2.17: (a) Parallel; (b) Dual-source and series. [27]

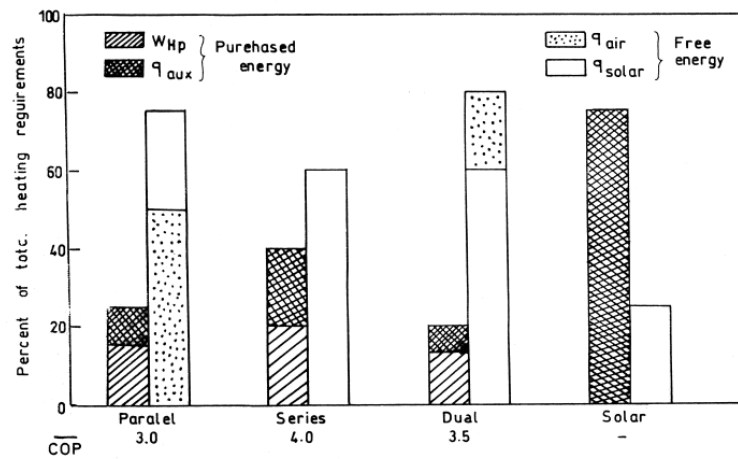


Figure 2.18: Heat contributions from all possible sources and COP for the considered operating modes.

seasonal COP with respect to series and dual configurations. Series mode operates with the highest COP, but the HP can work only when there is hot or warm water on the evaporator side, leading to higher purchased energy fraction.

We can conclude that the optimal configuration with respect to the considered geographical region seems to be the dual one: dual source heat pump system takes advantage of the best features of the series and parallel systems, working with an intermediate COP and the lowest purchased energy fraction. But the most important result is that solar and heat pump combination seem to have great potentiality in terms of energy saving and efficiency improvements.



# Chapter 3

## Methodology

In this chapter is described the numerical model of the plant represented in figure 3.1 developed in this work. The theoretical background of the governing equations of the model is explained in chapter 2.

### 3.1 Solar modules

#### 3.1.1 Thermal performance

According to the analysis performed in section 2.3, thermal performance is here modelled with equation (2.27). Both convective and radiative heat losses are taken into account linearising the behaviour of the system.

$$\eta_{panel} = \eta_{opt} - a_1 \cdot \frac{(T_{rec} - T_{amb})}{G} - a_2 \cdot \frac{(T_{rec} - T_{amb})^2}{G} \quad (2.27)$$

Where  $G$  is the *effective* radiation reaching the surface,  $T_{rec}$  is the average temperature of the receiver,  $\eta_{opt}$  is the optical efficiency and  $a_1$  and  $a_2$  are coefficients provided by manufacturers. A detailed database for solar thermal modules is available on SPF website. [28]

Optical efficiency is function of the incidence angle, and is calculated as follows:

$$\eta_{opt} = \eta_{opt}|_{\vartheta=0} \cdot IAM \quad (2.22)$$

Where  $\eta_{opt}|_{\vartheta=0}$  is the optical efficiency calculated with incidence angle equal to zero (i.e. sun rays normal to the surface), and  $IAM$  is the incidence angle modifier, a factor that takes into account the optical losses related to the incidence angle; in this work the Incidence Angle Modifier is calculated with the correlation proposed by De Soto et al. [29].

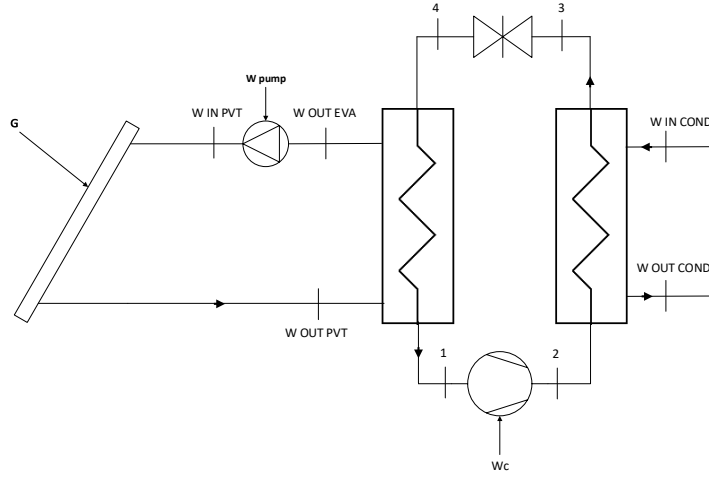


Figure 3.1: Schematic of the modelled system.

Notice that optical efficiency should also include the cosine effect, that is the reduction of "useful" receiving surface from sun point of view. This loss is taken into account upstream in the problem, since the effective radiation is considered. Practically, this value can be measured with a pyranometer positioned exactly with the same orientation and tilt angle of the module.

With the previous equations the thermal power absorbed by the solar panel is calculated as follows:

$$\dot{Q}_{panel} = GA\eta_{panel} \quad (3.1)$$

Where  $A$  is the aperture area of the modules.

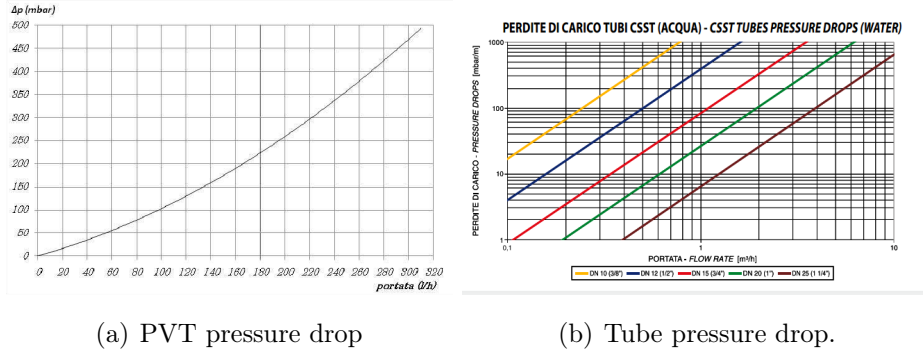
Water flowing inside the modules heats up, and the thermal power absorbed by water must be equal to the power transferred by the modules. This fact is considered in equation (3.2) with a simple energy balance:

$$\dot{Q}_{panel} = \dot{Q}_{w,panel} = \dot{m}_{w,panel} cp_w (T_{w,panel,out} - T_{w,panel,in}) \quad (3.2)$$

Where  $T_{w,panel,in}$  and  $T_{w,panel,out}$  are the temperatures of water entering and exiting the solar panel. Temperature difference for such applications is quite low, so  $cp_w$  is assumed to be constant.

Notice that in SAHP applications the fluid could reach temperatures lower than zero, therefore a water-glycol mixture could be required. In that case  $cp$  value should be updated with mixture's one; however, the equations presented in this chapter does not change their physical meaning.

Water flows into the hydraulic circuit thanks to a rotative pump, modelled as



(a) PVT pressure drop

(b) Tube pressure drop.

Figure 3.2: Pressure drops.

follows

$$\dot{W}_{pump} = \dot{m}_{w,panel} \frac{v \Delta p}{\eta_p} \quad (3.3)$$

Pump efficiency is assumed to be constant equal to 0.07, a typical value for small centrifugal pumps[30], and the pressure drop is calculated considering three components:

$$\Delta p = \Delta p_{hx} + \Delta p_{circuit} + \Delta p_{modules} \quad (3.4)$$

where  $\Delta p$  are calculated as follows:

- Heat exchanger: pressure drop, in kPa, is calculated with this correlation:  $\Delta p = 750 \cdot m_{w,eva}^2$ , where  $m_{w,eva}$  is expressed in kg/s.
- Modules pressure drops are computed with the curve reported in figure 3.2 (a).
- Pressure drops in the tubes are computed with the curve in figure 3.2 (b). The tubes have a DN15 diameter and an equivalent length of 7m.

However, a fraction of this power results in a pressure rise while the other part is dissipated as heat:

$$\dot{Q}_{diss,pump} = \dot{m}_{w,panel} \frac{v \Delta p}{\eta_p} (1 - \eta_p) \quad (3.5)$$

### 3.1.2 Electrical performance

The power produced by the PV panel is here modelled by means of equation (2.17) on p.13 as function of cell temperature  $T_c$  and incident solar radiation  $G$ ;

$$P_{el} = P_{el,ref} \frac{G}{G_{ref}} (1 + \gamma(T_c - T_{c,ref})) \quad (2.17)$$

While  $G$  is an operating parameter of the model (i.e. it is an input parameter),  $T_c$  depends on many parameters. For a conventional PV, it can be determined according

to equation (2.18).

$$T_c = T_{amb} + \frac{NOCT - T_{amb,NOCT}}{G_{NOCT}} \cdot G \quad (2.18)$$

In a PV-T module, however, water flowing on the back makes this method ineffective, since heat transfer from the fluid and the module takes place. In this work a simplified approach is adopted in order to estimate cell's temperature during SAHP operation, assuming

$$T_c = T_{m,htf} + 10 \quad (3.6)$$

Where  $T_{m,htf}$  is the average temperature of the heat transfer fluid flowing in the panel.

## 3.2 Heat pump

### 3.2.1 Model selection

The model of the heat pump can be built adopting many strategies. In the extensive work by Hadorn [24] on IEA Solar Heating and Cooling Programme, mentioned in section 2.5.3, a comparison between the main possible solutions is presented and discussed. In particular, physical models are not recommended for annual energy performance simulations, since they would require a too high computational time. One of the suggested solutions is the *black-box* model: the behaviour of some components is not represented physically, but in a simplified way: for instance, polynomial equations based on experimental data can be used in order to describe compressor's electric power. Such models are sufficiently accurate, and the required data are usually provided by the manufacturers.

This second approach is adopted in this work. In particular, the behaviour of the compressor (i.e. flow rate and electric power) is described by two polynomial equations as function of evaporating and condensing temperature.

### 3.2.2 Evaporator

The evaporator is a plate heat exchanger that transfers heat from water to the working fluid of the heat pump. This component is modelled by means of equation (3.7), that is the governing equation of heat exchangers.

$$\dot{Q}_{eva} = UA|_{eva} \vartheta_{lm} \quad (3.7)$$

Where:

$\dot{Q}_{eva}$  is the thermal power [W];

$UA_{eva}$  is the thermal transmittance [W/K];

$\vartheta_{lm}$  is the logarithmic mean temperature difference(LMTD) [K].

The calculation of  $UA_{eva}$  is developed in section 3.2.5, where design parameters calculation procedure is described.

In order to avoid the presence of liquid phase at the compressor inlet, a  $\Delta T_{sh}$  equal to  $10^\circ C$  is assumed.[31]

Therefore, the evaporator should be modelled as a two-zones heat exchanger. However, such a superheating is quite small in terms of thermal power, and the evaporation process can be assumed to occur at constant temperature.

In conclusion, the evaporator is here modelled as a one-zone heat exchanger.

Equation (3.7) is developed as follows:

$$\dot{Q}_{eva} = UA|_{eva} \frac{(T_{w,eva,in} - T_e) - (T_{w,eva,out} - T_e)}{\ln \frac{(T_{w,eva,in} - T_e)}{(T_{w,eva,out} - T_e)}} \quad (3.8)$$

The evaporator model is completed with the energy balance on both water and refrigerant sides.

$$\dot{Q}_{eva} = \dot{m}_{ref}(h_1 - h_4) \quad (3.9)$$

$$\dot{Q}_{eva} = \dot{m}_{w,eva} c_p (T_{w,eva,in} - T_{w,eva,out}) \quad (3.10)$$

Where:

$\dot{m}_{ref}$  is the mass flow rate of the refrigerant;  $h_4$  and  $h_1$  are the enthalpies at the points of the thermodynamic cycle according to Figure 3.3;

In particular,

$$h_1 = h(p_e, T_e + \Delta T_{sh}) \quad (3.11)$$

$$h_4 = h_3 \quad (3.12)$$

Equation (3.12) represents the behaviour of the valve: the refrigerant undergoes a pressure drop with no enthalpy change.

### 3.2.3 Compressor

The behaviour of the heat pump, in particular of the compressor, is not described with a physical model.  $\dot{m}_{ref}$  and  $\dot{W}_{comp}$  are calculated via polynomial equations as function of  $T_e$  and  $T_c$ . Such equations are provided by manufacturers in the form of equations (3.13) and (3.14). The performance curves of the compressor are plotted

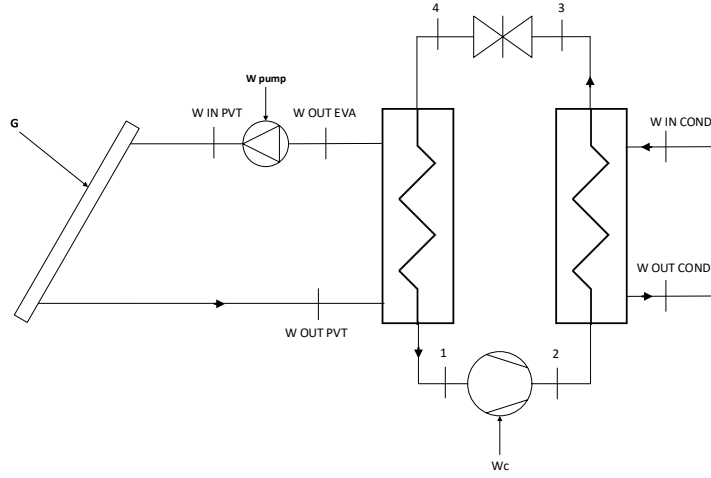


Figure 3.3: Schematic of the modelled system.

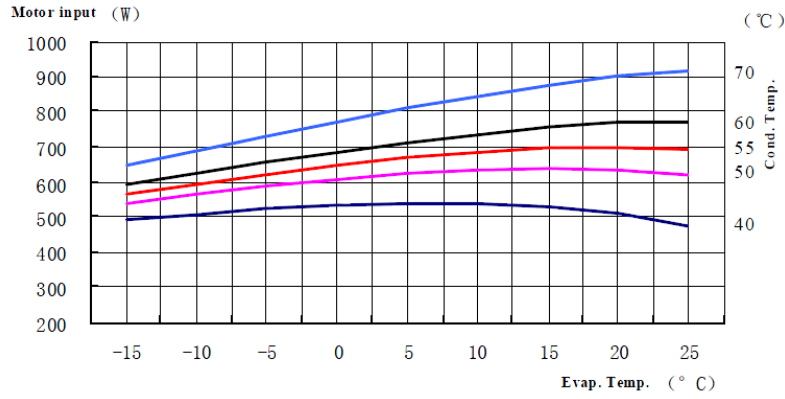


Figure 3.4: Motor input curves of the compressor.

in figure 3.4. The coefficients adopted in this work are in appendix A.

$$\begin{aligned} \dot{m}_{ref} = & a_0 + a_1 T_e + a_2 T_c + a_3 T_e^2 + a_4 T_e T_c + \dots \\ & + a_5 T_c^2 + a_6 T_e^3 + a_7 T_c T_e^2 + a_8 T_e T_c^2 + a_9 T_c^3 \end{aligned} \quad (3.13)$$

$$\begin{aligned} \dot{W}_{comp} = & b_0 + b_1 T_e + b_2 T_c + b_3 T_e^2 + b_4 T_e T_c + \dots \\ & + b_5 T_c^2 + b_6 T_e^3 + b_7 T_c T_e^2 + b_8 T_e T_c^2 + b_9 T_c^3 \end{aligned} \quad (3.14)$$

However, part of the electric power absorbed by the compressor is dissipated as heat to the environment. This heat is assumed to be 10% of  $\dot{W}_{comp}$ , and this

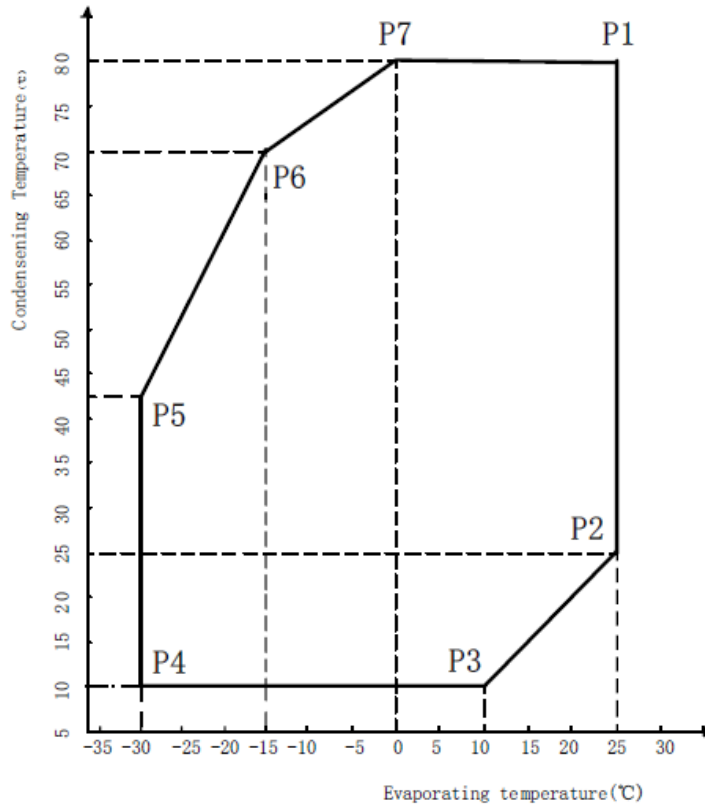


Figure 3.5: Operating field of the compressor.

assumption is taken into account by means of equation (3.15).

$$h_2 = h_1 + 0.9 \cdot \frac{\dot{W}_{comp}}{\dot{m}_{ref}} \quad (3.15)$$

The refrigerant at point 2 is superheated vapour and enters the condenser.

The compressor can work in a defined range of temperatures, defined by the envelope in figure 3.5. If the operating point of the compressor exits the envelope the machine stops.

### 3.2.4 Condenser

This component is a plate heat exchanger as well as the evaporator, so it is modelled in a similar way. In figure 3.6 we can see that the superheating of the refrigerant is much larger than in the previous case, and a two zone model must be implemented. In the first zone the refrigerant undergoes a de-superheating transformation, that ends when it reaches saturated vapour conditions; The second zone is the condensing one, and the fluid is assumed to reach point 3 in saturated liquid conditions.

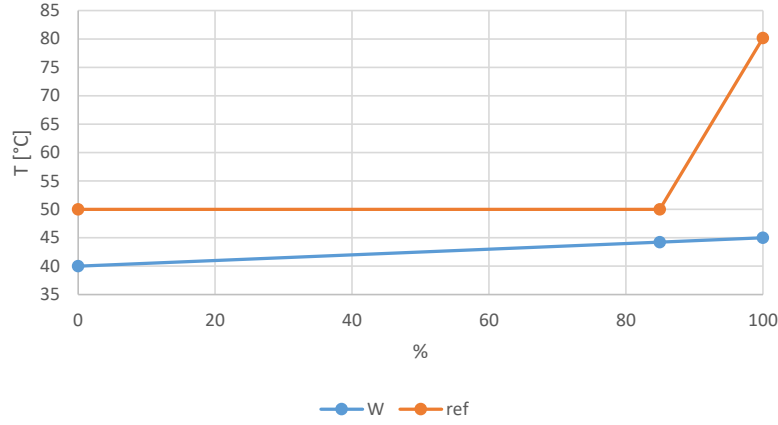


Figure 3.6: T-Q diagram of the condenser in nominal conditions.

$$h_{sv} = h(T_c, x = 1) \quad (3.16)$$

$$h_4 = h(T_c, x = 0) \quad (3.17)$$

Since the heat exchanger model is here built as a two-zones model, the sum of  $A_{desh}$  and  $A_{cond}$  (i.e. the total heat exchange area of the condenser) is constant, but its partition in the two zones can change. Moreover, heat transfer coefficients change with fluid and operating pressure, and this fact must be taken into account with suitable correlations.

This point is more extensively treated in section 3.2.5 and 3.2.6.

Condensing process is described with the same equations of the evaporator, developed as follows:

$$\dot{Q}_{desh} = UA|_{des} \frac{(T_2 - T_{w,cond,out}) - (T_c - T_{w,cond,int})}{\ln \frac{(T_2 - T_{w,cond,out})}{(T_c - T_{w,cond,int})}} \quad (3.18)$$

$$\dot{Q}_{cond} = UA|_{cond} \frac{(T_c - T_{w,cond,int}) - (T_c - T_{w,cond,in})}{\ln \frac{(T_c - T_{w,cond,int})}{(T_c - T_{w,cond,in})}} \quad (3.19)$$

Where:

$UA_{cond}$  and  $UA_{des}$  are the thermal transmittances [W/K].

$\dot{Q}_{desh}$  and  $\dot{Q}_{cond}$  are the thermal powers, respectively, of de-superheating and condensing zone;

$T_{w,cond,int}$  is the temperature reached by the water on the boundary between the two zones;

$T_{w,cond,in}$  and  $T_{w,cond,out}$  are the temperatures of the water entering and exiting the condenser;



$T_2$  is calculated as follows:

$$T_2 = T(p_c, h_2) \quad (3.20)$$

These thermal powers must be equal to the ones calculated with the energy balances:

$$\dot{Q}_{desh} = \dot{m}_{w,c} c p_w (T_{w,cond,out} - T_{w,cond,int}) = \dot{m}_{ref} (h_2 - h_{sv}) \quad (3.21)$$

$$\dot{Q}_{cond} = \dot{m}_{w,c} c p_w (T_{w,cond,int} - T_{w,cond,out}) = \dot{m}_{ref} (h_{sv} - h_3) \quad (3.22)$$

### 3.2.5 Design conditions

The calculation of the thermal transmittances  $UA$  is performed through the calculation of the performances with design specifications, reported in table 3.1.

$T_{eva}$	$T_{w,eva,in}$	$T_{w,eva,out}$	$T_{cond}$	$T_{w,cond,in}$	$T_{w,cond,out}$
-4	11	2,5	50	40	45

Table 3.1: Temperatures in design conditions.

With these data, the only unknowns of the equations of the model previously described are  $UA_{eva}$ ,  $UA_{cond}$  and  $UA_{desh}$ .

The results are the following:

- $UA_{eva,d} = 148.55$  [W/K];
- $UA_{cond,d} = 226.10$  [W/K];
- $UA_{desh,d} = 23.17$  [W/K];

### 3.2.6 Off-design

The boundary conditions of the problem (i.e. condenser inlet temperature, mass flow rate of water in the condenser, sun radiation and ambient temperature) during normal operation of the plant are different from the design ones. This imply changes in the behaviour of the machine.

In particular, heat transfer coefficients are affected by mass flow rate and pressure of the fluid in the heat exchangers.

## Evaporator

Evaporator is treated as a one-zone heat exchanger, so the area is always constant. Since  $UA_{eva,d}$  is known from section 3.2.5, it is possible to modify the whole term with a correction function. This approach, proposed by Pennati and Turrini [32], is used for the evaporator model.

A correction factor  $k$  is introduced in order to estimate the variation of heat exchange properties with respect to design conditions:

$$k = \frac{UA}{UA_d} \quad (3.23)$$

The calculation of the factor  $k$  is based on the following assumptions:

- Convective heat transfer coefficients  $\alpha$  are function of Reynolds number.

$$\alpha = C \cdot Re^n \quad (3.24)$$

Therefore,

$$\alpha \propto Re^n \propto \dot{m}^n \quad (3.25)$$

- Conductive heat transfer resistance is neglected.
- The heat exchanger is brazed-plate type: heat exchange area is the same for both water and refrigerant side.

$$\frac{A_w}{A_r} = 1 \quad (3.26)$$

- The ratio between convective heat transfer coefficient of water and refrigerant is equal to 1.

$$\frac{\alpha_w}{\alpha_r} = 1 \quad (3.27)$$

With such assumptions, the formulation of  $k$  is obtained:

$$k = \frac{2}{\left(\frac{\dot{m}}{\dot{m}_d}\right)_w^{-n_w} + \left(\frac{\dot{m}}{\dot{m}_d}\right)_r^{-n_r}} \quad (3.28)$$

Where both  $n_w$  and  $n_r$  are assumed to be equal to 0.5.

### Condenser

From section 3.2.5  $UA_{cond}$  and  $UA_{desh}$  are known. Now heat exchange correlations are introduced in order to estimate convective heat transfer coefficients in design and off-design conditions. After that, the global area of the heat exchanger will be calculated.

The approach used for the estimation of heat transfer coefficients is the same adopted by Barella [33].

- single-phase regions: Kim correlation [34];
- condensation region: modified Shah correlation [35].

The first of the two is proposed in equation 3.29.

$$Nu = 0.295 Re^{0.64} Pr^{0.32} \left(\frac{\pi}{2}\right)^{0.09} \quad (3.29)$$

Where  $Nu$  is the Nusselt number

$$Nu = \frac{\alpha D_h}{k} \quad (3.30)$$

$Re$  is the Reynolds number

$$Re = \frac{GD_h}{\mu} \quad (3.31)$$

and  $Pr$  is the Prandtl number

$$Pr = \frac{\mu c_p}{k} \quad (3.32)$$

In equation 3.31  $G$  is calculated as follows:

$$G = \frac{\dot{m}}{NBt} \quad (3.33)$$

where  $N$  is the number of channels,  $B$  the width of the base of the plates and  $t$  the thickness of the section of the channel.

$D_h$  is the hydraulic diameter, calculated as follows under the assumption of  $t \ll d$ :

$$D_h = \frac{4Bt}{2B + 2t} \approx 2t \quad (3.34)$$

The second correlation is shown in equation (3.35).

$$\alpha = c_1 Re_{SL}^{c_2} Pr_{SL}^{c_3} \frac{k_{SL}}{D_h} \left( (1-x)^{d_1} + \frac{3.8x^{d_2}(1-x)^{0.04}}{p^{*0.38}} \right) \quad (3.35)$$

Where the subscript "LS" means that the value must be evaluated in saturated liquid

conditions,  $k$  is the thermal conductivity,  $p^*$  is the dimensionless pressure, and the coefficients are  $c_1 = 0.2092$ ,  $c_2 = 0.78$ ,  $c_3 = 0.33$ ,  $d_1 = 0.80$ ,  $d_2 = 0.76$ .

The value of  $\alpha$  must be evaluated as the average on the steam quality.

Now it is possible to evaluate the overall heat transfer coefficients  $U_{des}$  and  $U_{cond}$ . Therefore, the heat exchange areas for both de-superheating and condensing zone in design conditions are calculated.

$$A_{des,h,d} = \frac{UA_{des,h,d}}{U_{des,h,d}} \quad (3.36)$$

$$A_{cond,d} = \frac{UA_{cond,d}}{U_{cond,d}} \quad (3.37)$$

$A_{des,h}$  and  $A_{cond}$  change during operation, but the sum of the two terms remains constant.

$$A_{cond,tot} = A_{des,h,d} + A_{cond,d} \quad (3.38)$$

### 3.3 Numerical solution

The model developed in previous sections requires a suitable numerical method in order to be solved, that has been implemented in MATLAB®.

The model is a system of non-linear equations, that can be solved with the native function *fsolve*.

First, input parameters must be specified:

- Ambient operating parameters:  $G$ ,  $T_{amb}$ , date, time; date and time are required in order to calculate the incidence angle  $\theta_s$ . Notice that  $G$  is the *effective* radiation reaching solar modules, as explained in subsection 3.1.1 on page 27.
- Thermal load specifications:  $T_{w,cond,out}$ ,  $T_{w,cond,in}$ ;
- evaporator/PVT mass flow rate:  $m_{w,eva}$ .

Then, a first guess is made on the five variables of the model:  $T_e$ ,  $T_c$ ,  $T_{w,eva,out}$ ,  $A_{cond}$ ,  $A_{des,h}$ . With these values, all the equations of the system can be solved.

The last step is performed by the function *fsolve*, and consists in iteratively changing the values of the five variables so that the equations of the model give coherent results; it means that the following five conditions must be respected:

$$m_{ref}(h_2 - h_3) = (UA\Delta T_{LM})_{des,h} + (UA\Delta T_{LM})_{cond} \quad (3.39)$$

$$m_{ref}(h(p_{cond}, x = 1) - h_3) = (UA\Delta T_{LM})_{cond} \quad (3.40)$$

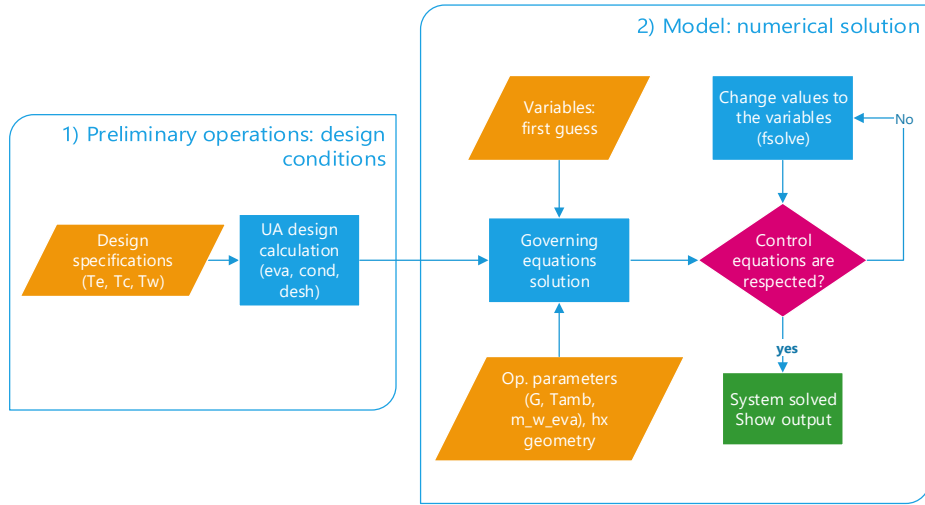


Figure 3.7: Block diagram: model solution procedure.

$$m_{ref}(h_1 - h_4) = (mc_p \Delta T)_{w,eva} \quad (3.41)$$

$$m_{ref}(h_1 - h_4) = (UA \Delta T_{LM})_{eva} \quad (3.42)$$

$$A_{tot,cond} = A_{desh} + A_{cond} \quad (3.43)$$

## 3.4 Model recap

In figure 3.7 is reported the block digram of the procedure explained in this chapter. As we can see, the procedure is split in two main steps:

1. The first step is the calculation of design conditions. In this situation,  $T_e$  and  $T_c$  are imposed, as well as water-glycol temperatures at the extremes of the two heat exchangers.

Therefore, thermal and electric power can be computed. Since temperatures and thermal power are now known, thermal transmittances (i.e.  $UA_{eva}$ ,  $UA_{desh}$  and  $UA_{cond}$ ) can be computed by means of equation (3.7), (3.18) and (3.19).

2. The second step is the numerical solution of the model. Given operating parameters and geometry of the heat exchangers, the result is a system of 5 equations and 5 variables (cfr. 3.3). The solution is obtained with the function *fsolve*, starting from a user-defined first guess.

## 3.5 Annual simulation

### 3.5.1 Considered cases

The yearly simulation have been carried out with diverse plant configurations, in order to get a wider range of solutions and comparisons.

#### Case A: 2.8kW HP + 3 PVT

The first case considered is the model of the heat pump experimentally investigated (c.f.r. chapter 4).

But since this system can produce a thermal power not higher than 3 kW it would be unsuitable to supply DHW and heating demand to the considered load. Therefore, it is important to consider also more powerful systems in the simulation.

#### Case B: 5.6kW HP + 4-6-8 PVT

Looking to the heat pump modelled before and the thermal load (cfr. 3.5.4), we see that the system could be not enough powerful. A possible solution is to choose a heat pump with higher rated capacity and consequently increase PVT aperture area. The solution adopted is to change the specifics of the validated heat pump in order to reach a greater size(cfr. Appendix A.). In particular, a compressor of double power is adopted and the new heat pump is modelled in three configurations, coupling it with 4(case B1). 6(case B2) and 8(case B3) PVT.

The heat exchangers are dimensioned with the same procedure of section 3.2.5.

#### Case C: 18kW HP + 9-12-15 PVT

In this case a heat pump with higher heating capacity is modelled. choosing the compressor with specifics reported in Appendix A and properly sizing the heat exchangers. In this case a scroll compressor is adopted instead of rotative one due to the higher size of the system. The procedure is the same adopted in the other cases. This heat pump is studied combining it with 9(case C1), 12(case C2) and 15(case C3) PVT modules.

The goal is to cover 50% of the demand in a typical winter day.

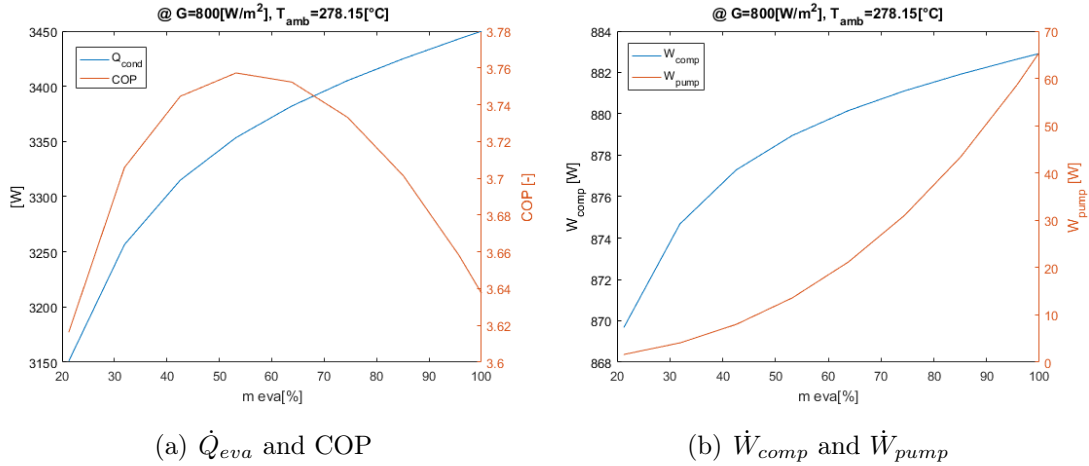


Figure 3.8: Variation of the main energy parameters of the model (B2) with respect to evaporator water-glycol mass flow rate.

### 3.5.2 Performance maps

#### Why performance maps

The numerical solution of the model for each time step of the year would require a too high computation time. Therefore, in order to speed up the simulation, the model is solved in a discrete mesh for representative values of the input variables  $G$ ,  $T_{amb}$  and  $\theta_s$  in order to obtain 3-d *performance maps*. In the simulation, then, the results will be obtained through the interpolation of the maps, saving computational time.

#### Operating modes

It is important to say that the system can be operated in two different modes. The mass flow rate of the secondary fluid in the evaporator (i.e. in the PV-Ts) can be optimized in order to maximize the efficiency or the thermal power at the condenser. In figure 3.8 we can see that a higher water-glycol mass flow rate results in higher thermal power at the condenser, but also in higher electric power absorbed by the circulating pump and the compressor. Moreover, pump electric power increases quadratically with upward concavity, creating an optimal operating point. Therefore, in order to maximize the COP, an iterative optimization is required; for the maximum power mode the mass flow rate is fixed at the highest value allowed. In particular, the limit is set by PVT modules, specified by the manufacturer at 2 l/min.

## Efficiency

The measure of the performance of the system should take into account both the useful outputs:  $\dot{W}_{el.pvt}$  and  $\dot{Q}_{cond}$ . But since the variations of the electric power produced by the PVT modules are quite low with respect to water-glycol mass flow rate changes, the conventional COP parameter can be adopted.

In figure 3.8 (a) we can see the variation of  $\dot{Q}_{cond}$  and COP with respect to  $\dot{m}_{w.eva}$ .

### 3.5.3 Storage

The storage is modelled as an ideal storage (i.e. no thermal losses) of infinite capacity. Such assumptions will result in an overestimation of the performance of the system, since the simulation does not take into account some technological limits of storage tanks and thermal losses.

However, in the simulation carried out the analysis is performed on a daily basis, making impossible to use the excess of energy in the following day. This assumption is detrimental with respect to the yearly performance factors.

Moreover, water temperatures at the condenser are fixed: in this work water is assumed to enter at 45°C and exit at 50°C. This operating condition could overestimate or underestimate the performance with respect to reality, since water temperature inside the condenser could be at lower or higher than the assumed one.

### 3.5.4 Thermal load

In this work the heat demand profile is modelled with the data represented in table 3.2, and the load is assumed to be constant along each month. Moreover, since the storage tank is modelled as an ideal storage and the thermal power is produced at a fixed temperature, the time profile along the day is neglected and the whole daily load is considered.

Heating season starts on October. Therefore the month is split in two parts: October1, that ends the 15<sup>th</sup> day of the month, and October2. The first half has the same heat demand of September, since heating systems are not turned on, and the second one has the same thermal load of November.

The same procedure is applied in April.

We can also see that when domestic heating is turned off the demand is very low, since the only request is domestic hot water.



Table 3.2: Annual thermal load.

Month	Load [kWh/d]
Jan	88.314
Feb	76.538
Mar	29.438
Apr1	29.438
Apr2	6.331
May	6.331
Jun	6.331
Jul	5.427
Aug	5.427
Sep	6.331
Oct1	6.331
Oct2	70.651
Nov	70.651
Dec	88.314

### 3.5.5 Weather Data

Weather data used in this simulation are the data collected by the weather station at SolarTech Lab (section 4.1.3) from September 2015 to September 2016.

### 3.5.6 Control logic

As mentioned before, the system can be operated in two modes. The choice of the operating mode and of the moments when eventually turn off the system is the key variable of the simulation. The control logic adopted in this work is represented in the schematic of figure 3.9. The aim is to satisfy the thermal load in the most efficient way possible. In other words, minimizing the electric power consumed.

The first choice is always to operate the system maximizing the  $COP$ , and keeping the SAHP on in the moments with better performances. But if the load is not covered, the consequent step is the attempt to cover the load operating in maximum power mode, with a penalty in terms of  $COP$ . The model switches to this mode starting from the time steps that suffer a lower efficiency penalty.

If the load is not satisfied even with the system operating always in this mode, the only solution is to use an auxiliary heat source: in this work the source is assumed to be a natural gas-fired condensing boiler with efficiency  $\eta_{th} = 95\%$ .

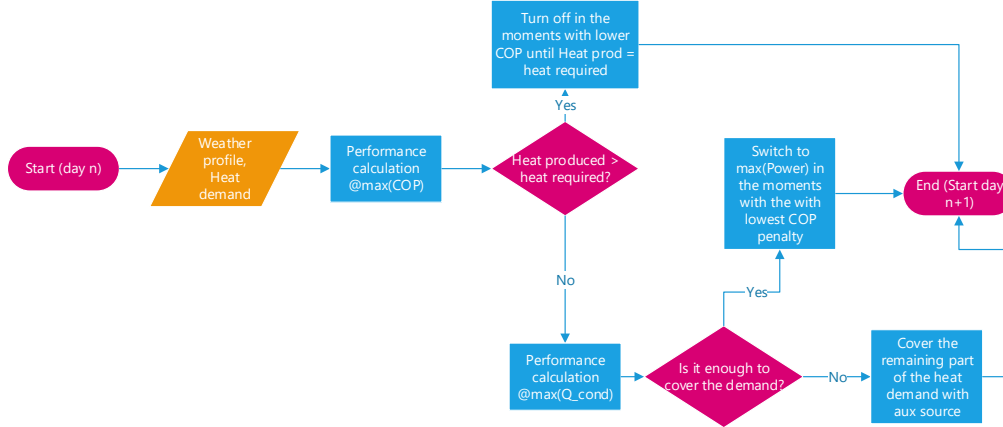


Figure 3.9: Block diagram of the control logic.

## 3.6 Economic Analysis

The analysis is performed for all the considered configurations. The main assumptions are reported in the following tables. Notice that lower-case term  $c$  is relative to a specific cost (€/kW), while upper-case  $C$  to a generic expense (€).

The present economic analysis compares all the previously described configurations with a reference case where all the thermal load is supplied with a natural gas-fired condensing boiler with efficiency  $\eta_{th} = 95\%$ . Therefore, the costs considered in this analysis are calculated as *cost differences* with respect to reference case.

### 3.6.1 Investment cost

In table 3.3 are reported the main costs relative to the initial investment. The cost of the heat pump and of the PVT are real data provided by manufacturers, while the others are assumptions based on average market prices.

Specific cost of PVT modules and inverter are equal to 1800 and 800 €/kW. Therefore the cost of solar modules and inverter are calculated as follows:

$$C_{pvt+inv} = (c_{pvt} + c_{inv}) \cdot Pnom \quad (3.44)$$

Where  $Pnom$  is the nominal power of the overall PVT system.

Heat pump cost is calculated by means of equation (3.45) assuming a scale factor  $n = 0.66$ .

$$C_{hp} = C_{hp,ref} \cdot \left( \frac{Q_{c,nom}}{Q_{c,nom,ref}} \right)^n \quad (3.45)$$

Where  $Q_{c,nom}$  and  $Q_{c,nom,ref}$  are the powers at the condenser in design conditions for

Table 3.3: Initial investment parameters assumed.

Cost	unit	value
$C_{hp,A}$	€	700
$C_{BOP,th}$	€	1500
$C_{BOP,el}$	€	1000
$c_{pvt}$	€/kW	1800
$c_{inverter}$	€/kW	800
$n$	-	0.66

the considered case and the reference case (i.e. case A).

In this way is taken into account the fact that cost increases less than proportionally to capacity.

The investment must take into account also the *balance of plant*, both for thermal and electric side. This parameter takes into account the cost of all the auxiliary components that must be installed in order to operate the system, such as wires, tubes, switches, valves and so on.

Such costs are assumed to be the same for all the cases and equal to 1500€ for the thermal part and 1000€ for the electric one.

Finally, the investment cost relative to the boiler is not considered, because there is no cost difference with the reference case. In chapter 5 on page 63 it has been shown that even in case C3 can occur days where the demand must be satisfied entirely with the auxiliary source: therefore, the boiler must have the same capacity of the reference case and the cost is the same.

The overall investment  $INV$  is calculated as the sum of all the previous components, and it is recorded in the first year of operations.

$$INV = C_{pv} + C_{inverter} + C_{hp} + C_{BOP,el} + C_{BOP,th} \quad (3.46)$$

### 3.6.2 Net Cash Flow

The installation of a solar-assisted heat pump generates energy (and cash) flows throughout the years. In particular, the heat pump absorbs electric power and produces thermal power at the condenser. Such thermal power generates savings, because less natural gas have to be purchased. Savings are considered as positive cash flows, while extra costs as negative ones. Finally, also the electric power produced by PVT modules is taken into account.

The determination of the annual energy balance have been performed in chapter 5.

In this analysis a cash flow is associated to every energy flow. The relation between energy and economic values is given by the *price*, calculated as follows.

For natural gas, the price given by the Italian Energy Authority on November 2016 is adopted.[36] With a price equal to  $0.72 \text{ €/Sm}^3$  and a  $LHV=0.0386 \text{ GJ/Sm}^3$  the value obtained is equal to

$$c_{ng} = \frac{price_{ng}}{LHV} = \frac{0.7223 \frac{\text{€}}{\text{Sm}^3}}{0.0386 \frac{\text{GJ}}{\text{Sm}^3}} = 18.71 \frac{\text{€}}{\text{GJ}} = 0.067 \frac{\text{€}}{\text{kWh}} \quad (3.47)$$

Analogously, electricity is assumed equal to  $c_{el} = 0.185 \text{ €/kWh}$  as follows referring to the same source. [37] Such prices are considered to change during the years according to an inflation rate  $i = 0.5\%$ .

Another cost that has to be taken into account is related to *operation&maintenance*. In this work is assumed to be  $150\text{€}$  for case A, and the 10% of this cost is scaled up proportionally to the nominal rated power of the heat pump for the other configurations.

Net cash flows are calculated considering the energy savings or the extra energy demand given by the system and the specific cost of energy; the net cash flow will be positive if the energy is exiting the system (i.e. excess of electric energy produced and natural gas saved) or negative if extra energy has to be purchased with respect to reference case.

Therefore, the annual cost of electricity will be

$$C_{el} = c_{el} \cdot (E_{el,pvt} - E_{el,HP}) \quad (3.48)$$

where  $E_{el,pvt}$  and  $E_{el,HP}$  are the annual energy produced by the solar modules and absorbed by the heat pump (compressor+pump).  $c_{el}$  and all the other annual specific costs change year by year because of inflation, according to the following equation:

$$c_{el}^k = c_{el}^{k-1} \cdot (1 + i) \quad (3.49)$$

where the superscript identifies the year and  $i$  the inflation rate.

Natural gas cost will be a positive cash flow, since only savings can occur thanks to the heat production by the solar-assisted heat pump.

$$C_{ng} = c_{ng} \cdot \frac{Q_{SAHP}}{\eta_{boiler}} \quad (3.50)$$

where  $Q_{DSHP}$  is the overall heat production of the system and  $c_{ng}$ , as said before, is

Table 3.4: Other economic assumptions.

Cost	unit	value
$c_{el}$	€/kWh	0.185
$c_{ng}$	€/kWh	0.067
$i$	-	0.5%
$c_c$	-	3%
$UL$	y	20
$FV$	€	0

evaluated like electricity cost:

$$c_{el}^k = c_{el}^{k-1} \cdot (1 + i) \quad (3.51)$$

Now it's possible to define the Net Cash Flow, distinguishing between the first year

$$NCF = INV + C_{el} + C_{ng} + C_{om} \quad (3.52)$$

and the following ones, when the investment cost is not present.

$$NCF = C_{el} + C_{ng} + C_{o\&m} \quad (3.53)$$

Notice that the value/disposal cost ( $FV$ ) of the system at the end of its useful life is assumed to be zero.

### 3.6.3 Investment evaluation

Thanks to the parameter defined in previous subsections it is now possible to evaluate the economic convenience of the system considering the cash flows throughout its the useful life.

The system is assumed to remain in service for a useful life  $UL$  equal to 20 years.

The last parameters that has to be considered is the cost of capital  $c_c$ , that in this work is assumed to be 3%.

A recap of the main assumptions of the analysis can be found in [table 3.3 on page 45](#) and [table 3.4](#).

The convenience of the investment is evaluated by means of two parameters: *Net Present Value* and *Internal Rate of Return*. The first, calculated with equation

(3.54), represents the actual value of a series of cash flows in a time span.

$$NPV = \sum_{k=0}^{UL-1} \frac{NCF_k}{(1 + c_c)^k} \quad (3.54)$$

From a theoretical point of view, the whole succession of cash flows in the useful life is equivalent to a single cash flow equal to NPV occurring now. Therefore, positive NPV means that the investment leads to a profit, while with a negative value would lead to a loss.

The IRR is defined as the value of  $c_c$  that makes the Net Present Value of an investment equal to zero.

$$IRR = c_c \mid \sum_{k=0}^{UL-1} \frac{NCF_k}{(1 + c_c)^k} = 0 \quad (3.55)$$

Practically it represents the rate at which the investment breaks even, or the return rate of the investment.

# Chapter 4

## Experimental campaign

In this chapter is described the experimental part of this work.

In section 4.1 a is described the whole experimental apparatus; then, section 4.2 shows the results of the experimental campaign and in section 4.3 are reported the conclusions.

### 4.1 System configuration

#### 4.1.1 Heat Pump

The first component of the plant is the heat pump. The model tested is a  $2.8 \text{ kW}_{th}$  water-water heat pump derived from a commercial air-water heat pump. Figure 4.2 shows the scheme of the commercial model provided by the manufacturer (a) and a photograph of the water-water prototype installed in the laboratory(b).

The first thing to note is that the air evaporator is replaced by a brazed-plate heat exchanger identical to the condenser. Accurate technical data are available in Appendix A.

#### 4.1.2 Solar modules

In the first part of the experimental campaign four mono-silicon with sheet-and-tube heat exchangers modules were installed. But after the diagnosis of malfunctions they have been replaced with poly-silicon modules with roll-bond heat exchangers. In figure 4.3 we can see the pictures of the panel in this second configuration. We can see that the back of the modules is covered with an insulating layer, and that each module is connected with its own inverter, in order to separately measure the electric performance of each module.

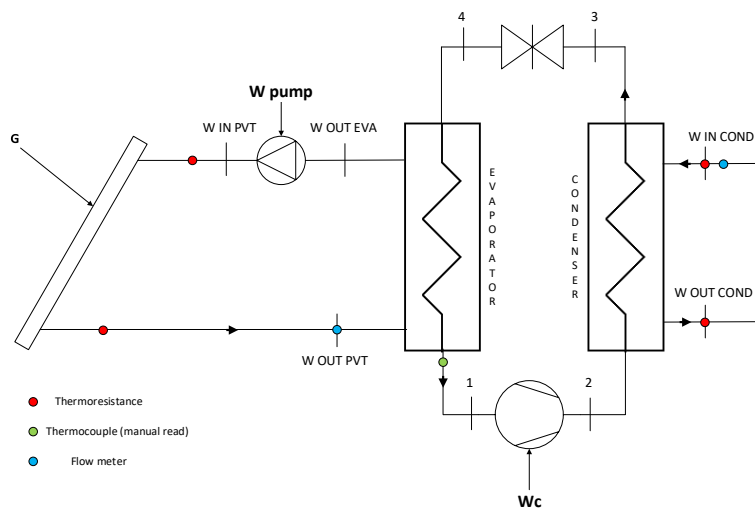


Figure 4.1: Plant scheme and instruments position.

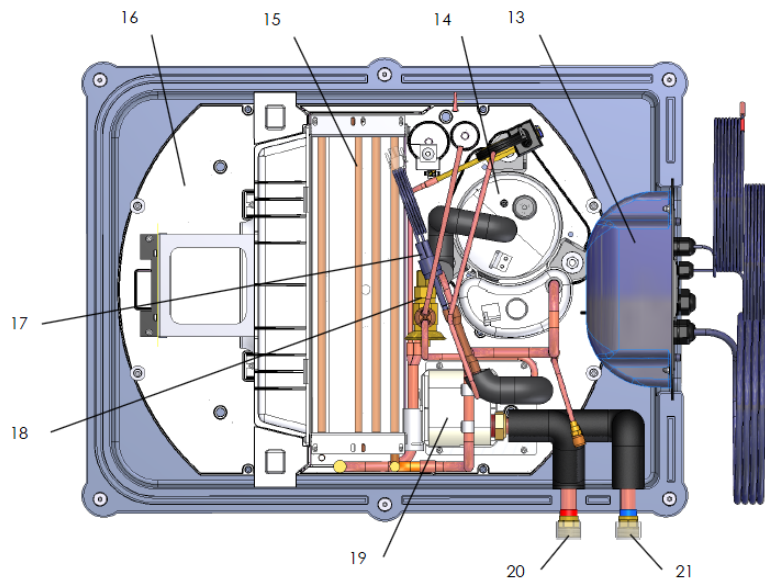
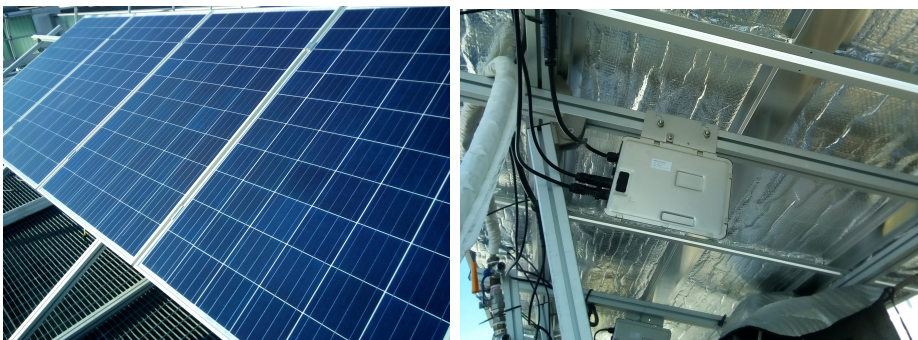


Figure 4.2: Scheme of the commercial air-source heat pump.



(a) Front

(b) Back

Figure 4.3: Poly-silicon roll-bond PVT at SolarTech Lab.



### 4.1.3 Measuring apparatus

The performances of the system are evaluated by means of temperature, power and volume flow rate measurements. The position of the instruments is represented in the schematic of figure 4.1.

Detailed data on the instruments are reported in table 4.1.

Table 4.1: Measuring instruments specifications.

Instrument	Range	U
Pyranometer (LSI, DPA252)	$<2000 \text{ W/m}^2$	$\pm 2\% \text{ RV}$
Thermoresistance Pt100	$[-30 \text{ } 70] \text{ } ^\circ\text{C}$	1/3 B (DIN EN 60751)
Thermoresistance Pt100	$[-50, 250] \text{ } ^\circ\text{C}$	1/10 B (DIN EN 60751)
Flow meter	$[0.9 \text{ } 15] \text{ l/min}$	$\pm 1\% \text{ FS}$
Wattmeter		$\pm 1\% \text{ FS}$
Inverter	$[0 \text{ } 300] \text{ W}$	$\pm 1\% \text{ RV}$

#### Temperature

In figure 4.1 we can see that the temperature is measured at the inlet and outlet of the condenser (water side) and of the solar panel. Together with flow rate measurements it is possible to compute the thermal power exchanged.

Temperature measurements are performed with thermoresistances Pt100 (1/10 B) inserted in the hydraulic circuit.(fig. 4.4 (a))

#### Flow Rate

Volume flow rate measurements are performed with a flow meter whose operating principle is based on Von Karman's vortices: the flow rate is related to the frequency of this phenomenon. (fig. 4.4 (b))

#### Electric power

Each PVT module is coupled with an inverter that communicates with a computer: in this way it's possible to measure the power produced by the single modules.

The power absorbed by the heat pump is measured with a watt-meter. However, in this measure is included the power absorbed by the pump of the evaporator circuit, since it is connected to the heat pump.



(a) Front

(b) Back

Figure 4.4: Pt 100 thermoresistances and flow meter.

### Weather station

On the lab is present a weather station that measures every two seconds ambient temperature (with a thermoresistance Pt100 1/3 B), relative humidity and solar radiation in the diffuse (pyranometer with shadow band) and direct (pyranometer) components. Also a measure of the global irradiance on a south-oriented, 30°tilted surface is performed with a pyranometer.

### Data acquisition

The instruments are connected with data acquisition boards that constantly communicate the data to a LabView program, that stores all the informations collected and controls some components of the system.

## 4.2 Experimental results

In this section are presented the results of the experimental campaign carried out from October to November 2016.

### 4.2.1 SAHP

The results show an abnormal behaviour both of the heat pump and the thermal collectors. In the following figures are showed the measures of a typical day in

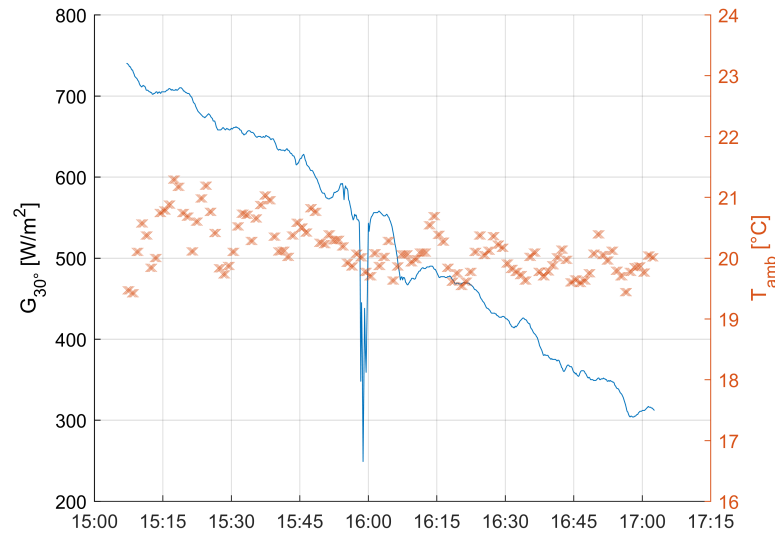


Figure 4.5: Weather data in the considered sample.

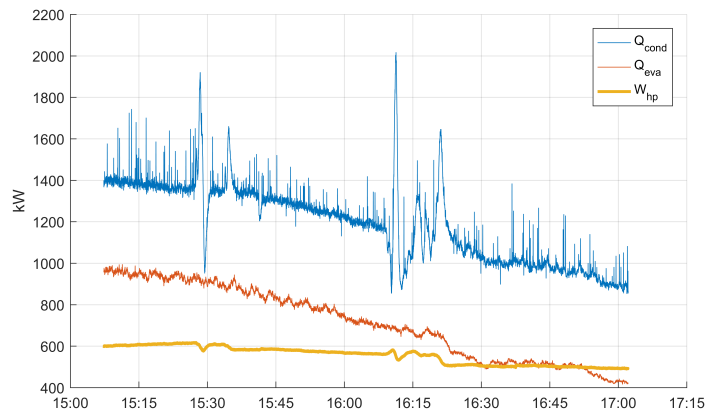


Figure 4.6: Thermal and electric powers data.

October. In the considered sample, with favourable weather conditions (cfr. figure 4.5), the system generated a very low thermal power compared to the expected values. In figure 4.6 we can see that even with an incident effective radiation of  $700 \text{ W/m}^2$  and an ambient temperature around  $20^\circ\text{C}$ , the heat pump exchanges less than 1 kW at the evaporator producing less than 1.5 kW at the condenser. Operating condition description is completed with figure 4.7, where the temperatures of secondary fluids are plotted. Looking to the heat pump alone, that receives water at the evaporator between 10 and  $15^\circ\text{C}$ , we should expect power values close to nominal ones or higher, also because at the condenser heat is produced below  $45^\circ\text{C}$ .

But also on the collectors side the data highlight a problem. Theoretically, thermal efficiency of the collectors should be close to or higher than the optical one

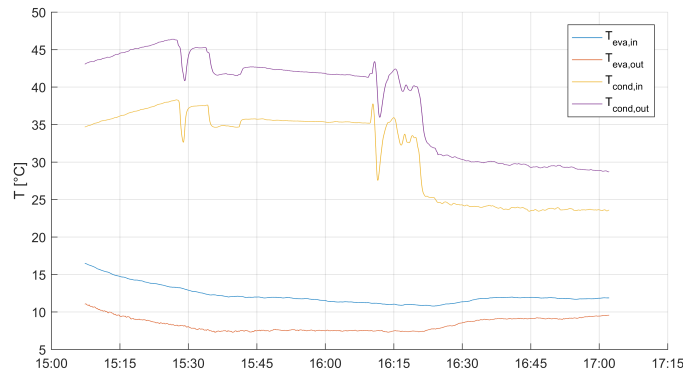


Figure 4.7: Temperature measures for the considered sample interval.

(58%), because water flowing inside them is at a temperature lower than  $T_{amb}$ . The aperture area of the collectors was equal to  $1.58 \cdot 4 = 6.32 \text{ m}^2$ , and considering an incident radiation of  $500 \text{ W/m}^2$  the power transferred to the fluid should be roughly equal to 1.8 kW, while the experimental data show that thermal power does not reach 1 kW even at higher solar radiations.

In figure 4.8 we can see one of the thermal images taken at SolarTech Lab during operations. The image shows that only a small part of the module is cooled by the heat transfer fluid flowing on the back, while in the remaining part an ineffective heat exchange occurs. The cause of this behaviour is ascribable to sheet's detachment on the back of the PV. Only the blue-coloured region is in contact with the sheet&tube heat exchanger, and can be cooled by the water flowing on the back.

However, in such condition a heat pump operating correctly would have absorbed a higher thermal power; water temperature, together with  $T_{eva}$ , would have decreased increasing the power absorbed by the modules reaching a new equilibrium or exiting the envelope of the compressor.

Looking to the COP, we can see in figure 4.9 that the system reaches quite low values considering solar radiation available and ambient temperature. Cop values of 2.5 are typical values reached by state of the art machines when ambient conditions are very unfavourable and evaporation temperature is close to the lower limit of compressor's operating field.

This low value is strictly related to the low thermal power input at the evaporator:  $W_c$  and  $W_p$ , being constant-speed machines, do not change significantly with respect to operating parameters, while  $Q_{eva}$  does. Therefore, such COP values are due to the malfunction observed on evaporator and solar collectors.

A wider picture of the situation is obtained looking also to the working fluid temperature. The heat pump is equipped with a thermocouple that measures the

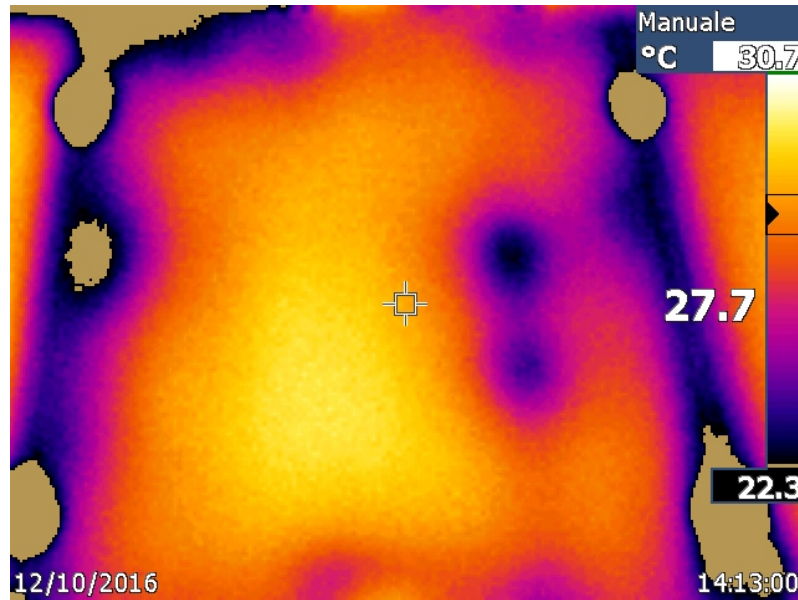


Figure 4.8: PVT thermal image.

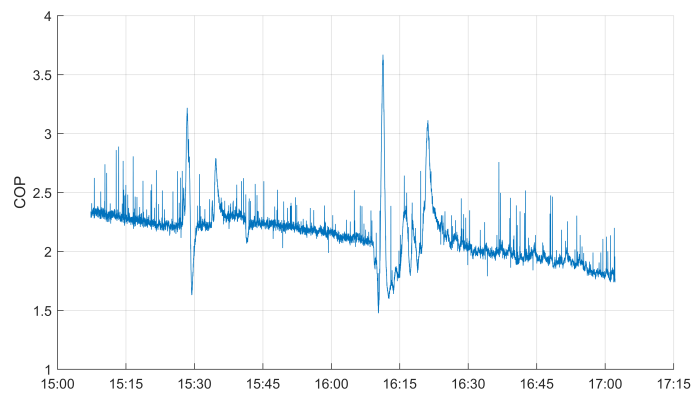


Figure 4.9: COP calculated in the considered sample interval.

temperature at the outlet of the evaporator. This measure can be read only manually on the display of the heat pump, and for this reason only few data are available, but it's enough to understand the problem. In table 4.2 we can see the data collected on November, 16<sup>th</sup> with volume flow rate and temperature relative to secondary fluid; in the last column the temperature of the refrigerant exiting the evaporator is reported. Such measures are performed after the substitution of the broken collectors with new ones.

As we can see, temperature difference at evaporator's outlet between refrigerant and water-glycol mixture is higher than 15°C, a value much higher than expected. Moreover, considering that the refrigerant is superheated vapour,  $T_{eva}$  is even lower than the measured value. This superheating could be even higher than in normal conditions, because after the high pressure drop across the valve the fluid could be almost evaporated, and the superheating increases. A high superheating could be compatible with such higher  $\Delta T$  because if the refrigerant is in vapour phase its convective heat exchange coefficient decreases, increasing temperature difference and lowering the thermal power exchanged.

The possibility of problems in the heat exchanger have been excluded, since an accurate wash of the water-side have been carried out.

Data collected on November, 30<sup>th</sup> with a different system configuration showed some improvement with respect to the previous one.

In figure 4.10 we can see that test day is characterized by clear sky and ambient temperatures between 0 and 8 °C. In figures 4.11, 4.12 and 4.13 are plotted powers, temperatures and COP data.

Looking to temperature's figure, we can see how evaporator's temperatures follow the shape of solar radiation curve, with a peak during central hours of the day. Notice that with respect to November, 16<sup>th</sup>, temperature difference at evaporator's outlet slightly decreased. Now the measured  $\Delta T$  value is close to 10 °C, while before ranged between 22 and 15 °C. Although this is an effective improvement in the system, the heat exchanger still operates with too high temperature differences. In fact, the measured refrigerant's temperature value is at evaporator's outlet: the effective  $T_e$  should be 10 °C lower leading to much higher  $\Delta T_{LM}$ . Such values are still far from operating conditions of conventional machines, that in design conditions (evaporator water temperatures are close to nominal ones) should present lower values.

Powers and COP also show an improvement with respect to the first measures performed.  $\dot{Q}_e$  decreases together with  $G$ . Compressor electric power absorbed increases with time, coherently with the decrease of  $T_e$  and the increase of water temperature at the condenser, that reached 45°C at the end of the test. COP, that at 11:30 was equal to 3, decreased with time because of compressor's power input

Table 4.2: 16/11/2016 experimental data with refrigerant temperature at evaporator outlet.

Time	$T_{in,c}$ [°C]	$T_{out,c}$ [°C]	$\dot{V}_{w,c}$ [l/min]	$T_{in,e}$ [°C]	$T_{out,e}$ [°C]	$\dot{V}_{w,e}$ [l/min]	$\dot{W}_{hp}$ [W]	$T_{ref}$ [°C]
12:26:00	20,42	25,36	4,81	17,07	14,44	8,12	550,26	-6,10
12:27:00	20,64	25,62	4,84	16,75	14,04	8,13	552,77	-6,10
12:28:00	20,83	25,71	4,81	16,49	13,92	8,06	555,23	-6,70
12:29:00	21,00	25,81	4,79	16,26	13,68	8,10	557,69	-6,70
12:30:00	21,33	26,14	4,87	16,05	13,43	8,15	560,10	-6,60
14:08:00	32,64	36,62	4,82	5,67	3,81	8,27	596,94	-12,10
14:15:00	32,66	36,68	4,74	5,09	3,21	8,37	592,47	-12,60
14:15:34	32,71	36,69	4,81	5,03	3,18	8,33	590,08	-12,60
14:39:28	32,47	37,37	4,84	7,55	5,61	8,29	607,05	-
14:45:00	32,80	37,01	4,86	5,73	3,91	8,36	589,21	-9,50
14:50:00	33,11	37,07	4,86	4,51	2,76	8,41	583,26	-11,10
14:55:00	33,43	37,20	4,81	3,61	1,91	8,31	579,53	-12,10
15:00:00	33,53	37,24	4,86	3,01	1,30	8,33	575,81	-12,80
15:05:00	33,64	37,28	4,84	2,51	0,84	8,28	572,76	-13,20
15:10:00	33,54	37,02	4,88	2,21	0,55	8,29	567,31	-13,70
15:15:00	33,70	37,19	4,83	2,01	0,36	8,23	563,51	-13,80
15:20:00	33,38	36,85	4,82	1,84	0,31	8,17	564,95	-13,80
15:25:00	33,61	36,94	4,79	1,68	0,16	8,21	566,64	-14,10
15:30:00	33,59	36,98	4,82	1,46	-0,01	8,25	568,63	-14,30

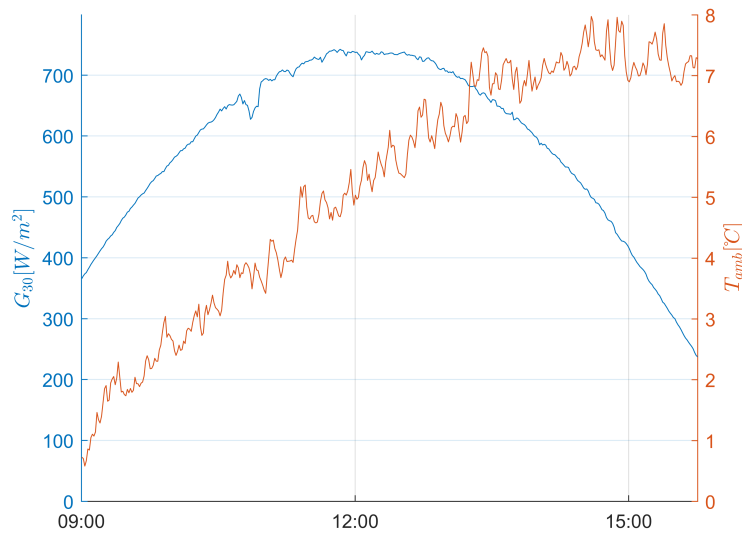


Figure 4.10: Weather profile, November, 30<sup>th</sup> 2016.

increase.

Such results are not satisfactory, although they represent an improvement with respect to the previous situation.

After such theoretical considerations, we can conclude that the unexpectedly poor performance of the heat pump can be due to its prototype nature; the substitution of the air evaporator with a brazed-plate heat exchanger and maybe an inaccurate re-calibration of the internal control system of the machine could be the main causes of such operating condition.

Further investigations could be done by opening the covering of the heat pump, checking components' condition.

### 4.2.2 PVT cooling effect

In this section the cooling effect of PVT collectors coupled with the heat pump is discussed.

PVT collectors, in fact, during heat pump operation, undergo to heat transfer with the fluid flowing on their back. The fluid (i.e. water-glycol mixture in the experimental set-up), is generally at low temperatures, because it comes from HP evaporator. The result is a cooling effect and a cell temperature decrease, that can lead to a higher electric power production.

This effect is highlighted by data collected on November, 30<sup>th</sup> with respect to the three mono-silicon, roll-bond PVT modules and two mono-silicon conventional PV modules with nominal power equal to, respectively, 245 and 285 W. (technical data



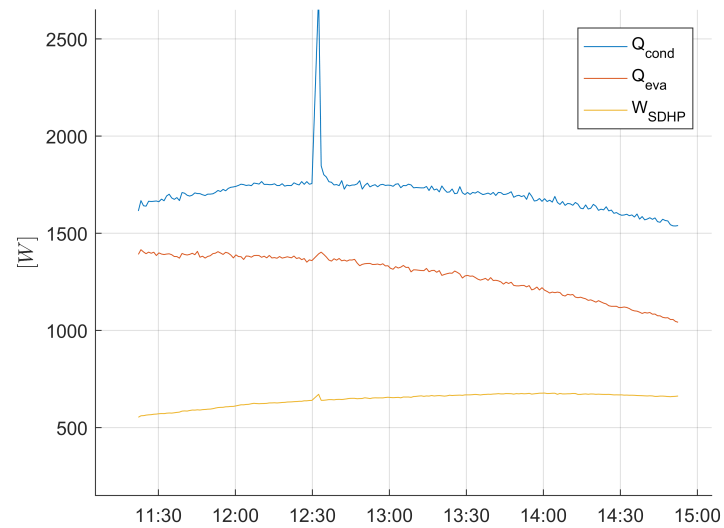


Figure 4.11: SAHP thermal and electric power, November, 30<sup>th</sup> 2016.

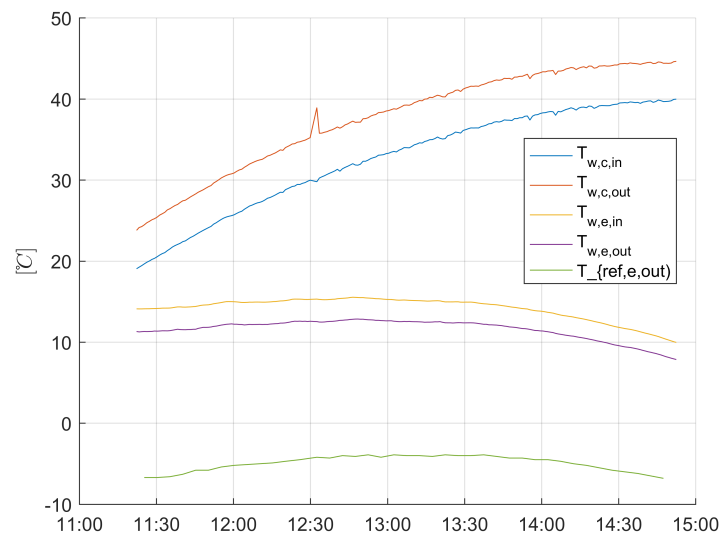


Figure 4.12: Evaporator and condenser temperatures, November, 30<sup>th</sup> 2016.

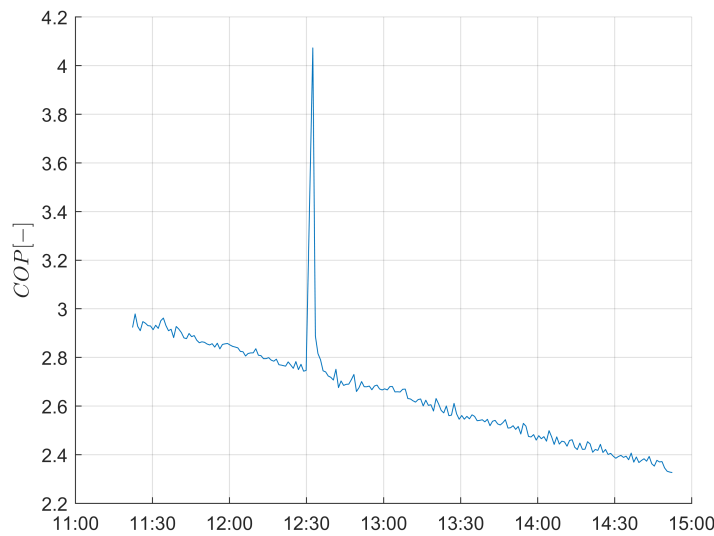


Figure 4.13: COP, November, 30<sup>th</sup> 2016.

available in table [A.4 on page 93](#)).

Results, reported in figure 4.14, show the relative electric power (i.e.  $\dot{W}/\dot{W}_{nom}$ ) produced by the modules. The figure shows also solar radiation behaviour.

We can see that the three pvt collectors work with a ratio  $\dot{W}/\dot{W}_{nom}$  around 5 percentage point more with respect to conventional PV cells. Notice that ambient temperature is between 5 and 8°C (cfr. figure 4.10), and water-glycol mixture flowing in PVT modules ranges between 8 and 15°C (cfr. figure 4.12).

Such results show that cooling effect occurs on PVT collectors, with an advantage in terms of electric power production. Notice that in winter, when  $T_{amb}$  is close to °0, PV cell temperature is lower than in other seasons. During summer, for example, with much higher temperatures and solar radiations,  $T_{c,PV}$  is expected to increase significantly, while water-glycol mixture temperature should remain below 15°C. The consequence is a higher operating cell temperature difference and a consequent higher efficiency difference between the two technologies.

### 4.3 Conclusions

The experimental investigation revealed the presence of problems in the system. Collected data showed a bad thermal efficiency of the modules and an unexpected behaviour of the evaporator. COP,  $\dot{Q}_{eva}$  and  $\dot{Q}_{cond}$  were lower than expected, and at the outlet of the evaporator  $T_{ref,e}$  reached values lower than -12°C while water-glycol mixture was at 5 °C.

The problem with the solar collectors, where the detachment of the sheet&tube heat

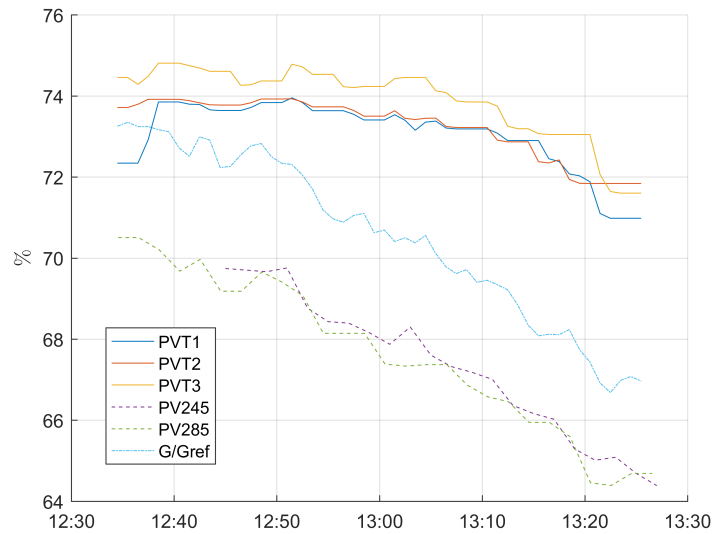


Figure 4.14: Comparison between PVT and PV electric power production with respect to nominal values on November, 30<sup>th</sup> 2016..

exchanger occurred, have been solved substituting the modules with new ones.

The evaporator, after being washed, did not improved his behaviour, and the cause of the poor performances have been attributed to the prototype nature of the heat pump: the heat exchangers could require a new design phase in water-source mode, and the simple substitution of the air-source evaporator with a brazed-plate heat exchanger identical to the condenser could be an unsuitable choice. Also the thermostatic valve should be checked, since the poor performance could be due to a wrong calibration of the component.

PVT collectors cooling is investigated with a comparison with conventional PV modules. Results show a 5 percentage points performance improvement in PVT collectors in the considered sample, thanks to water-glycol mixture flowing in the roll-bond heat exchanger at temperatures between 8 and 15°C.



# Chapter 5

## Results

The model developed in chapter 3 is here used to carry out a yearly simulation of the performance of the system.

The results of the experimental campaign presented in chapter 4 showed that the heat pump operates in an abnormal and inefficient condition. Therefore, experimental data are not used in this simulation, and the model is operated assuming conventional parameters described in chapter 3.

The analysis is carried out considering 7 different configurations (cfr 3.5.1 on page 40), changing rated power and PVT aperture area. Finally, a system with PVT will be compared to a SAHP coupled with conventional collectors.

### 5.1 Performance Maps

The first result of the simulation is the creation of the performance maps. Such maps represent the behaviour of the modelled systems as a function of the three operating parameters  $G$ ,  $T_{amb}$  and  $\theta_s$ .

All the following plots and considerations are referred to case B2, but can be extended to all the other cases.

In figure 5.1 we can see the maps of COP and  $Q_{cond}$  at  $\theta_s = 0$ .

As expected, thermal power produced and COP are proportional to ambient temperature and solar radiation. Notice that if the thermal power available to the evaporator is too high  $T_{eva}$  exits the envelope of the compressor and the heat pump can't operate in that condition.

In figure 5.2 we can see that the evaporation temperature can reach values higher or close to the ambient one. The region where this operating condition occurs is at low  $T_{amb}$ , that is typically during heating season. This behaviour could result

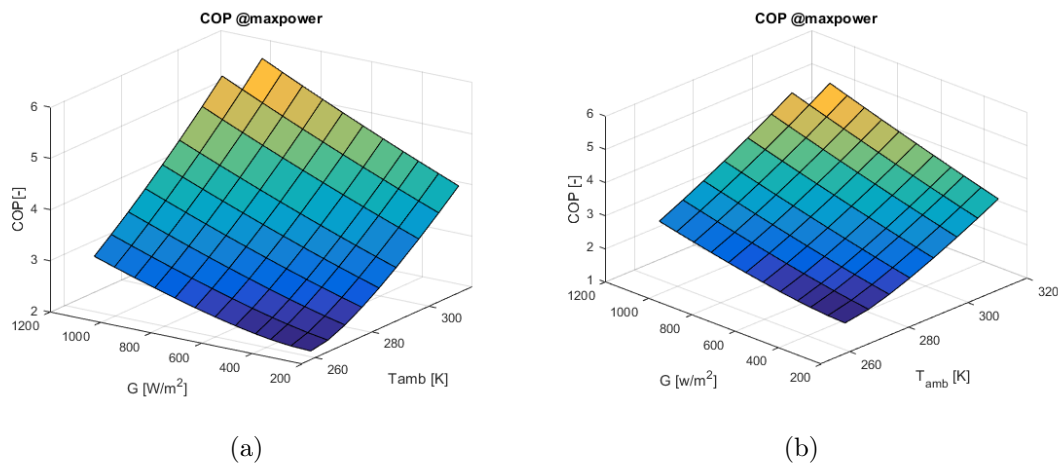


Figure 5.1: Condenser thermal power (a) and COP (b) performance maps for case B2 with  $\theta_s = 0$ .

in an advantage with respect to air-source heat pumps, that must evaporate at temperatures lower than  $T_{amb}$ .

## 5.2 Daily results - Winter

In the following plots are represented the behaviours of the diverse systems in a sunny winter day (in figure 5.3 is shown the weather data).

As expected, the parameter that affects mostly the performance is the solar radiation  $G$ . In figure 5.4 (a) we can see that in the central hours of the day, when a higher radiation is available, the thermal power at the evaporator and at the condenser are higher. We can also see the the difference between the diverse groups of plants: We can easily distinguish group A, B and C.

Obviously, configurations with a higher number of modules can produce a higher thermal power ranging from the 1.5 kW of case A to the 7.5 kW of case C3.

Notice that such differences between the cases in terms of thermal power at the condenser is not that relevant considering the electric power of the compressor. In figure 5.5 (a) we can see that  $W_c$  is quite the same for the three cases of group B and for the ones of group C. Therefore, we can expect that the configuration with a higher number of collectors will produce more power in a more efficient way.

This behaviour can be observed in figure 5.5 (b), representing the COP. Case A and B3 show the highest values. We can observe that, as expected, a higher aperture area of the collectors results in better performances of the system. Similarly, a lower number of collectors corresponds to lower COP values. It's important to say that in winter days (like in this case) the system is not able to cover the load, and operates

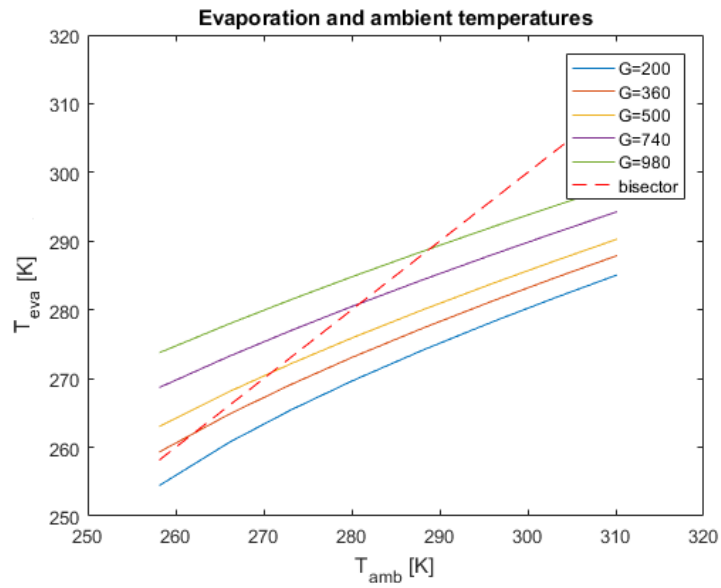
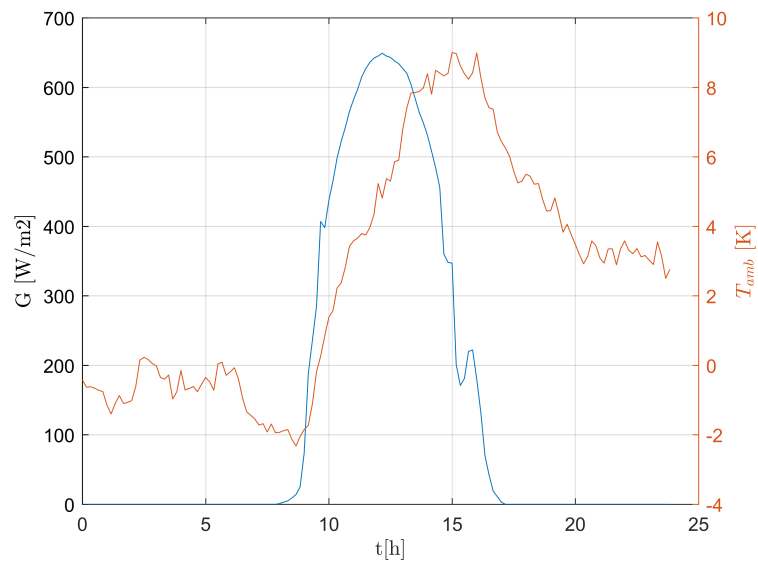


Figure 5.2: Ambient and evaporation temperature behaviour.

Figure 5.3:  $G$  and  $T_{amb}$  in the considered winter day.

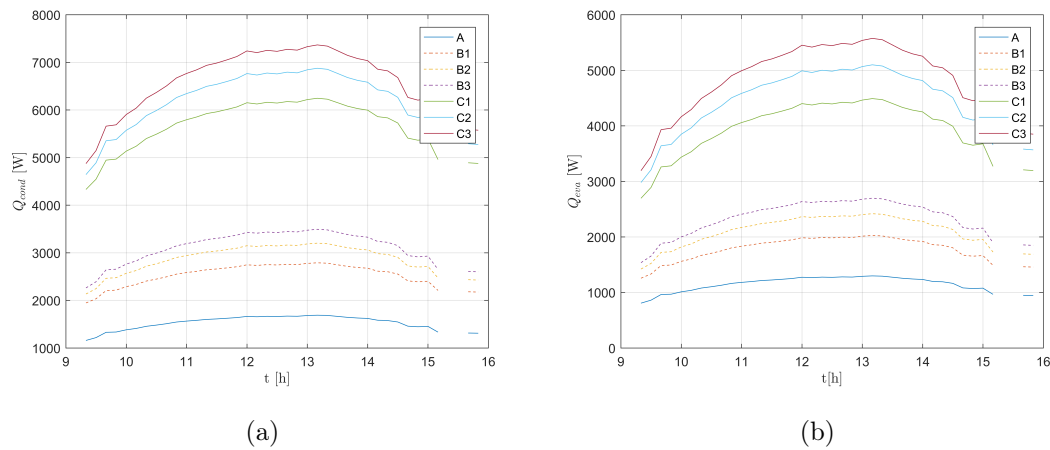


Figure 5.4: Condenser (a) and evaporator (b) thermal power for all the configurations in the considered winter day.

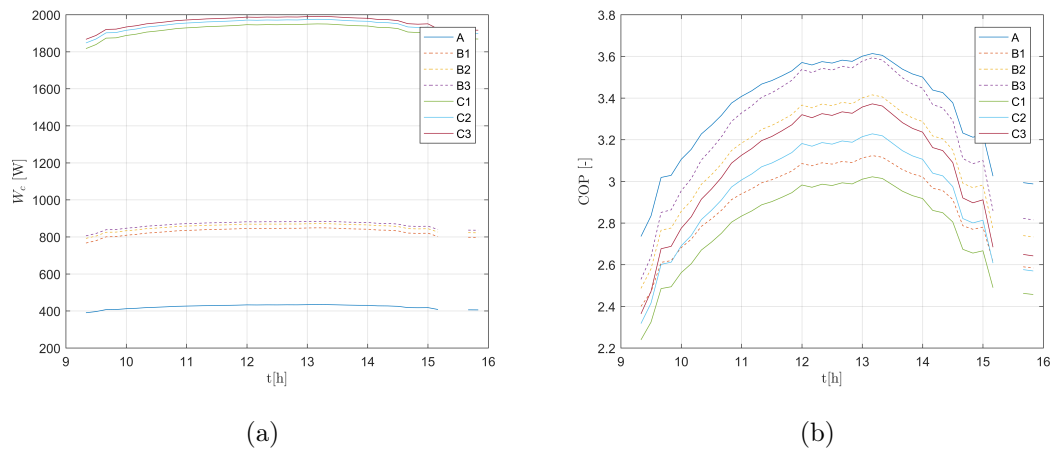


Figure 5.5: Compressor electric power consumption (a) and COP (b) for all the configurations in the considered winter day.

producing the maximum power possible, with lower COP.

COP behaviour is explained also by the relation with  $T_{eva}$ . In figure 5.6 (a) we can see that evaporation temperature is higher during the central hours of the day, thanks to higher solar radiation and ambient temperature. Analogously, water-glycol mixture's average temperature, represented in figure 5.6 (b) inside the collectors reach higher values in the same hours.

Notice that the operating field of the compressor, represented by the envelope in figure 3.5 on page 33, has a lower bound at  $T_{eva} = -30$  °C. However, such condition would be reached only with no solar radiation available, and the heat exchange on the collectors would take place only by convection; in this work, in order to avoid operating conditions that could compromise the system, the SAHP stops when the



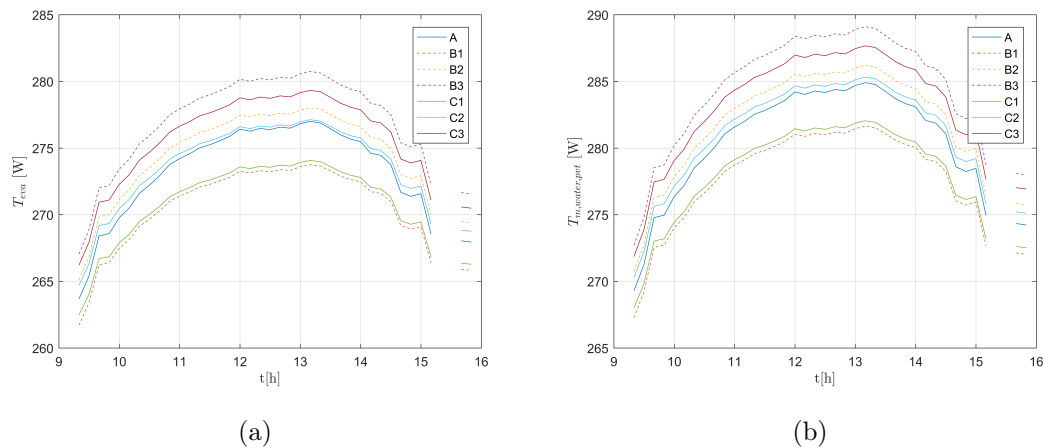


Figure 5.6: Evaporation temperature (a) and average fluid temperature in PVT (b) for all the configurations in the considered winter day.

solar radiation falls below  $200 \text{ W/m}^2$ .

An important parameter useful in order to understand if system's size is suitable with respect to the load is the fraction of the demand that the system is able to cover.

Figure 5.7 shows that case A is actually undersized, while configuration B and especially C reach more interesting values. Case C3 reaches the maximum value, close to 60%, while the cases B range between 25% and 30%.

### 5.3 Daily results - Mid-season

The second day considered is a mid-season one. In such part of the year the thermal demand is much lower than in winter (roughly 30 kWh). In figure 5.8 we can see that in the considered day solar radiation is available for a larger number of hours than in winter; It means that the systems are more likely to produce enough to satisfy the load and the SAHP could operate at the operating mode that maximizes COP.

In fact, we can see in figure 5.9 (a) that the more powerful systems are able to satisfy the demand working only in the central hours of the day, when ambient operating parameters are favourable and the COP is higher.

This fact has implications in the production of electric power of the PVT modules, because the cooling effect caused by the water-glycol mixture is not present when the system is not working. In figure 5.9 (b) we can see the step in the PVT electric power curve when the solar assisted heat pump is turned off (The figure shows only case C1, C2 and C3 because the step is more evident). Green points highlight the moments when the HP is turned on and cooling effect occurs. In a real situation a

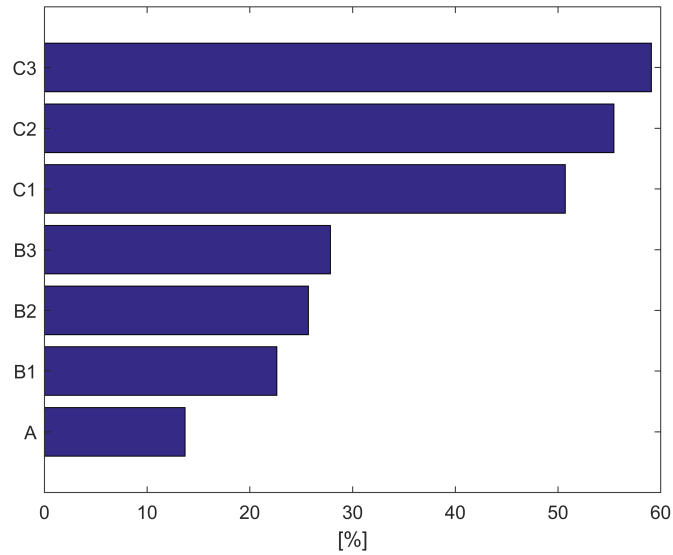


Figure 5.7: Fraction of daily heat demand satisfied by the diverse systems in the considered winter day.

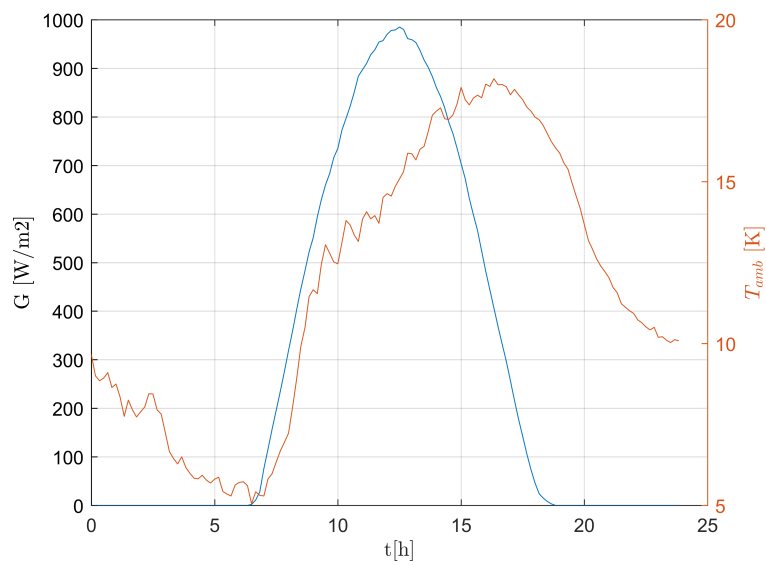


Figure 5.8: Weather profile for the considered mid-season day.

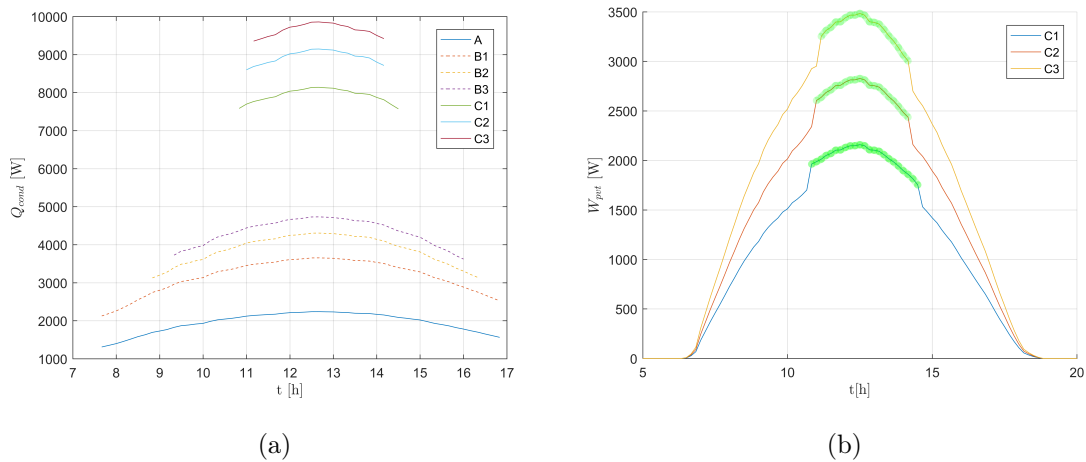


Figure 5.9: Condenser thermal power (a) and PVT electric power profile.

transient would occur, but since the model is steady-state we see a step. According to model's assumption (cfr. subsection 3.1.2 on page 29) while the system is not working the NOCT method is used; while it's working  $T_c$  is assumed to be 10 K higher than the average temperature of the fluid.

With respect to system capacity, the only configuration that is not able to satisfy the load is A. System A, in fact, is able to supply only 60% of the daily demand. All the other configurations can supply the requested heat. The main difference is the number of working hours, that is quite low in case C. Indeed configuration B works for a larger number of hours, exploiting more the system capacity, but during heating season the lower capacity is paid with higher natural gas expenses as auxiliary source.

## 5.4 Annual and monthly results

After considering the daily behaviour of the system, a wider point of view can be considered looking to the monthly and annual performance.

### 5.4.1 Load supply

In figure 5.11 we can see the energy produced and the extra energy required by the system for each day of the year.

Both cases B2 and C2 are almost able to cover the demand in mid-season days; a significant difference is observed during heating season, when case B1 is able to cover only 25% of the load during sunny days. During summer both the configurations cover without problems domestic hot water supply. Therefore there is a trade-off between the capacity of the system and the auxiliary thermal power that have to be

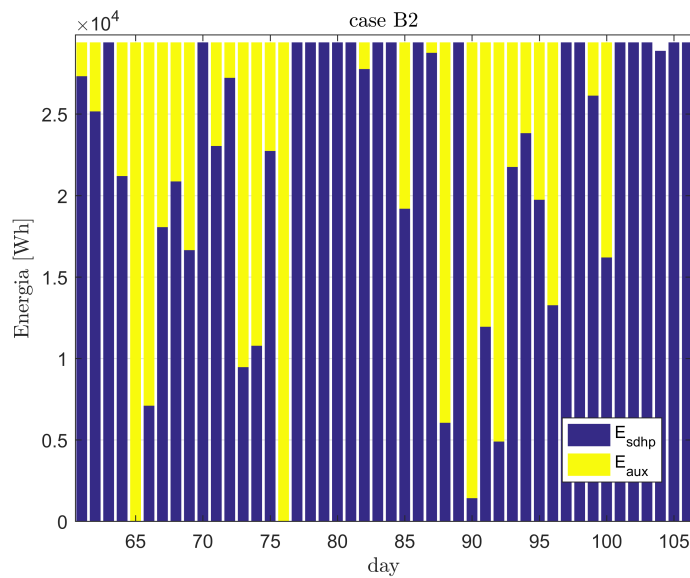


Figure 5.10: Mid season (spring) energy production and auxiliary energy requirement, case B2.

purchased.

Higher capacity (i.e. a more powerful system, like in configuration C) means higher thermal power produced by the solar-assisted heat pump, but higher investment cost. A smaller system, like in configuration B, is less expensive in terms of investment but will require higher expenses for natural gas. This topic is treated in section 5.5 on page 78.

Looking to figure 5.10 we can see that in mid season an alternation of sunny and cloudy days sometimes occur. In such situation, in a sunny day the model turns off the system when it reaches the required daily energy; in a real condition the SAHP produce more heat storing it for the following day. The result is that the simulation considers a conservative situation, and with respect to this issue real performance could be better.

In table 5.2 is shown, for each month, the number of days characterized by high ( $>4 kWh/m^2$ ), medium ( $2 < E < 4 kWh/m^2$ ) or low ( $< 2 kWh/m^2$ ) solar energy available; in the right part of the table are reported the values of the energy produced by each system in each slot. The picture is completed by table 5.1, representing the monthly productivity of each configuration.

From the analysis of the results we can observe that in mid-season months there are both days with high and low solar energy available, but in figure 5.10 we can see that sunny days seem to be grouped together. Moreover, during heating season the SAHP never matches the load even in configuration C3. Therefore, the possible inaccuracy of the simulation due to the impossibility to store the energy for the day

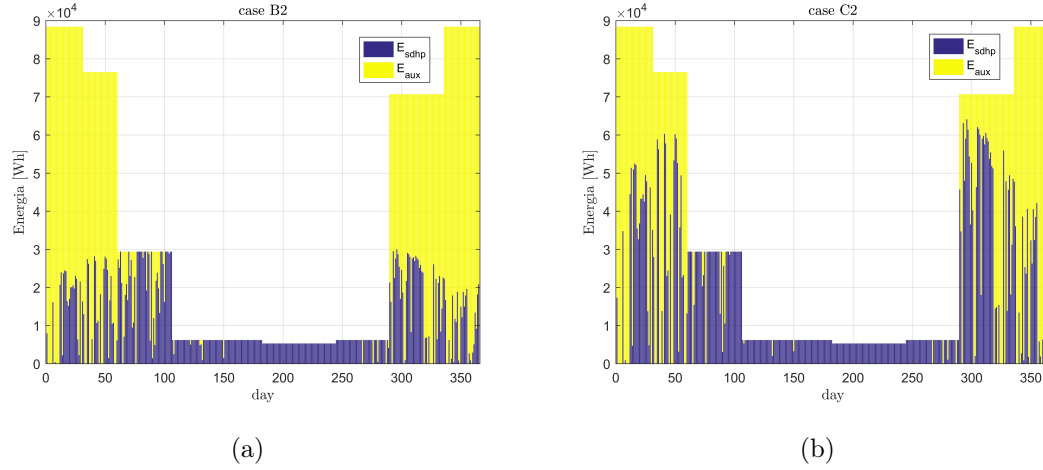


Figure 5.11: Yearly energy production for case B2 and C2

Table 5.1: Monthly load and thermal energy production. Values in kWh.

Month	Load	A	B1	B2	B3	C1	C2	C3
Jan	2740.40	193.16	319.50	364.32	395.71	715.59	784.59	837.88
Feb	2218.50	180.12	297.97	341.68	372.47	666.95	734.13	786.35
Mar	911.40	358.11	591.18	648.07	672.68	768.27	776.98	783.68
Apr	534.00	294.57	423.74	449.74	462.10	509.45	513.40	515.34
May	192.20	168.04	176.42	178.52	179.98	184.58	185.03	185.38
Jun	186.00	186.00	186.00	186.00	186.00	186.00	186.00	186.00
Jul	164.30	164.30	164.30	164.30	164.30	164.30	164.30	164.30
Aug	164.30	162.74	164.30	164.30	164.30	164.30	164.30	164.30
Sep	186.00	179.80	179.80	179.80	179.80	179.80	179.80	179.80
Oct	1224.20	233.33	342.96	385.82	416.21	680.52	745.55	796.57
Nov	2121.00	259.62	429.55	495.02	541.33	960.86	1061.34	1139.88
Dec	2740.40	148.17	244.96	278.54	302.00	549.04	600.77	640.58

Table 5.2: Thermal energy produced in days with high, medium and low radiation.

	Esun <i>kWh/m<sup>2</sup></i>	$n_d$ -	A kWh	B1 kWh	B2 kWh	B3 kWh	C1 kWh	C2 kWh	C3 kWh
Jan	E>4	5	62.95	104.11	119.38	130.12	233.04	256.47	274.67
	2<E<4	12	119.93	198.36	225.84	245.06	444.38	486.70	519.33
	E<2	14	10.27	17.02	19.10	20.53	38.17	41.42	43.88
Feb	E>4	9	124.30	205.66	236.77	258.75	460.05	507.79	545.06
	2<E<4	3	25.30	41.81	47.80	52.01	93.67	102.86	109.97
	E<2	17	30.52	50.50	57.11	61.71	113.23	123.48	131.32
Mar	E>4	18	279.91	461.91	500.72	512.66	529.20	529.20	529.20
	2<E<4	6	59.66	98.60	112.56	122.34	170.34	172.67	174.48
	E<2	7	18.54	30.66	34.79	37.67	68.73	75.11	80.01
Apr	E>4	20	214.71	299.85	309.08	309.60	309.60	309.60	309.60
	2<E<4	8	75.94	117.43	133.30	144.51	185.37	187.93	188.80
	E<2	2	3.91	6.46	7.36	8.00	14.48	15.87	16.94
May	E>4	21	130.20	130.20	130.20	130.20	130.20	130.20	130.20
	2<E<4	4	22.75	24.80	24.80	24.80	24.80	24.80	24.80
	E<2	6	15.09	21.42	23.52	24.98	29.58	30.03	30.38
Jun	E>4	27	167.40	167.40	167.40	167.40	167.40	167.40	167.40
	2<E<4	3	18.60	18.60	18.60	18.60	18.60	18.60	18.60
	E<2	0	0.00	0.00	0.00	0.00	0.00	0.00	0.00
Jul	E>4	28	148.40	148.40	148.40	148.40	148.40	148.40	148.40
	2<E<4	3	15.90	15.90	15.90	15.90	15.90	15.90	15.90
	E<2	0	0.00	0.00	0.00	0.00	0.00	0.00	0.00
Aug	E>4	28	148.40	148.40	148.40	148.40	148.40	148.40	148.40
	2<E<4	1	5.30	5.30	5.30	5.30	5.30	5.30	5.30
	E<2	2	9.04	10.60	10.60	10.60	10.60	10.60	10.60
Sep	E>4	23	142.60	142.60	142.60	142.60	142.60	142.60	142.60
	2<E<4	6	37.20	37.20	37.20	37.20	37.20	37.20	37.20
	E<2	1	0.00	0.00	0.00	0.00	0.00	0.00	0.00
Oct	E>4	14	150.44	224.70	254.44	275.56	456.25	501.87	537.74
	2<E<4	8	67.54	100.98	113.45	122.27	202.92	222.06	237.02
	E<2	9	15.36	17.28	17.93	18.38	21.36	21.62	21.81
Nov	E>4	14	192.06	317.87	367.39	402.50	710.70	786.66	846.22
	2<E<4	4	44.16	73.02	83.76	91.32	163.47	179.94	192.75
	E<2	12	23.39	38.66	43.88	47.51	86.70	94.74	100.91
Dec	E>4	0	0.00	0.00	0.00	0.00	0.00	0.00	0.00
	2<E<4	14	125.91	208.12	236.98	257.15	466.43	510.82	545.02
	E<2	17	22.26	36.84	41.57	44.85	82.62	89.96	95.55

after is negligible for this kind of analysis.

Table 5.1 shows that system A could be a suitable solution for domestic hot water production, since in almost all the months produce more than 160 kWh, that is DHW demand for the considered load, constant throughout the year. But the relevance of this system in a domestic heating application would be significant only during summer, since in mid-season it would satisfy about 50% of the demand and during heating season a very small fraction.

In the same table we can see that on September all the systems produced the same amount of energy, lower than the one required by the user.

The explanation to this fact can be found on table 5.2: we can observe that in this month there is only one day with low solar energy available, and looking to weather data (not reported in this work because of their size), we see that in this day solar radiation and ambient temperature were too low for the system to start.

This fact highlights one of the limits of solar-assisted heat pumps, that can only operate with favourable operating conditions.

The yearly analysis is completed with figure 5.12, showing the fraction of annual heat demand covered by the systems. Case A is able to supply only the 20% of the overall demand, and seems to be suitable only for domestic hot water production. Case B reach values around 30%, and the 50% is reached only by the biggest case (C3).

In the figure we can distinguish the three groups of systems characterized by similar performances. The optimal ratio between aperture area and heating capacity will be investigated in chapter 5.5.

On the electric side we can see in figure 5.13 that in all the considered systems the electric energy produced along the year is higher than the absorbed. Also notice that the electric energy absorbed by the heat pump remains almost constant with respect to PVT number for a fixed heat pump size.

On monthly basis, however, the situation is quite unbalanced between winter and summer. In table 5.3 we can see that during heating season electricity production and consumption are quite balanced because the heat pump always works if solar radiation is available and the power absorbed is comparable with  $\dot{W}_{el,pvt}$ . During summer the heat pump works only few hours per day while the solar modules always produce. The result is a positive energy balance, that positively influences the yearly performance. This unbalance is not a problem, because the solar-assisted heat pump is assumed to be connected to the national electric grid, modelled as an infinite and perfect storage (i.e. the Italian "scambio sul posto").

However, with respect to a system with PV modules only (i.e. without HP), SAHP systems are characterized by a significant advantage. In fact, high electric

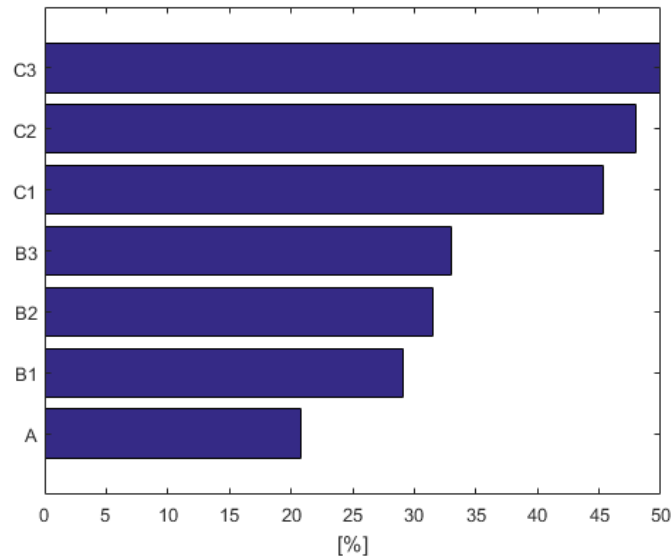


Figure 5.12: Fraction of annual heat demand supplied by the solar-assisted heat pump for each configuration.

energy self-consumption occurs, because the heat pump works only when there is solar radiation available, that is when electric power is produced by PVT. In table 5.4 are reported the fractions of electric energy produced by PVT directly used by the heat pump. We can see that during winter electricity self-consumption reach values close to 100%, because heat pump and PVT both work all day long. During summer, more solar energy is available and heat demand is low. The systems work with higher efficiency, and increasing system's size for a lower number of hours. PVT instead, produce more with respect to winter, and the result is a low self-consumption fraction, especially for larger systems that work only few hours per day.

In figure 5.14 we can see that on annual basis systems' self consumption fractions range from 47% to 27%, decreasing with system size and pvt number.

### 5.4.2 Primary Energy

In terms of primary energy the system generates two main effects:

- Natural gas: consumption reduction thanks to thermal power production at the condenser.
- Electric power: PVT modules produce power, while the heat pump absorbs it. Energy balances showed which term is prevalent.



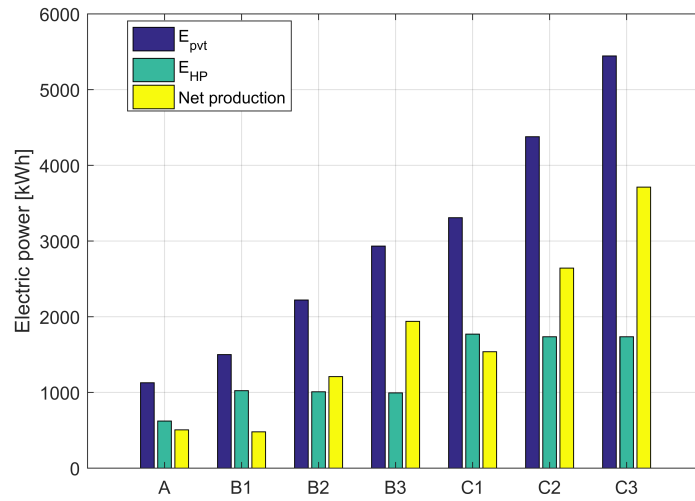


Figure 5.13: Electric energy produced and absorbed by the system on annual basis

Table 5.3: Net electric energy production on monthly basis.

kWh	A	B1	B2	B3	C1	C2	C3
Jan	-0.38	-32.10	-1.97	29.11	-82.07	-36.61	9.59
Feb	1.46	-26.17	2.06	31.08	-67.03	-24.48	18.64
Mar	3.87	-45.91	21.50	88.92	66.65	172.73	276.31
Apr	43.26	34.06	114.18	193.15	193.50	314.01	430.53
May	77.77	106.27	185.49	260.14	281.65	401.66	509.75
Jun	88.66	124.68	209.93	294.30	321.67	449.48	567.37
Jul	104.82	142.88	234.07	326.49	356.33	495.95	629.26
Aug	102.47	140.48	230.20	321.94	351.63	485.40	621.77
Sep	73.98	105.51	180.70	255.12	276.80	391.18	495.42
Oct	14.65	-1.86	43.21	88.58	11.90	75.84	145.58
Nov	-2.04	-41.62	-4.97	32.73	-104.02	-48.80	7.14
Dec	-1.89	-27.45	-4.78	18.69	-69.60	-35.36	-0.48

Table 5.4: SAHP electricity self-consumption.

	A [%]	B1 [%]	B2 [%]	B3 [%]	C1 [%]	C2 [%]	C3 [%]
Jan	82.98	87.61	83.18	72.03	87.49	86.68	80.72
Feb	77.97	85.20	78.03	67.75	85.05	82.18	75.48
Mar	78.35	89.40	73.99	59.30	58.75	47.08	37.56
Apr	51.26	52.64	40.76	31.58	31.25	24.32	19.56
May	28.65	25.19	15.36	11.45	13.20	7.86	6.80
Jun	29.12	24.08	14.92	9.96	11.88	7.43	6.35
Jul	22.85	19.75	12.05	7.37	9.64	5.41	3.77
Aug	22.35	19.03	11.91	7.42	9.39	6.20	3.80
Sep	32.00	25.11	16.33	11.26	12.94	8.26	7.06
Oct	66.46	66.85	58.45	48.69	59.28	56.94	50.24
Nov	84.65	89.09	84.68	73.28	88.97	88.33	81.95
Dec	77.94	78.97	77.95	70.62	78.81	78.60	76.71

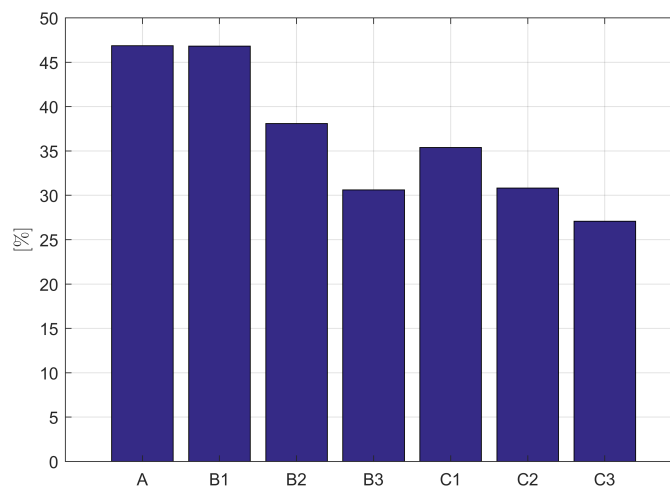


Figure 5.14: Electric energy self-consumption on annual basis.

In order to compare electric energy and thermal energy (natural gas), a conversion factor equal to 52% is assumed for electricity.

$$PE_{el} = \frac{E_{el}}{\eta_{conv}} \quad (5.1)$$

Natural gas savings are equal to the thermal energy production of the heat pump, taking into account boiler thermal losses.

$$Q_{ng,saved} = \frac{Q_{hp}}{\eta_{boiler}} \quad (5.2)$$

where we assume  $\eta_{boiler} = 0.95$ . Detailed data about SAHP thermal energy production are reported in table 5.1 on page 71.

With the data previously explained we can compute the effects of system's installation in terms of primary energy. Thermal reference case have been already defined: thermal load as in table 3.2 on page 43 entirely supplied with a natural gas-fired boiler. The electric demand is assumed to be equal to 3.3 MWh/y. Therefore, for the reference case the annual primary energy demand is calculated:

$$PE_{ref} = \frac{Q_{load}}{\eta_{boiler}} + \frac{E_{el,ref}}{\eta_{conv}} = \frac{13.383 \text{ MWh}}{0.95} + \frac{3.3 \text{ MWh}}{0.52} = 20.434 \text{ MWh} \quad (5.3)$$

For the other cases, electric and thermal energy produced are subtracted to the reference consumption:

$$PE = \frac{Q_{load} - Q_{SAHP}}{\eta_{boiler}} + \frac{E_{el,ref} - E_{el,net,SAHP}}{\eta_{conv}} \quad (5.4)$$

In figure 5.15 is shown the annual primary energy demand of the considered systems. Blue bars represent the effective primary energy demand of the user, that is the auxiliary energy that has to be purchased. Cyan and yellow bars represent, respectively, thermal and electric contribution of the solar-assisted heat pump to the primary energy consumption of the system.

Notice that system C1 has one PVT more than B1, but its contribution to primary energy is lower because compressor power input is higher, and this can be found in the higher thermal contribution of the heat pump. The point is that a good balance between PVT and heat pump have to be found in order to optimize the efficiency and the convenience of the system.

We can also see that while in terms of thermal energy the only system able to supply the 50% of the load was C3, in terms of overall primary energy also case C2 reaches this target.

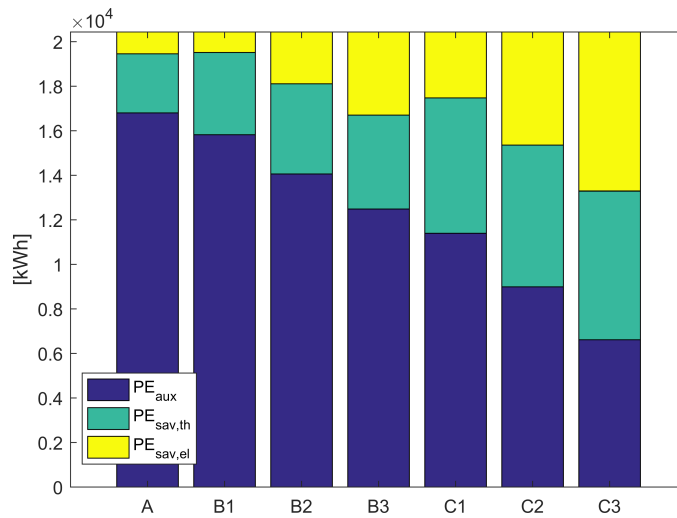


Figure 5.15: Primary energy demand and savings contributions.

## 5.5 Economic results

In section 3.6 on page 44 the adopted procedure and the main assumptions of the economic analysis carried out in this work have been described.

The first results presented are relative to the cost structure of the investment. In figure 5.16 we can see all the components of the initial investment.

The first thing to say is that the main cost is associated to PVT modules, that represent roughly 50% of the investment.

The smaller systems pay the assumption of fixed costs for the *balance of plant*, that become relatively less relevant for higher sizes. However, such costs include storage and grid connection, that generally does not change significantly with respect to the size of the plant.

An important consideration with respect to such cost analysis is that while heat pump and inverter are consolidated technologies and significant cost reduction are not expected in the following years, PVT modules, that are the most expensive component, could reduce their cost thanks to possible improvements in the design and in the manufacturing process. Such effects will be further investigated in this section.

Looking to NPV and IRR, results show that the economic convenience of the system is not reached in all the considered configurations. In table 5.5 are reported Net Present Value and Internal Rate of Return of the investments.

We can see that that under current assumptions all the considered configurations are associated to a negative NPV, meaning that the investment is not convenient and leads to a loss. Case C3 is the only one with a value close to 0, meaning that in

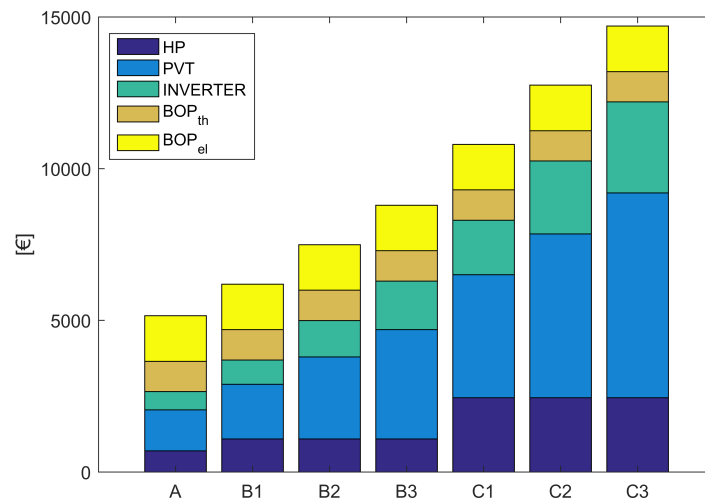


Figure 5.16: Investment cost structure.

economic terms there is a very low difference with the reference case, and the system almost able to pay back the investment.

This result is quite important, because it demonstrate that the SAHP is able to efficiently supply a domestic load, with significant primary energy consumption reduction, at costs almost competitive with respect to conventional technologies.

IRR gives the same informations about the convenience or not of the investment, all the systems are characterized by an IRR lower than the capital cost (assumed to be 3%).

But the other information that we can read in such results is that, keeping fixed all the other parameters, system B3 and C2 could result convenient if the investor is able to lower the capital cost to, respectively, 1.5% and 1.34%. Case C3 would become convenient with a capital cost equal to 2.79%, that is not too far from today's real values.

The other configurations, however, have a negative IRR and can't become convenient even with a capital cost equal to zero.

Further analysis can be carried out with respect to the costs. In particular, figure 5.16 shows that PVT modules represent the larger part of the investment, and this cost is expected to decrease in the next years. In figure 5.17 we can see the effect of a decrease of this cost on the Net Present Value.

The sensitivity analysis shows that a slight decrease of PVT cost, in the order of 5%, would lead to break even configuration C3. Such cost reduction seems to be quite a realistic forecast, and in the next years improvements of the manufacturing processes will be crucial.

Table 5.5: Economic analysis results: NPV and IRR

	NPV [€]	IRR [%]
A	-3111	-5.96
B1	-3295	-4.57
B2	-2119	-0.62
B3	-1078	1.50
C1	-3383	-1.06
C2	-1724	1.34
C3	-259	2.79

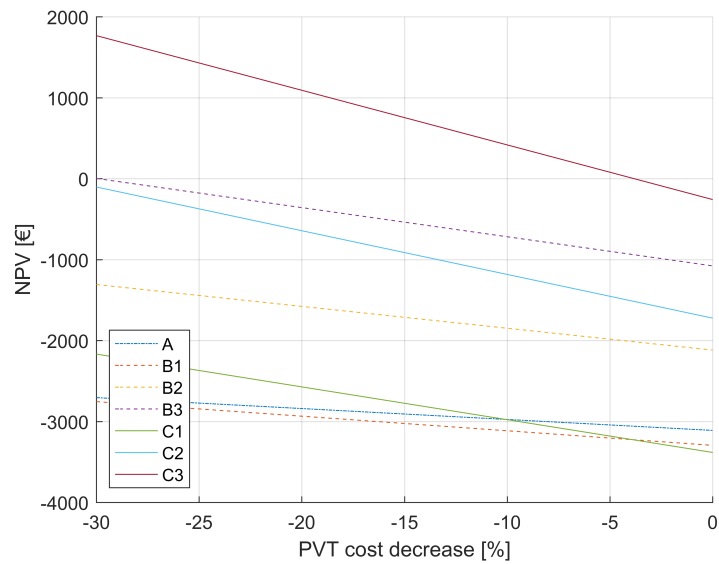


Figure 5.17: PVT cost sensitivity analysis.

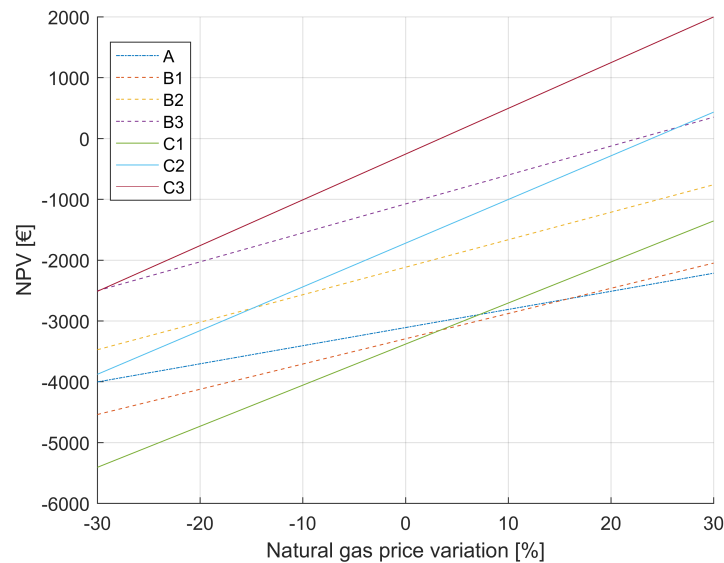


Figure 5.18: Natural gas price sensitivity analysis.

Configuration B3 and C2 are the only other systems that could reach break even under this assumptions, but this event would require a 30% cost reduction of PVT cost.

The other factors that generally change in the years are natural gas and electricity price. In this situation, an increase of such costs would result in higher revenues/savings, and would have a positive effect on the overall investment.

In figures 5.18 and 5.19 are represented the effects of natural gas and electricity price variations on NPV. Notice that while PVT cost is expected to not increase, in this cases energy price could decrease as well as increase.

We can see that energy price become more important on the overall investment increasing the size of the plant. Also notice that this influence is comparable to PVT cost one, because a similar relative variation (lower than 5%) would lead to break-even configuration C3. However, a huge difference is represented by the fact that energy price could also decrease, critically lowering the NPV.

## 5.6 Comparison with a system with conventional modules

In this section is presented a comparison between configuration C2 and a similar system equipped with conventional PV and thermal collectors instead of PVT ones (config. D).

In particular, in system D the aperture area of thermal collectors is selected in

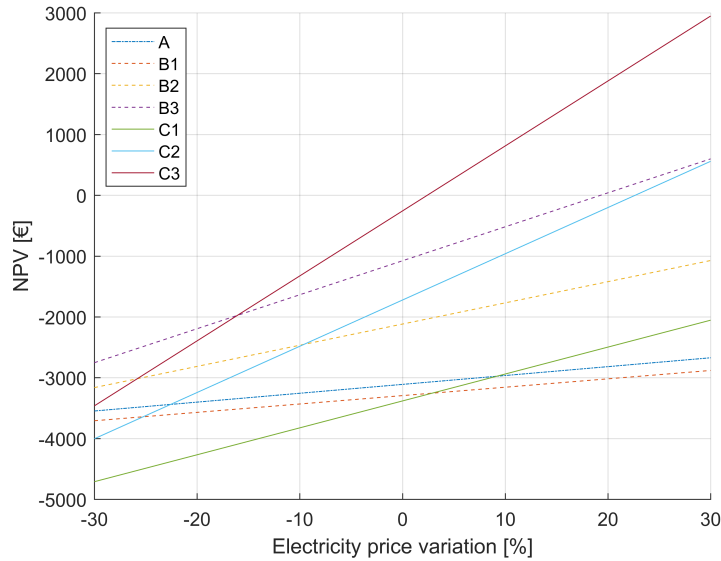


Figure 5.19: Electricity price sensitivity analysis.

order to perform in the same way in design conditions, and the overall area has to be the same of case C2. In Appendix A are reported the details of the modules used for the simulation.

Notice that the conventional flat-plate thermal collector is characterized by a higher optical efficiency and a lower loss coefficient, requiring a smaller aperture area in order to provide the same thermal power. The consequence is that only 4 conventional thermal collectors ( $A_{ap} = 2.295 \text{ m}^2$ ) are able to satisfy design requirements. The remaining area is covered with PV modules with the same technology of case B2.

The main advantage of system D is the reduction of the initial cost; thermal collectors' cost is assumed to be  $300\text{€}/\text{m}^2$  and PV modules cost  $700\text{€}/\text{kW}$ , while PVT collectors  $1800\text{€}/\text{kW}$ . However, the lower number of PV modules will lower the energy production of the system, resulting in lower savings in terms of primary energy.

In figure 5.20 are compared  $\dot{W}_{pvt}$  and  $\dot{Q}_c$  of the two systems in the reference winter day (weather profile in figure 5.3 on page 65). We can see that the two configurations have a similar thermal behaviour coherently with design specifications. Notice that the system equipped with pvt works with a better thermal power output at the condenser. In fact, PVT have a higher heat exchange coefficient, that when  $T_{amb}$  is higher than fluid's temperature (this situation occurs especially in the second half of the day) leads to better thermal performances because of convective heat transfer.

On the electric side we can see that the produced power in case D is roughly 50% of the other one because of the number of modules installed.



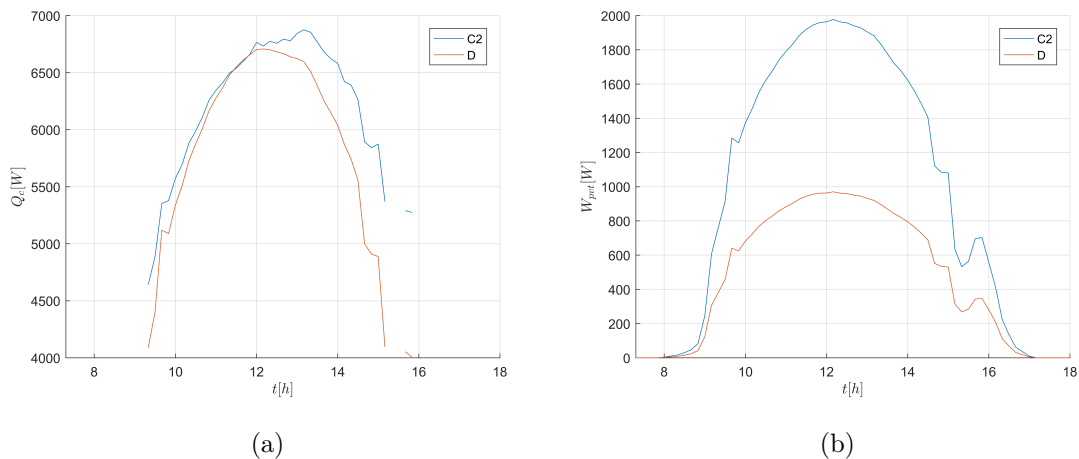


Figure 5.20: Condenser thermal power (a) and electric power profile (b) in the reference winter day.

We can conclude that hybrid PVT modules represent an efficient energy solution, able to increase in this application both thermal and electric power with respect to conventional technologies. We can also observe that the operating field of the collectors, with fluid temperatures frequently lower than ambient ones, is optimal for PVT collectors, because the higher heat transfer coefficient in this situation turns into an advantage. Analogously, PVT modules are not recommended for direct DHW production, because the higher heat transfer coefficient would be detrimental.

In table 5.6 are reported energy production and consumption of the two systems on monthly basis.

As said before, heat pump thermal production is similar for the two cases. The advantage of PVT use can be seen with respect to electric energy: configuration C2 is able to compensate heat pump consumption in winter time, when heat demand is higher and solar radiation lower, and can produce a significant power excess during summer. System D is not able to compensate heat pump consumption in winter, and the extra electric energy produced during mid-season and summer is much lower than case C2. On annual basis, in fact, net electricity production in case D is close to zero.

Such considerations show the energy convenience of PVT, especially in this application where fluid temperatures are close to ambient ones. In fact, the better thermal insulation of conventional thermal collectors turns into a disadvantage if  $T_w < T_{amb}$ .

In table 5.7 we can see the fraction of PV electric energy directly used by the heat pump. Configuration D directly exploits a larger energy fraction with respect to C2. This trend is more evident during mid season, when the systems work only few hours per day. Such increase in self-consumption fraction is ascribable to the

Table 5.6: Energy production and consumption on monthly basis in case C2 and D.

<i>kWh</i>	$Q_{hp}$		$Q_{aux}$		$W_{PV}$		$W_{HP}$	
	C2	D	C2	D	C2	D	C2	D
Jan	784.59	725.83	1955.81	2014.57	221.06	108.59	257.66	309.38
Feb	734.13	665.06	1484.37	1553.44	205.19	100.34	229.67	274.74
Mar	777.82	761.38	134.42	153.91	382.25	189.26	209.52	239.01
Apr	511.73	510.77	20.60	31.20	442.63	223.90	128.62	156.12
May	171.02	198.52	7.17	8.47	441.41	226.76	39.75	52.41
Jun	176.79	205.99	0.00	0.00	485.60	249.11	36.12	48.71
Jul	143.14	154.39	0.00	0.00	524.33	270.26	28.37	35.85
Aug	163.87	154.95	0.00	0.00	519.16	267.78	33.76	37.94
Sep	170.77	185.92	6.20	6.20	428.01	219.59	36.83	47.01
Oct	754.12	659.62	478.65	561.37	290.94	143.81	215.10	252.61
Nov	1061.34	932.87	1059.66	1188.13	268.97	130.86	317.77	379.32
Dex	600.77	535.30	2139.63	2205.10	167.00	82.37	202.36	241.93

lower PV modules installed in configuration D, that leads to a decrease of the overall electric energy production.

However, the increase in self-consumption fractions is negligible in winter and ranges between 2 and 10 percentage points in the other months. Therefore, the advantages for the national electric grid seem to be not significant, especially comparing them with the worse energy performance of case D.

Figure 5.21 compares the primary energy supply of the two systems. The lower installed power for PV technology zeroes the annual balance between heat pump and PV production. Therefore, in the global balance (b) only a negligible fraction of electricity demand can be supplied by PV modules. The thermal energy that the solar-assisted heat pump is able to supply in the two configurations is quite the same (slightly higher in case C2), therefore the primary energy that has to be externally provided in case D is higher.

In figure 5.22 we can see that the contribution of solar modules to the overall investment decreased in case D. The cost for the modules in case D is lower than in case C2; we can also see that in system D the cost for solar modules is mainly due to thermal collectors, while PV cost is less relevant. Moreover, also inverter cost is lower because the nominal electric power is 50% of case C2.

Global economic results show that the configuration with conventional solar modules is much less convenient with respect to the one with PVT. Case C2 presented

Table 5.7: Electricity self-consumption fraction on monthly basis for cases C2 and D.

	C2 [%]	D [%]
Jan	86.681	87.06083
Feb	82.18457	84.46259
Mar	47.08361	58.69969
Apr	24.32484	31.70971
May	7.863914	13.17169
Jun	7.42676	12.5696
Jul	5.411611	8.693789
Aug	6.202074	8.635833
Sep	8.255198	12.75564
Oct	56.94392	57.9871
Nov	88.32798	88.45673
Dec	78.59681	78.19384

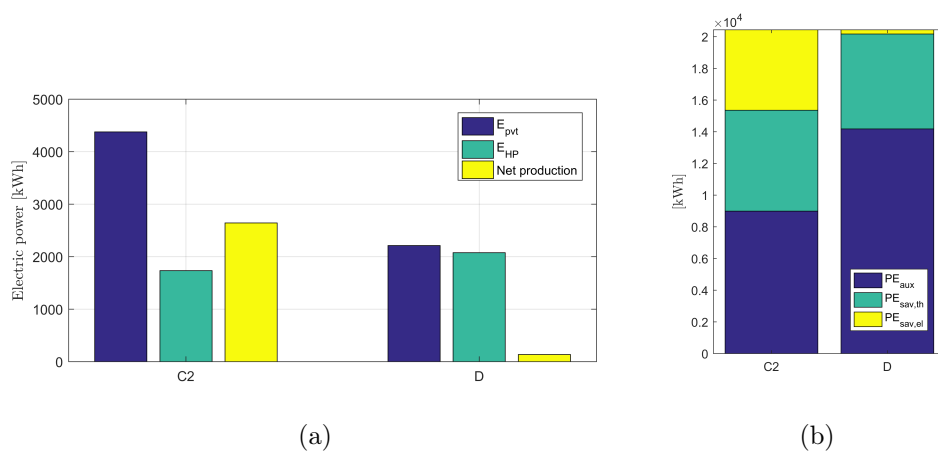


Figure 5.21: Electric energy balance (a) and primary energy supply to the load (b) for systems C2 and D.

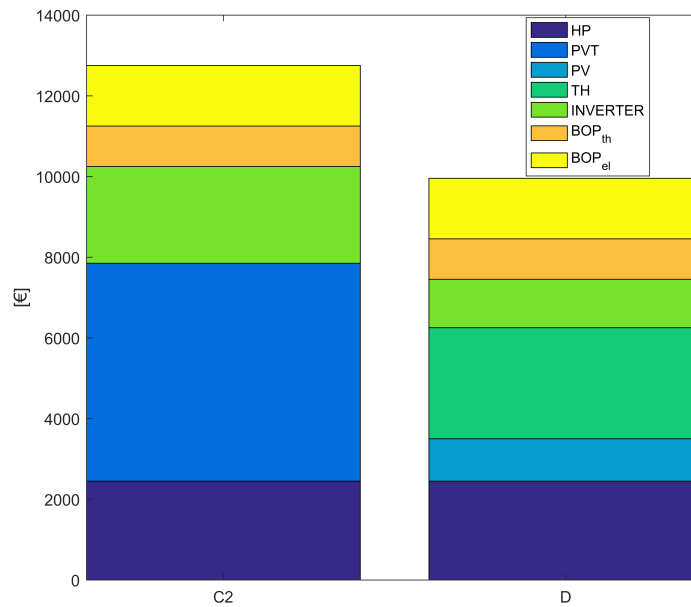


Figure 5.22: Cost structure in case C2 and D

a Net Present Value and an Internal Rate of Return equal to -1274€ and 1.34%. Case D shows a NPV equal to -6649€ and an IRR equal to -7.34%. It is clear that the advantage of a lower investment cost is not balanced in terms of revenues, that decreased more than proportionally to initial cost reduction. Notice that NPV of the system with conventional modules is the lowest of all the cases considered in the analysis of the previous section.

Such results show the importance of PVT technology for solar-assisted heat pump applications, both in energy and economic terms. Indeed the higher cost of this technology is more effectively balanced by energy production than for conventional technologies, even if it is not able to cover all the expenses. Moreover, flat-plate collectors pay the fact that they are designed for heat production at mid-temperature, and the expense for this technology is not justified by SAHP applications.

The previous considerations, in fact, are strictly related to solar assisted heat pump, and in general to low-temperature heat production, since the high loss coefficients of PVT would reduce critically the efficiency at higher temperatures.

# Chapter 6

## Conclusions

In this work a solar-assisted heat pump with photovoltaic-thermal collectors have been studied.

Different system configurations are taken into account and modelled, with three heat pump capacities and different numbers of solar collectors, in order to find the best configuration for domestic hot water and heating supply and to understand the behaviour of the system. The smallest of such systems is object of a preliminary experimental investigation, carried out at the SolarTech Lab, Energy Department of Politecnico di Milano.

The heat pump present in the laboratory is a water-source heat pump, derived from a commercial air-source one where the air evaporator have been substituted with a brazed-plate heat exchanger identical to the condenser. PVT collectors in the first part of the campaign were mono-silicon sheet&tube collectors, and in the second part poly-silicon with roll-bond heat recovery. Collected data, in fact, showed the presence of problems in the first set of solar collectors, whose efficiency was significantly lower than expected.

But the experimental campaign also showed that the heat pump did not perform as expected. The power exchanged at the evaporator was low, and the consequence was a COP not comparable with state of the art heat pumps. Further analysis, and the measure of refrigerant temperature at evaporator outlet, showed that the logarithmic mean temperature difference in the component was really high: for example,  $T_{eva}$  reached  $-12\text{ }^{\circ}\text{C}$  while water-glycol mixture was at  $5\text{ }^{\circ}\text{C}$ . The ineffective heat transfer at the evaporator affected the performance of the whole system, that worked with COP and power values lower than expected. A possible cause of this working condition can be found in the fact that the heat pump is a prototype, derived from a air-source heat pump replacing the air heat exchanger with a brazed plate one identical to the condenser.

Experimental results also showed the beneficial effect of cold water-glycol mixture flowing in PVT modules' back with respect to electric power production. In a winter day characterized by clear sky and  $T_{amb}$  between 5 and 8°C, electric power produced by PVT was 5 percentage points higher with respect to conventional PV modules.

For the reasons previously explained, the mathematical model of the system was developed assuming heat exchange properties similar to state of the art machines, in order to simulate the working condition of a commercial heat pump instead of a prototype. In order to perform an annual simulation without excessive computational resources a black-box steady-state model have been adopted.

Thermal performance of the solar modules have been modelled with the loss coefficients provided by the manufacturer, while compressor behaviour have been described via polynomial equations obtained from technical data sheets.

The nature of the system defines two different operating modes, that maximize, respectively, COP and thermal power output. Such operating modes are obtained changing water mass flow rate at the evaporator (and in the solar collectors), with variations in terms of heat exchange properties and electric power absorbed by the circulating pump.

Therefore, the model produced two different performance maps: one at maximum COP and one at maximum power.

Results show that the performance of the system is strictly related to solar radiation available. Thanks to solar energy the heat pump can evaporate the working fluid at temperatures higher than ambient ones, with a significant advantage in terms of COP with respect to air-source heat pumps. However, when solar radiation is too low, the system is not able to produce any thermal power.

Annual simulations, carried out assuming a storage of infinite capacity with no thermal losses, showed that the smallest configuration is suitable only for domestic hot water supply applications. The biggest of the configurations was able to supply 50% of the annual thermal demand. Both systems with intermediate and big heat pump were able to supply the demand during mid season. In winter season, only cases C (i.e. with the more powerful heat pump) were able to supply a significant fraction of the demand.

On the electric side, especially in summer can be seen the cooling effect of the PV cells thanks to the fluid coming from the evaporator circulating on the back of the PVTs. However, for the systems of higher size this effect is less relevant on daily basis since the heat pump works only few hours a day because of the low heat demand.

Electric energy balances show that while the SAHP is working the electric power absorbed by the heat pump is comparable with the one produced by the modules. During summer the heat pump works only few hours per day, and on annual basis

all the systems are characterized by a surplus of electric energy production.

The economic analysis showed that the largest configuration reached break-even in its useful life. Looking to the initial investment, the main cost is related to PVT technology, affecting significantly the Net Present Values. A higher number of PVT, however, tends to increase the NPV, meaning that the higher investment cost is balanced by extra-revenues.

The choice of PVT instead of conventional thermal collectors and PV modules is justified comparing a configuration equipped with PVT with a configuration with conventional modules, fixed the overall collectors' area and the design conditions. The result is that on annual basis the conventional system supplied slightly less thermal energy to the load, and PV collectors roughly covered heat pump's electric consumption. Of course this system is initially less expensive than the one with PVT collectors, but the economic analysis showed that the lower electricity production reduces a lot net cash flows, leading to a Net Present Value lower than all the other considered systems.

In conclusion, SAHP systems represent a promising technology for domestic heating and hot water production. In fact, this system, in configuration C3 is able to co supply 50% of annual thermal load and to reduce 65% primary energy demand with costs comparable to a conventional technology.

The price of PVT modules is expected to decrease in the next years thanks to improvements in design and manufacturing process.

Moreover, the advantages of this technology could be coupled with other systems thanks to dual configurations. For instance, the addition of an air-source evaporator would let the system operate even without solar radiation. Another possible investigation could concern the use during summer of PVT collectors as conventional water heaters, bypassing the heat pump. This solution would result in a decrease of electric power consumption of the heat pump but also a decrease of the electric power produced by the modules, being removed cell's cooling.

Finally, with a more accurate storage model, able to take into account capacity limits and thermal losses, it will be possible in future works to study other control logics and make more precise annual energy and economic assessments.





# Appendix A

## Technical specifications

### A.1 Compressors

In the following tables are reported the polynomial coefficients used in this work for the modelling of electric power and mass flow rate of the heat pump.

Table A.1: Polynomial equations coefficients for compressor Highly 02830, used in case A.

	$\dot{m}_{ref}[kg/s]$	$\dot{W}_{comp}[W]$
a0	0,844992929	-1471,964903
a1	0,000398085	-4,167225778
a2	-0,051296084	112,4036051
a3	7,4493E-06	-0,247210947
a4	2,27735E-06	0,110356095
a5	0,001038585	-2,122125446
a6	-7,70124E-08	-0,001493486
a7	-6,84528E-08	0,003228433
a8	-4,18152E-08	0,000839386
a9	-6,92385E-06	0,01414766

Table A.2: Polynomial equations coefficients for compressor Highly 05100, used in case B.

	m_ref[kg/s]	Wc
a0	7,404E-01	6,970E+03
a1	7,699E-04	1,831E-01
a2	-4,416E-02	-3,848E+02
a3	1,741E-05	-6,754E-01
a4	8,919E-06	-1,363E-01
a5	8,938E-04	8,083E+00
a6	-1,651E-07	-1,774E-03
a7	-1,011E-08	9,138E-03
a8	-1,267E-07	5,003E-03
a9	-5,963E-06	-5,391E-02

Table A.3: Polynomial equations coefficients for compressor Tecumseh VSC 9538 ZXG, used in case C.

	Pa	Qm
c0	9.00E+02	5.24E-02
c1	1.01E+01	1.83E-03
c2	2.23E+01	2.82E-05
c3	4.66E-01	2.15E-05
c4	-4.43E-01	7.52E-06
c5	1.51E-01	-6.86E-07
c6	6.10E-03	2.77E-08
c7	-1.46E-02	1.30E-07
c8	7.60E-03	-8.83E-08
c9	2.33E-03	-7.07E-09

## A.2 Solar modules

Table A.4: Solar modules specifications

type		PVT	PV	Thermal	PV1	PV2
use			model	model	exp	exp
$W_{nom}$	W	250	250		245	285
NOCT	°C	56	46		47	48
$\gamma$	%/°C	-0.42	-0.42		-0.48	-0.4
$A_{ap}$	$m^2$	1.45	4.45	2.295		
$a_1$	$W/m^2K$	15.529		4.47		
$a_2$	$W/m^2K^2$	0.01		0.0069		
$\eta_{opt}$	-	0.588		0.791		



# List of Figures

1.1	World Total Primary Energy Supply - IEA . . . . .	1
1.2	Annual growth rates of world renewables supply from 1990 to 2014.[4]	2
1.3	2014 fuel shares in world total primary energy supply. [4] . . . . .	2
1.4	2014 product shares in world renewable energy supply. [4] . . . . .	3
1.5	RES share in Italy. . . . .	4
1.6	Renewable energy exploitation in Italy by source. [7] . . . . .	4
2.1	Effect of Rayleigh scattering and atmospheric absorption on spectral distribution of beam irradiance. [9] . . . . .	6
2.2	Air mass at different solar altitudes. [10] . . . . .	7
2.3	Declination change during the year. [11] . . . . .	7
2.4	Equation of time. [11] . . . . .	8
2.5	n-type and p-type silicon cristal lattice.[11] . . . . .	11
2.6	Cross section of a silicon solar cell.[9] . . . . .	11
2.7	Model and I-V curve of a PV cell. [9] . . . . .	12
2.8	Multi-layer and multi-junction principle. [12] . . . . .	15
2.9	Types of collectors and applications.[12] . . . . .	16
2.10	Cross section of a flat plate collector. [9] . . . . .	16
2.11	Thermal network for a single collector; case (c) represents a simplified approach. [13] . . . . .	18
2.12	Plot of equation 2.27 for diverse collectors. . . . .	19
2.13	Sheet and tube and roll bond configurations of PVT modules. . . . .	20
2.14	Heat pump scheme.[18] . . . . .	21
2.15	Schematic diagram of a DX-SAHP system.[25] . . . . .	23
2.16	Schematic of indirect expansion solar-assisted heat pump. . . . .	24
2.17	(a) Parallel; (b) Dual-source and series. [27] . . . . .	25
2.18	Heat contributions from all possible sources and COP for the consid- ered operating modes. . . . .	25
3.1	Schematic of the modelled system. . . . .	28

3.2	Pressure drops. . . . .	29
3.3	Schematic of the modelled system. . . . .	32
3.4	Motor input curves of the compressor. . . . .	32
3.5	Operating field of the compressor. . . . .	33
3.6	T-Q diagram of the condenser in nominal conditions. . . . .	34
3.7	Block diagram: model solution procedure. . . . .	39
3.8	Effect of $\dot{m}_{w,eva}$ . . . . .	41
3.9	Block diagram of the control logic. . . . .	44
4.1	Plant scheme and instruments position. . . . .	50
4.2	Scheme of the commercial air-source heat pump. . . . .	50
4.3	Poly-silicon roll-bond PVT at SolarTech Lab. . . . .	50
4.4	Pt 100 thermoresistances and flow meter. . . . .	52
4.5	Weather data in the considered sample. . . . .	53
4.6	Thermal and electric powers data. . . . .	53
4.7	Temperature measures for the considered sample interval. . . . .	54
4.8	PVT thermal image. . . . .	55
4.9	COP calculated in the considered sample interval. . . . .	55
4.10	Weather profile, November, 30 <sup>th</sup> 2016. . . . .	58
4.11	SAHP thermal and electric power, November, 30 <sup>th</sup> 2016. . . . .	59
4.12	Evaporator and condenser temperatures, November, 30 <sup>th</sup> 2016. . . . .	59
4.13	COP, November, 30 <sup>th</sup> 2016. . . . .	60
4.14	Comparison between PVT and PV electric power production. . . . .	61
5.1	Condenser thermal power (a) and COP (b) performance maps for case B2 with $\theta_s = 0$ . . . . .	64
5.2	Ambient and evaporation temperature behaviour. . . . .	65
5.3	$G$ and $T_{amb}$ in the considered winter day. . . . .	65
5.4	$Q_{cond}, Q_{eva}$ in winter day. . . . .	66
5.5	$W_c, COP$ in winter day. . . . .	66
5.6	$T_{eva}, T_{m,w,pvt}$ in winter day. . . . .	67
5.7	% of load supplied by the system in winter. . . . .	68
5.8	Weather profile for the considered mid-season day. . . . .	68
5.9	Condenser thermal power (a) and PVT electric power profile. . . . .	69
5.10	Mid season energy production, case B2. . . . .	70
5.11	Yearly energy production for case B2 and C2 . . . . .	71
5.12	Fraction of annual heat demand supplied by the SAHP. . . . .	74
5.13	Electric energy produced and absorbed by the system on annual basis . . . . .	75

---

5.14	Electric energy self-consumption on annual basis. . . . .	76
5.15	Primary energy demand and savings contributions. . . . .	78
5.16	Investment cost structure. . . . .	79
5.17	PVT cost sensitivity analysis. . . . .	80
5.18	Natural gas price sensitivity analysis. . . . .	81
5.19	Electricity price sensitivity analysis. . . . .	82
5.20	Condenser thermal power (a) and electric power profile (b) in the reference winter day. . . . .	83
5.21	Electric energy balance (a) and primary energy supply to the load (b) for systems C2 and D. . . . .	85
5.22	Cost structure in case C2 and D . . . . .	86





# List of Tables

3.1	Temperatures in design conditions. . . . .	35
3.2	Annual thermal load. . . . .	43
3.3	Initial investment parameters assumed. . . . .	45
3.4	Other economic assumptions. . . . .	47
4.1	Measuring instruments specifications. . . . .	51
4.2	16/11/2016 experimental data with refrigerant temperature at evaporator outlet. . . . .	57
5.1	Monthly load and thermal energy production. . . . .	71
5.2	Thermal energy produced in days with high, medium and low radiation. . . . .	72
5.3	Net electric energy production on monthly basis. . . . .	75
5.4	SAHP electricity self-consumption. . . . .	76
5.5	Economic analysis results: NPV and IRR . . . . .	80
5.6	Energy production and consumption on monthly basis in case C2 and D. . . . .	84
5.7	Electricity self-consumption fraction on monthly basis for cases C2 and D. . . . .	85
A.1	Polynomial equations coefficients for compressor Highly 02830, used in case A. . . . .	91
A.2	Polynomial equations coefficients for compressor Highly 05100, used in case B. . . . .	92
A.3	Polynomial equations coefficients for compressor Tecumseh VSC 9538 ZXG, used in case C. . . . .	92
A.4	Solar modules specifications . . . . .	93



# Acronyms

**SAHP** Solar-Assisted Heat Pump

**DX-SAHP** Direct-expansion Solar-Assisted Heat Pump

**IDX-SAHP** Indirect-expansion Solar-Assisted Heat Pump

**HP** Heat Pump

**PV** Photovoltaics

**DHW** Domestic Hot Water

**IEA** International Energy Agency

**GSE** Gestore Servizi Energetici

**AM** Air Mass

**DNI** Direct Normal Irradiance

**GHI** Global Horizontal Irradiance

**NOCT** Nominal Operating Cell Temperature

**IAM** Incidence Angle Modifier

**NPV** Net Present Value

**IRR** Internal Rate of Return



# Bibliography

- [1] International Energy Agency. *Statistics*. 2016. URL: <http://www.iea.org/statistics>.
- [2] British Petroleum. *BP statistical review of world energy*. 2016.
- [3] Intergovernmental Panel on Climate Change. *Climate Change 2014 - Synthesis Report*. 2014. URL: <https://www.ipcc.ch>.
- [4] IEA. “Key Renewables Trends”. In: *Paris, France* (2016).
- [5] GSE. “Rapporto Statistico 2015-Solare Fotovoltaico”. In: *www.gse.it* (2015).
- [6] *Official Journal of the European Union*. 2016. URL: [eur-lex.europa.eu](http://eur-lex.europa.eu).
- [7] GSE. “Rapporto Statistico 2014 - Energia da fonti rinnovabili”. In: *www.gse.it* (2014).
- [8] William B Stine and Michael Geyer. *Power from the Sun*. Power from the sun. net, 2001.
- [9] John A Duffie and William A Beckman. *Solar engineering of thermal processes*. Vol. 3. Wiley New York, 2013.
- [10] ABB SACE. *Quaderni di applicazione tecnica N.10. Impianti fotovoltaici*. ABB, 2013.
- [11] Christiana Honsberg and Stuart Bowden. *PV education*. 2014. URL: <http://pveducation.org>.
- [12] Giampaolo Manzolini. *Power production from renewable energy, notes of the course*. Milan, 2016.
- [13] Soteris A. Kalogirou. *Solar Energy Engineering - processes ad systems*. Boston: Academic Press, 2009.
- [14] Daniele Cocco, Pierpaolo Puddu, and Chiara Palomba. *Tecnologie delle energie rinnovabili*. Servizi grafici editoriali, 2010.

- [15] H.A. Zondag et al. “The yield of different combined PV-thermal collector designs”. In: *Solar Energy* 74.3 (2003), pp. 253–269. URL: <http://www.sciencedirect.com/science/article/pii/S0038092X0300121X>.
- [16] Niccolò Aste, Claudio del Pero, and Fabrizio Leonforte. “Water flat plate PV-thermal collectors: A review”. In: *Solar Energy* 102 (2014), pp. 98–115. URL: <http://www.sciencedirect.com/science/article/pii/S0038092X14000437>.
- [17] Paola Bombarda et al. “Thermal and electric performances of roll-bond flat plate applied to conventional {PV} modules for heat recovery”. In: *Applied Thermal Engineering* 105 (2016), pp. 304–313. URL: <http://www.sciencedirect.com/science/article/pii/S1359431116308511>.
- [18] Michael J Moran et al. *Fundamentals of engineering thermodynamics*. John Wiley & Sons, 2010.
- [19] Phillip Sporn and ER Ambrose. “The heat pump and solar energy”. In: *Proc. of the World Symposium on Applied Solar Energy. Phoenix, US*. 1955.
- [20] Wikipedia. *Pompa di calore elio-assistita*. 2016. URL: [it.wikipedia.org](http://it.wikipedia.org).
- [21] SK Chaturvedi, DT Chen, and A Kheireddine. “Thermal performance of a variable capacity direct expansion solar-assisted heat pump”. In: *Energy Conversion and management* 39.3 (1998), pp. 181–191.
- [22] Raghad S. Kamel, Alan S. Fung, and Peter R.H. Dash. “Solar systems and their integration with heat pumps: A review”. In: *Energy and Buildings* 87 (2015), pp. 395–412. URL: <http://www.sciencedirect.com/science/article/pii/S037877881400961X>.
- [23] Mahmut Sami Buker and Saffa B. Riffat. “Solar assisted heat pump systems for low temperature water heating applications: A systematic review”. In: *Renewable and Sustainable Energy Reviews* 55 (2016), pp. 399–413. URL: <http://www.sciencedirect.com/science/article/pii/S1364032115012368>.
- [24] Jean-Christophe Hadorn. *Solar and Heat Pump Systems for Residential Buildings*. John Wiley & Sons, 2015.
- [25] T.T. Chow et al. “Potential use of photovoltaic-integrated solar heat pump system in Hong Kong”. In: *Applied Thermal Engineering* 30.8–9 (2010), pp. 1066–1072. URL: <http://www.sciencedirect.com/science/article/pii/S1359431110000268>.

- [26] K Kaygusuz and T Ayhan. “Experimental and theoretical investigation of combined solar heat pump system for residential heating”. In: *Energy Conversion and Management* 40.13 (1999), pp. 1377–1396. URL: <http://www.sciencedirect.com/science/article/pii/S0196890499000266>.
- [27] John A Duffie and William A Beckman. *Solar engineering of thermal processes*. Vol. 3. Wiley New York etc., 1980.
- [28] *SPF Institute für Solartechnik*. 2016. URL: <http://www.spf.ch/>.
- [29] W. De Soto, S.A. Klein, and W.A. Beckman. “Improvement and validation of a model for photovoltaic array performance”. In: *Solar Energy* 80.1 (2006), pp. 78–88. URL: <http://www.sciencedirect.com/science/article/pii/S0038092X05002410>.
- [30] *Grundfos*. 2016. URL: <http://it.grundfos.com>.
- [31] RIES GmbH. *Hitachi-Highly Rotary R134a Heat Pump Compressors*. 2016. URL: <http://www.ries-gmbh.de>.
- [32] Gabriele Turrini and Carlo Pennati. “Analisi energetica di sistemi edificio impianto con pompa di calore: sviluppo di un modello e sua validazione”. In: (2012).
- [33] Andrea Barella. “Ottimizzazione del frazionamento della potenza in pompe di calore multicompressore di tipo acqua-acqua”. In: (2014).
- [34] YS Kim. “An experimental study on evaporation heat transfer characteristics and pressure drop in plate heat exchanger”. PhD thesis. MS thesis, Yonsei University, 1999.
- [35] M.M. Shah. “A general correlation for heat transfer during film condensation inside pipes”. In: *International Journal of Heat and Mass Transfer* 22.4 (1979), pp. 547–556. URL: <http://www.sciencedirect.com/science/article/pii/0017931079900589>.
- [36] *Autorità per l’Energia Elettrica, il Gas e il Sistema Idrico*. 2016. URL: <http://www.autorita.energia.it/it/dati/g3.htm>.
- [37] *Autorità per l’Energia Elettrica, il Gas e il Sistema Idrico*. 2016. URL: <http://www.autorita.energia.it/it/dati/eep35.htm>.